Condensed Matter Science

Electronic Structure

Angle-dependent soft x-ray emission spectra of hexagonal boron nitride
Muramatsu, Y., R.C.C. Perera

Cu metallic quantum well states on Cu/Ni/Cu(100) and Cu/Fe/Cu(100)
Danese, A., R.A. Bartynski, D.A. Arena, M. Hochstrasser, J. Tobin

Determination of formal oxidation state of Co in MBE-grown co-doped TiO_2(001) anatase epitaxial films by x-ray absorption spectroscopy
Chambers, S.A., T. Droubay, S. Thevuthasan, N.H. Hamdan

Development and evaluation of a new liquid cell system for soft x-ray absorption experiments
Matsuo, S., T. Kurisaki, H. Yamashige, P. Nachimuthu, R.C.C. Perera, H. Wakita

Electronic structure of alkali metal-doped M_8Si_{46} (M=Na, K) clathrates
Moewes, A., E.Z. Kurmaev, J.S. Tse, M. Geshi, M.J. Ferguson, V.A. Trofimova, Y.M. Yarmoshenko

Electronic structure of CMR compounds investigated by means of XES
Küpper, K., B. Schneider, S.G. Chiuzbaian, M. matteucci, D.D. Sarma

Electronic structure of divalent hexaborides
Denlinger, J.D., G.-H. Gweon, J.W. Allen, Z. Fisk

Electronic structure of graphite fluorides
Kurmaev, E.Z., A. Moewes, D.L. Ederer, H. Ishii, K. Seki, M. Yanagihara, F. Okino, H. Touhara

Fermi surface topology, bilayer splitting, and (π,0) dispersion kinks in Bi2212
Gromko, A.D., Y.-D. Chuang, A.V. Fedorov, J.D. Koralek, Y. Aiura, Y. Yamaguchi, K. Oka, Y. Ando, D.S. Dessau

Infrared conductivity of photocarriers in organic molecular crystals
Weber, C., Ch. Kloc, M. Martin, J.H. Schoen, B. Batlogg, J. Orenstein

Investigation of surface and bulk half-metallic character of Fe_3O_4 by spin resolved photoemission
Morton, S.A., G.D. Waddill, S. Kim, I.K. Schuller, S.A. Chambers, J.G. Tobin

Magnetic circular dichroism in the x-ray absorption spectra of the CMR compound, $Yb_{14}MnSb_{11}$
Holm, A.P., S.M. Kauzlarich, S.A. Morton, G.D. Waddill, W.E. Pickett, J.G. Tobin

Multi-atom resonant photoemission effects from solid surfaces and free molecules
Mannella, N., B.S. Mun, S.-H. Yang, A.W. Kay, F.J. Garcia de Abajo, E. Arenholz, A.T. Young, Z. Hussain, H. Wang, O. Hemmers, D.W. Lindle, M.A. Van Hove, C.S. Fadley

O 1s XAS of H_2O in the solvation shell of monovalent and trivalent ions
Näslund, L.- Å., Ph. Wernet, H. Ogasawara, D. Edwards, S. Myneni, A. Nilsson

Partial density of states of B-2*p* in AlB_2 type compounds
Nakamura, J., K. Kuroki, N. Yamada, T.A. Callcott, D.E. Ederer, J.D. Denlinger, R.C.C. Perera

Polarization-dependent soft-x-ray absorption of highly oriented ZnO microrod-array
Guo, J.-H., L. Vayssieres, C. Persson, R. Ahuja, B. Johansson, J. Nordgren

Quantum confinement observed in α-Fe_2O_3 nanorod-array
Guo, J.-H., L. Vayssieres, C. Såthe, S.M. Butorin, J. Nordgren.

Soft x-ray emission and absorption spectra in the Si *L* region of polysilanes
Muramatsu, Y., M. Fujino, E.M. Gullikson, R.C.C. Perera

Soft x-ray emission spectroscopy of the liquid-solid interface between water and a $Cu(In,Ga)(S,Se)_2$ thin film solar cell absorber
Heske, C., U. Groh, O. Fuchs, L. Weinhardt, E. Umbach, Ch.-H. Fischer, Th. Schedel-Niedrig, M.Ch. Lux-Steiner, S. Zweigart, F. Karg, J.D. Denlinger, B. Rude, C. Andrus, F. Powell

Soft x-ray probe of bulk bandgaps in divalent hexaborides
Denlinger, J.D., J.W. Allen, Z. Fisk

Soft x-ray spectroscopy of noble gas atoms doped in solid matrices
Muramatsu, Y., R.C.C. Perera

Spectroscopic observation of polaron-lattice band structure in the conducting polymer polyaniline
Kurmaev, E.Z., M.I. Katsnelson, A. Moewes, M. Magnuson, J.-H. Guo, S.M. Butorin, J. Nordgren, D.L. Ederer, M. Iwami

Spin-resolved electronic structure studies of ultrathin films of Fe on singular and vicinal GaAs
Spangenberg, M., E.A. Seddon, E.M.M. McCash, T. Shen, S.A. Morton, D. Waddill, J. Tobin

VUV Photoionization of superfluid liquid helium droplets at the ALS
Peterka, D., A. Lindinger, L. Poisson, M. Ahmed, D. Neumark

XANES spectroscopy of Ti and V centers grafted onto mesoporous sieves: Preliminary results
Lin, W., D. Bruehwiler, H. Frei

X-ray absorption and emission spectroscopy at the nitrogen K-edge in dilute $GaAs_{1-x}N_x$
Adamcyk, M., A. Ballestad, A. Moewes, E. Nodwell, T. Tiedje, S. Tixier

X-ray absorption studies of the cBN composites with different bonding phases
Benko, E., K. Lawniczak-Jablonska, P. Nachimuthu, I.N. Demchenko, E. Piskorska, P. Klimczyk, R.C.C. Perera, A. Wlochowicz, A. Benko, T.L. Barr

X-ray emission spectra and electronic structure of charge transfer salts
Kurmaev, E.Z., A. Moewes, U. Schwingerschlögl, R. Claessen, M.I. Katsnelson, H. Kobayashi, S. Kagoshima, Y. Misaki, D.L. Ederer, K. Endo, M. Yanagihara

X-ray transitions for studying the electronic structure of 5d metals
Kurmaev, E.Z., A. Moewes, Z. Pchelkina, I. Nekrasov, T.A. Callcott, D.L. Ederer

Angle-Dependent Soft X-Ray Emission Spectra of Hexagonal Boron Nitride

Y. Muramatsu[1] and R. C. C. Perera[2]
[1]*Japan Atomic Energy Research Institute, Sayo-gun, Hyogo 679-5148, Japan*
[2]*CXRO, Lawrence Berkeley National Laboratory, Berkeley, California 94720, USA*

Hexagonal boron nitride (*h*-BN) is a basic boron compound, which has been widely used as a reference sample in soft x-ray spectroscopy. It adopts a layered structure similar to graphite. To obtain detailed structural information for *h*-BN using soft x-ray emission spectroscopy, we have measured its angle-dependent soft x-ray emission spectra.

Commercially obtained *h*-BN power pressed on indium sheets and pyrolytic (*p*) BN plate was used for spectroscopic measurements. Soft x-ray emission spectra in the B *K* and N *K* regions were measured using a grating x-ray spectrometer installed in the undulator beamline, BL-8.0.1. The photon energy of the monochromatized incident beam was tuned to about 230 eV (for B *K*) and 430 eV (for N *K*). The incident angle (θ) of the monochromatized beam to the sample surface was adjusted to 15, 45 and 75 degrees. Measured x-ray emission spectra were analyzed using discrete variational (DV)-Xα molecular orbital calculations.

Figure 1 shows the angle-dependent B *K* and N *K* x-ray emission spectra of *p*-BN. In the B *K* spectra, intensity of the high-energy shoulder near 184 eV increases as θ increases. Intensities of the low-energy satellite near 170 eV and the low-energy shoulder near 178 eV both decrease as θ increases. In the N *K* spectra, intensity of the high-energy peak at 398.5 eV drastically increases as θ increases, while intensity of the low-energy shoulders near 385 eV and 390 eV decrease as θ increases. Upper panels of Figure 2 show the calculated density-of-states (DOS) spectra of occupied B2p- and N2p-orbitals in the model cluster of $B_{48}N_{48}H_{24}$. These calculated DOS spectra reproduce the x-ray emission spectra measured with an incident angle of 45 degrees. Lower panels of Figure 2 show the B2p- and N2p-DOS spectra calculated by considering the contributions of σ- and π-components in x-ray emission. In the B2p-DOS spectra, intensity of the high-energy shoulder (near -4 eV) increases as θ increases. Intensities of the low-energy shoulder (-10 eV) and low-energy peak (-18 eV) decrease as θ increases. In the N2p-DOS spectra, intensity of the high-energy peak (-2 eV) increases as θ increases, while intensities of the low-energy shoulders (-6 eV and –10 eV) decrease as θ increases. These calculated spectra well reproduce the measured angle-dependent x-ray emission spectra. Thus, it can be confirmed that angle-dependent x-ray emission measurements will provide detailed structural information on *h*-BN.

We thank Dr. J. Denlinger of the Lawrence Berkeley National Laboratory for his help and support in performing x-ray emission measurements. This work is supported by the Hyogo Science and Technology Association and the US Department of Energy under contract No. DE-AC03-76SF00098.

Principal Investigator: Yasuji Muramatsu, Japan Atomic Energy Research Institute. Email: murama@spring8.or.jp. Telephone: +81-791-58-2601.

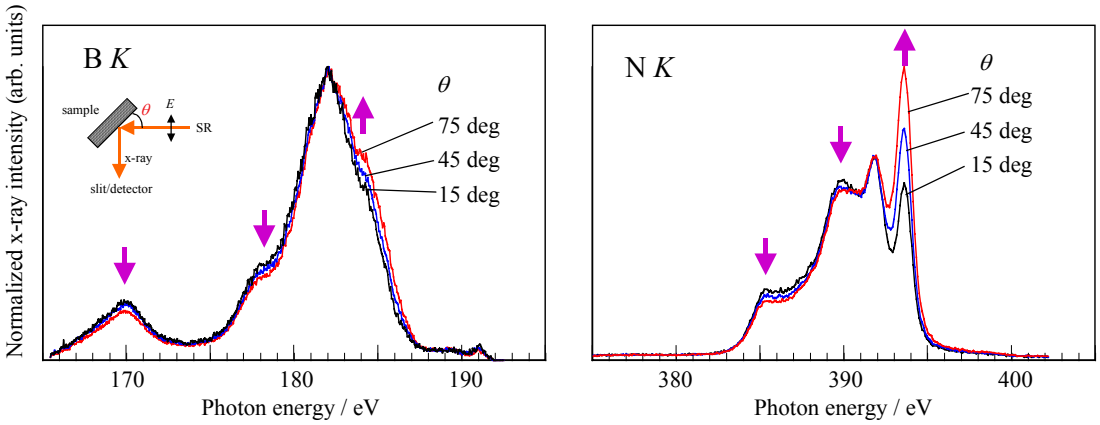

Figure 1 Angle-dependent x-ray emission spectra in the B *K* (left panel) and N *K* (right panel) regions of *p*-BN.

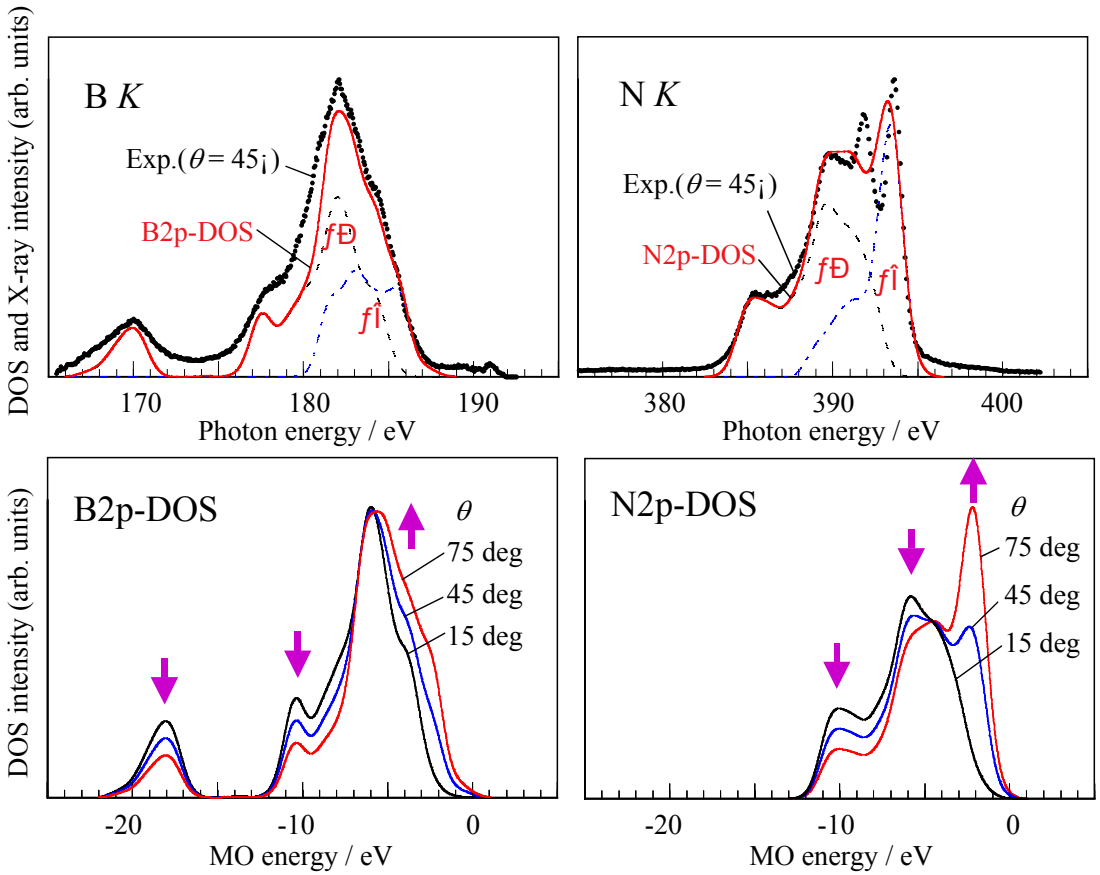

Figure 2 Upper panels show the occupied B2p- and N2p-DOS spectra of the $B_{48}N_{48}H_{24}$ model cluster. X-ray emission spectra measured with an incident angle of 45 degrees are superimposed on the calculated spectra. Lower panels show the angle-dependent B2p- and N2p-DOS spectra with incident angles of 15, 45 and 75 degrees.

Cu Metallic Quantum Well States on Cu/Ni/Cu(100) and Cu/Fe/Cu(100)

A. Danese,[1] R.A. Bartynski,[1] D.A. Arena,[2] M. Hochstrasser,[2] and J. Tobin[2]
[1] Department of Physics and Laboratory for Surface Modification
Rutgers University, 136 Frelinghuysen Rd., Piscataway, NJ 08855
[2]Lawrence Livermore National Laboratory

Ultrathin metal films grown epitaxially on metal substrates often exhibit so called metallic quantum well (MQW) states.[1-8] These are electronic states that are confined to the overlayer by reflectivity from projected band gaps in the substrate metal. Even in the absence of such band gaps, significant interface reflectivity can from intense quantum well resonances. Owing to band structure effects, a given MQW state will move to higher energy as the thickness of the overlayer increases. Furthermore, the periodicity with which these states cross the Fermi level is expected to be a function of the overlayer band structure and insensitive to the substrate.

Much of the work on MQW states has concentrated on the behavior of Cu on various transition metal substrates such as Ni and Co, owing to their importance in magnetic multilayers. In the unoccupied electronic states above the Fermi level, the Cu/Ni(100) system is unusual in that the Cu-induced levels disperse downward with increasing film thickness, rather than downward.[9, 10] It was thought that this might be due to strain in the Cu film. To test these ideas, we used photoemission and inverse photoemission to study the occupied and unoccupied overlayer electronic states of the Cu/Ni/Cu(100) system as a function of Cu and Ni thickness.

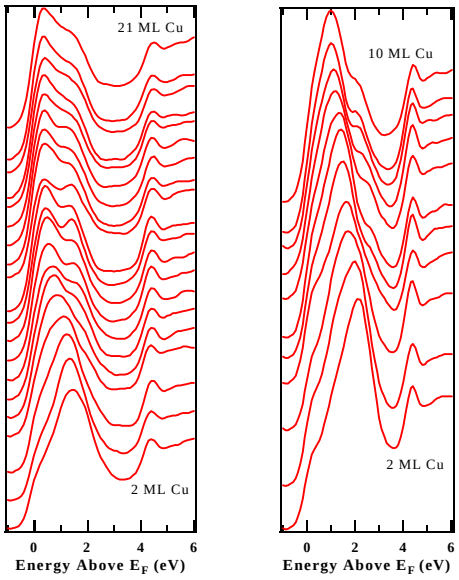

Fig. 1: Downward dispersion of unoccupied Cu states in the Cu/Ni/Cu(100) system.

In Fig. 1 we show inverse photoemission spectra from increasingly thick Cu overlayers on a 35 ML and on a 5 ML film of Ni grown on Cu(100). One can see that the results are qualitatively similar to eachother, and to the Cu/Ni(100) results, in that the Cu-induced states disperse downward as a function of increasing Cu film thickness. There are quantitative differences, however. The states of the Cu films grown on the thinner Ni layer are at higher energy than those on the thicker Ni film. Although it appears that the downward dispersion does not appear to arise from a strain effect, these quantitative differences may. To test this, we measured normal emission photoemission from wedges of Cu grown on two different thickness Ni films on the same Cu(100) substrate. A diagram of the sample geometry is shown in Fig. 2. Two identical Cu wedges were grown on Ni films of 7 ML and 35 ML thicknesses.

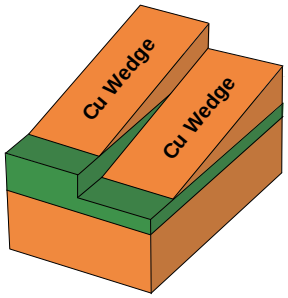

FIG.2: Sample geometry for photoemission studies.

Using the UltraESCA end station of Beamline 7.0.1, we have obtained photoemission data from the Cu/fccNi/Cu(100) system. The sample was prepared by depositing the Ni onto an atomically

clean, well-ordered Cu(100) surface. This was followed by deposition of a wedge-shaped Cu film whose thickness ranged from 0 to 40+ ML. Figure 3 show a series of normal emission photoemission data displayed as a 2-dimensional plot of Cu film thickness vs. binding energy. Light colors indicate high intensity and the dark colors low. These peaks are associated with metallic quantum well states in the Cu films. In contrast to the inverse photoemission data, the intensity maxima that move towards the Fermi level as the film thickness increases. Although the MQW states are less pronounced on the thicker Ni film, the period with which these Cu MQW states cross E_F appears are identical. As a change in the Cu lattice constant would change the electronic structure and thus change the periodicity of the Fermi level crossings, these results suggest that there is minimal change in strain in these Cu films. Strain in the Ni, however, may cause this effect. Quantitative structural studies and first principles electronic structure calculations are currently underway to investigate the low energy structures of these systems.

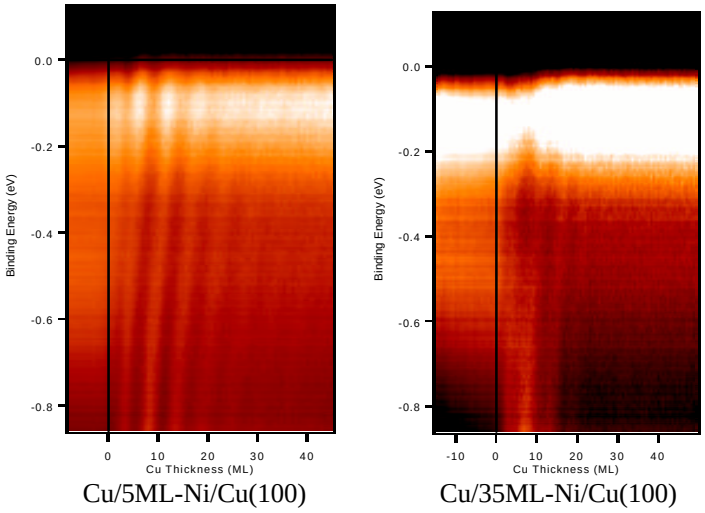

Fig. 3.: Normal emission from the Cu/Ni/Cu(100) systems as a function of Cu film thickness.

Another important observation is the sharp contrast between the upward dispersion of Cu MQW states below the Fermi level and the downward dispersion of Cu state above E_F. Most likely this difference arises because the Ni *d*-bands terminate about E_F + 0.1 eV. The downward dispersion if the Cu states on Ni is most likely associated with the interaction of the Cu and Ni *sp*-band.

Finally, we have also grown Cu/fccFe/Cu(100) quantum well structures and the exhibit a strong upward dispersion and cross EF with a periodicity that is, within experimental uncertainty, the same as that of the Cu/Ni system.

REFERENCES

[1] J.E. Ortega and F.J. Himpsel, Phys. Rev. Lett. **69**, 844 (1992).
[2] P. Segovia, E.G. Michel and J.E. Ortega, Phys. Rev. Lett. **77**, 2734 (1996).
[3] F.G. Curti, A. Danese and R.A. Bartynski, Phys. Rev. Lett. **80**, 2213 (1998).
[4] R.K. Kawakami et al., Phys. Rev. Lett. **80**, 1754 (1998).
[5] R.K. Kawakami et al., Nature. **398**, 132 (1999)
[6] R.K. Kawakami et al., Phys. Rev. Lett. **82**, 4098 (1999).
[7] A. Danese and R.A. Bartynski, Phys. Rev. B. (in press).
[8] A. Danese, D.A. Arena and R.A. Bartynski, Prog. Surf. Sci. **67**, 249 (2001).
[9] O. Rader and F.J. Himpsel, Appl. Phys. Lett. **67**, 1151 (1995).
[10] C. Hwang and F.J. Himpsel, Phys. Rev. B **52**, 15368 (1995).

This work is supported by NSF Grant DMR-98-01681 and Petroleum Research Fund Grant # 33750-AC5,6.

Principle Investigator: Robert A. Bartynski, Department of Physics and Laboratory for Surface Modification, Rutgers University. Email: bart@physics.rutgers.edu. Telephone: 732-445-4839

Determination of Formal Oxidation State of Co in MBE-Grown Co-doped TiO_2(001) Anatase Epitaxial Films by X-ray Absorption Spectroscopy

S.A. Chambers[1], T. Droubay[1], S. Thevuthasan[1], N.H. Hamdan[2]
[1]Fundamental Science Division, Pacific Northwest National Laboratory
Richland, WA 99352, U.S.A.
[2]Lawrence Berkeley National Laboratory, Berkeley, CA 94720, U.S.A.

INTRODUCTION

Diluted magnetic semiconductors (DMS) consist of nonmagnetic semiconducting materials doped with a few atomic percent of impurity magnetic cations. Magnetic coupling occurs by virtue of exchange interactions between the magnetic spins and free carriers in the semiconductor. The interaction can occur via *p-d* or *d-d* exchange, and can lead to antiferromagnetic or ferromagnetic coupling, depending on the concentration and the local structural environment of the magnetic impurity. DMS materials grown as thin epitaxial films can be used as spin injectors for semiconductor heterostructures, provided they are ferromagnetic.

Virtually all conventional DMS materials exhibit Curie temperatures of ~100K or less and must be *p*-type, which means that the exchange interaction leading to ferromagnetic behavior is hole mediated. Most of the effort expended to date on understanding the crystal growth and properties of thin-film DMS materials has focused on Mn-doped II-VI, III-V, and Group IV semiconductors.[1-4] Relatively little effort has gone into the investigation of "nontraditional" semiconductors, such as semiconducting oxides, to see if they are more robust magnetically. However, one such oxide - Co-doped TiO_2 anatase ($Co_xTi_{1-x}O_2$) - has recently been discovered to be the most magnetically robust DMS with regard to magnetic moment at saturation, coercivity, remanence, and Curie temperature.[5] Indeed, it is one of the very few DMS materials demonstrated to exhibit ferromagnetic behavior above 300K. In addition, it has been shown that the material can be grown epitaxially by both pulsed laser deposition (PLD)[6] and oxygen plasma assisted molecular beam epitaxy (OPA-MBE)[5] on $SrTiO_3$(001) and $LaAlO_3$(001). However, the resulting magnetic properties differed considerably for the two growth methods, with significantly better properties exhibited by OPA-MBE grown material.

In order to understand the mechanism of magnetism in this fascinating material, it is essential to know the charge state of the magnetic cation (Co), and the doping type. We have utilized Co L-edge x-ray absorption spectroscopy (XAS) at beamline 9.3.2 to determine the Co charge state.

EXPERIMENT

Epitaxial $Co_xTi_{1-x}O_{2-x}$ films of high structural quality were grown by OPA-MBE on $LaAlO_3$(001)[7] using a system at PNNL described in detail elsewhere.[8] The resulting samples were then transferred through air to beamline 9.3.2 and XAS measurements were made in total electron yield mode at the Co L-edge, Ti L-edge, and O K-edge. X-ray absorption near-edge spectra (XANES) were also recorded for several Co standards for comparison purposes. No surface cleaning was done, as the distribution of Co has been shown to be strongly modified by post-growth annealing at the temperatures required to rid the surface of carbon, or remove sputter damage.

RESULTS

We show in Fig. 1 Co L-edge XAS data for three films with different Co mole fractions (x) (Fig. 1a-c), and for standards containing Co in different oxidation states and local structural environments (Fig. 1d-g). The $CoTiO_3$ standard was a powder, CoO was a (001)-oriented bulk single crystal, γ-Co_2O_3 was a 100 nm thick (001)-oriented epitaxial film grown on MgO(001) at PNNL, and the Co metal standard was a polycrystalline film evaporated *in situ* in the XAS chamber. Comparison of all film spectra with those for the standards reveals a good fit with both $CoTiO_3$ and CoO, which both contain Co^{+2}, but a very poor fit for both γ-Co_2O_3, which contains Co^{+3}, and for Co metal. The fit to $CoTiO_3$ is better than that to CoO. However, there is some similarity between the reference spectra for CoO and γ-Co_2O_3, particularly in the vicinity of the feature at 784 eV. This result indicates that there may be some Co^{+3} in the CoO single crystal. The very high degree of similarity between the spectra for the Co-doped anatase films and the $CoTiO_3$ standard establishes that Co in the former is in the +2 formal oxidation state. Interestingly, using the Co evaporation rate and oxygen plasma beam intensity we have used for the growth of $Co_xTi_{1-x}O_{2-x}$ result in the epitaxial growth of metastable γ-Co_2O_3 on MgO(001). Therefore, the anatase lattice stabilizes the formation of Co(II), even though the conditions would result in Co(III) formation if pure Co oxide were allowed to grow under comparable

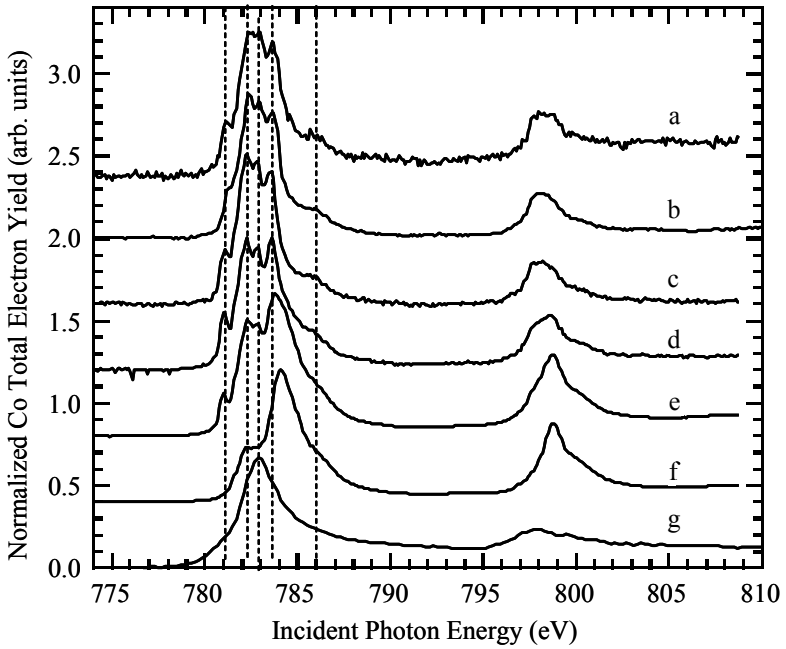

conditions.

Fig. 1 Co L-edge XAS for 20 nm thick films of epitaxial $Co_xTi_{1-x}O_{2-x}$ on $LaAlO_3$(001): (a) x = 0.01, (b) x = 0.06, (c) x = 0.08. Also shown are spectra for reference compounds containing Co in different formal oxidation states: (d) $CoTiO_3$, (e) CoO, (f) γ-Co_2O_3, and (g) Co metal.

SIGNIFICANCE

Ion channeling measurements conducted at PNNL reveals that Co substitutes for Ti in the anatase lattice. Furthermore, Hall effect measurements carried out at PNNL show that these films are *n*-type semiconductors as grown, despite the fact that no intentional *n*-type doping was carried out. The origin of the *n*-type doping may have to do with the presence of H in the film,

which has been detected by ^{19}F nuclear reaction analysis at PNNL at a concentration that is of the same order of magnitude as that of the free carriers – 10^{19} to 10^{20} cm^{-3}. H may be the direct dopant, as occurs in *n*-ZnO.[9] Alternatively, H_2, which is present in the growth chamber at a very low partial pressure, may partially reduce lattice oxygen during growth to produce OH and a free donor electron according to the reaction $O^{-2}_{(lattice)} + (1/2)H_2 \rightarrow OH^-_{(lattice)} + e^-$. This phenomenon is currently under more detailed investigation.

It thus appears that Co-doped anatase TiO_2 is ferromagnetic by virtue of *electron* mediated exchange interaction between Co^{+2} cations that substitute for Ti^{+4} in the lattice. In order to maintain charge neutrality, each substitutional Co^{+2} must be accompanied by an O^{-2} vacancy. However, such vacancies are uncharged and therefore do not contribute any donor electrons. In fact, *n*-type semiconducting behavior and Co substitution are independent phenomena; some highly resistive films are nonmagnetic despite having several at. % Co. Indeed, the magnetization depends as much on the free carrier concentration as on the presence of substitutional Co, as expected for a DMS.

Significantly, virtually all other known DMS materials are ferromagnetic by virtue of *hole* mediated exchange interaction, which has been thought to be the stronger interaction.[10] Therefore, Co-doped TiO_2 anatase is a highly unusual and potentially very important DMS in that it exhibits strong electron mediated exchange interaction at temperatures of at least 500K. No other known DMS exhibits these properties.

REFERENCES

1. R. Fiederling, M. Keim, G. Reuscher, W. Ossau, G. Schmidt, A. Waag, L.W. Molenkamp, Nature **402**, 787 (1999).
2. B.T. Jonker, Y.D. Park, B.R. Bennett, H.D. Cheong, G. Kioseoglou, A. Petrou, Phys. Rev. **B62**, 8180 (2000).
3. R.K. Kawakami, Y. Kato, M. Hanson, I. Malajovich, J.M. Stephens, E. Johnston-Halperin, G. Salis, A.C. Gossard, D.D. Awschalom, Science **294**, 131 (2001).
4. Y.D. Park, A.T. Hanbicki, S.C. Irwin, C.S. Hellberg, J.M. Sullivan, J.E. Mattson, T.F. Ambrose, A. Wilson, G. Spanos, B.T. Jonker, Science **295**, 651 (2002).
5. S.A. Chambers, S. Thevuthasan, R.F.C. Farrow, R.F. Marks, J.-U. Thiele, L. Folks, M.G. Samant, A.J. Kellock, N. Ruzycki, D.L. Ederer, U. Diebold, Appl. Phys. Lett. **79**, 3467 (2001), and, S.A. Chambers, Mat. Today, to appear, April issue (2002).
6. Y. Matsumoto, M. Murakami, T. Shono, T. Hasegawa, T. Fukumura, M. Kawasaki, P, Ahmet, T. Chikyow, S.-Y. Koshihara, H. Koinuma, Science **291**, 854 (2001).
7. S.A. Chambers, C. Wang, S. Thevuthasan, T. Droubay, D.E. McCready, A.S. Lea, V. Shutthanandan, C.F. Windisch, Jr., submitted to Thin Solid Films (2002).
8. S.A. Chambers, Surf. Sci. Rep. **39**, 105 (2000).
9. D.M. Hofman, A. Hofstaetter, F. Lieter, H. Zhou, F. Henecker, B.K. Meyer, S.B. Orlinskii, J. Schmidt, and P.G. Baranov, Phys. Rev. Lett. **88**, 045504-1 (2002).
10. T. Dietl, H. Ohno, F. Matsukura, J. Cibert and D. Ferrand, Science **287**, 1019 (2000).

The work was funded by a Laboratory Directed Research and Development grant associated with the PNNL Nanoscience and Technology Initiative, and by DOE BES Materials Science.

Principal Investigator – S.A. Chambers. Phone – (509) 376-1766. E-mail – sa.chambers@pnl.gov

Development and Evaluation of a New Liquid Cell System for Soft X-Ray Absorption Experiments

S. Matsuo[1], T. Kurisaki[2], H. Yamashige[2], P. Nachimuthu[3], R. C. C. Perera[4], and H. Wakita[1,2]
[1]Advanced Materials Institute, Fukuoka University, Nanakuma, Jonan-ku, Fukuoka 814-0180, Japan
[2]Department of Chemistry, Faculty of Science, Fukuoka University,
Nanakuma, Jonan-ku, Fukuoka 814-0180, Japan
[3]Department of Chemistry, University of Nevada Las Vegas, Las Vegas, NV 89154-4003, USA
[4]Center for X-ray Optics, Lawrence Berkeley National Laboratory, Berkeley, CA 94720, USA

INTRODUCTION

Soft X-ray is well used as a means available to investigate the electron state of valence band in a material, because the energy of soft X-ray is close to that of the valence band and strongly affects the material in the electronic state. The soft X-ray absorption spectrum provides information on the electron states between the absorbing atom and neighboring atom(s) in a material, in addition, the researches by the soft X-ray absorption spectroscopy are extensively developed with the increase of the number of the target atoms for the researches, because the elements absorbing the soft X-ray include not only the light elements, but also the elements which can cause the L- and M-shells excitation. So far, for solid samples, the soft X-ray absorption spectroscopy has been utilized for the studies of developments for functional materials, the speciation of pollution compounds, the mechanistic analysis of catalytic reactions and vital functions [1]. However, for the soft X-ray absorption experiments for liquid samples, it has really been difficult to design the liquid cell system which is able to measure the absorption spectra under atmospheric pressure. In this paper, we report on a new liquid cell system for the soft X-ray absorption experiments developed at ALS, and show the X-ray absorption near-edge structure (XANES) spectra for aqueous Al salt solutions by the use of the cell system.

APPARATUS

The setup of the developed cell system is depicted in Figure 1. This cell system has been installed in BL6.3.1, and has the vacuum system with two shutters to keep the pressure in the path, ca. 10^{-7} Torr. The window attached the silicon nitride (Si_3N_4) membrane, which has 150 nm in thickness and 1 mm square, is fixed on the end of the pressure path. A liquid sample is trapped between two other Si_3N_4 membrane windows, on which the polystyrene microspheres (ca. 10 μm in diameter) are dropped in advance. The liquid sample trapped is fixed on the sample holder, which is made of stainless steel and designed as the beam is transmitted by the sample liquid and detected by the silicon photodiode under the optimal condition, and then it is put on the sample stage. The end of the pressure path, sample stage, and detector are covered with the acryl case.

EXPERIMENTAL

Aluminum K-edge XANES spectra were collected by a transmission mode using the cell system for aqueous solution samples and by a total electron yield method for powder samples pressed onto the conductive carbon tape. The measured aluminum compounds were aluminum chloride ($AlCl_3$), aluminum nitrate nonahydrate ($Al(NO_3)_3 \cdot 9H_2O$), sodium aluminate, and aluminum ethylenediaminetetraacetate (Al-EDTA) complex. The aqueous solution of Al-EDTA was

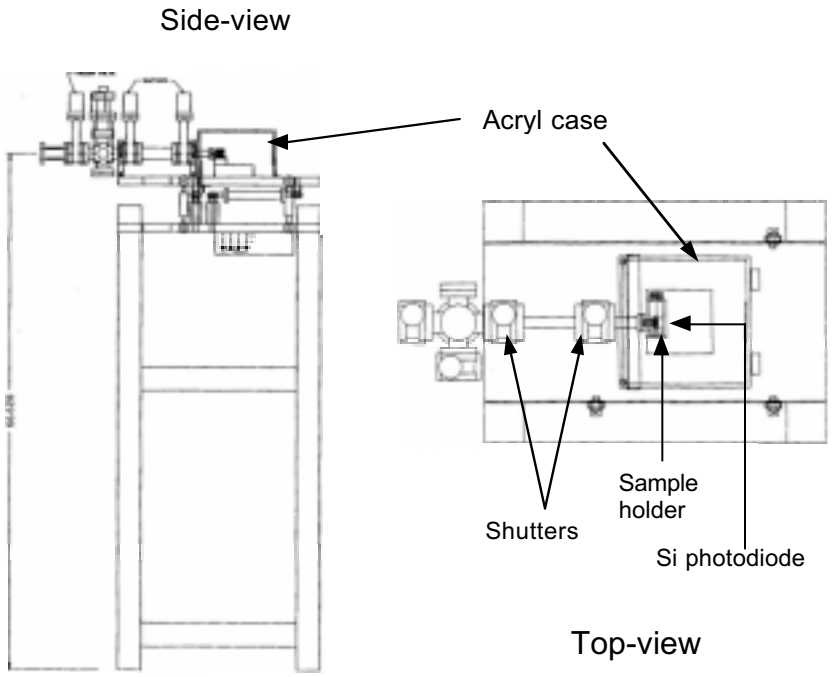

Figure 1. Setup of the XAFS cell system of soft X-ray absorption spectral measurements for solution samples.

prepared by adding 0.5 M $Al(NO_3)_3 \cdot 9H_2O$ aqueous solution (25 ml) to 0.5 M EDTA tripotassium salt aqueous solution (25 ml) and finally adjusted to pH 4.5. The other solution samples were high-concentrated aqueous solutions. Al-EDTA sodium salt dihydrate was purchased from DOJINDO Laboratories. Data were collected from 1550 to 1620 eV at intervals of 0.2 eV with the speed of 0.5 s a point. In the measurements, Helium gas was made to flow and to fill in the acryl case, which was covered with a black cloth.

RESULTS

The Al K-edge XANES spectra for the aqueous solutions of $AlCl_3$, $Al(NO_3)_3 \cdot 9H_2O$, sodium aluminate, and Al-EDTA are shown in Figure 2 with those for their powder samples. In the powder samples, all the peak tops of the XANES spectra appear in almost similar energy position. In the aqueous solution samples, on the other hand, the peak tops of the XANES spectra of $AlCl_3$ and $Al(NO_3)_3 \cdot 9H_2O$ are similar in the position to those in their powder samples, while those of sodium aluminate and Al-EDTA are different from those in their powder samples, and shift to the low energy side. These results indicate that the coordination numbers for $AlCl_3$ and $Al(NO_3)_3 \cdot 9H_2O$ little change between the powder and aqueous solution samples, and those for sodium aluminate and Al-EDTA show a change. In fact, by the NMR study the coordination number of Al-EDTA has

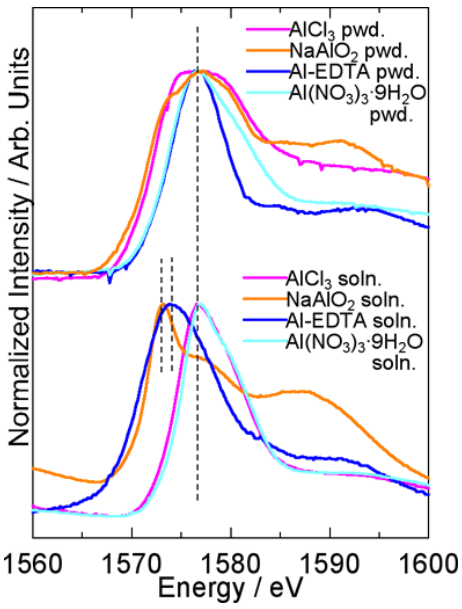

Figure 2. Al K-edge XANES spectra of powders and aqueous solution of various Al compounds.

been proposed to be six in powder and five in aqueous solution [2]. Accordingly, the peak position of the XANES spectra for Al-EDTA can be related with the coordination number. Furthermore, the relation between the peak position and coordination number would be also applied for all aluminum compounds.

CONCLUSION

The new liquid cell system for the soft X-ray absorption experiments developed at ALS enables us to record the spectra characteristic of chemical species in solution. For the XANES spectra of aqueous aluminum salt solutions obtained by the liquid cell system, the change of the peak position was related with the coordination structure, especially coordination number.

REFERENCES

1. H. Wakita, Bunseki (in Japanese) **1**, 24 (2002).
2. T. Yokoyama, Y. Tsuji, T. Kurisaki, and H. Wakita, presented at the IUPAC International Congress on Analytical Sciences 2001, Waseda University, Tokyo, Japan, 2001 (unpublished).

This work was supported by the Advanced Materials Institute, Fukuoka University and by the Director, Office of Energy Research, Office of Basic Energy Sciences, Materials Science Division, of the U.S. Department of Energy under Contract No. DE-AC03-76SF00098.

Principal investigator: Hisanobu Wakita, Advanced Materials Institute and Department of Chemistry, Faculty of Science, Fukuoka University. Email: wakita@fukuoka-u.ac.jp. Telephone: +81-92-801-8883.

Electronic structure of alkali metal-doped M_8Si_{46} (M=Na, K) clathrates

A. Moewes[1], E.Z. Kurmaev[2], J.S. Tse[3], M. Geshi[3], M.J. Ferguson[3], V.A. Trofimova[2], and Y.M. Yarmoshenko[2]

[1]University of Saskatchewan, Dept. of Physics and Engineering Physics, 116 Science Place, Saskatoon, SK S7N 5E2, Canada,

[2]Institute of Metal, Russian Academy of Sciences-Ural Division, 620219 Yekaterinburg, GSP-170, Russia,

[3]Steacie Institute for Molecular Sciences, National Research Council of Canada, Ottawa, Ontario, Canada K1A 0R6

INTRODUCTION

Silicon clathrates are networks of Si cages and can be considered as the Si-analog to fullerenes (C_{60}) with Silicon substituting the Carbon. The Si cages in clathrate structures share faces to satisfy the sp^3 bonding. All Si-atoms in clathrates are tetrahedrally coordinated with the Si-atoms occupying the centers of slightly imperfect tetrahedrons. Their indirect bandgap makes silicon clathrates promising candidates for optoelectronical and thermoelectrical devices. It has been shown recently that semiconductor clathrates also have thermoelectric properties [6] and can form three-dimensional arrays of nano-sized clusters [7]. Although pure silicon and germanium clathrates are predicted to be locally stable, experiments have been able to synthesize the metal-doped clathrate compounds only. The interaction between the metallic impurity atoms inside the clathrate and the semiconductor skeleton modifies the electronic structure of the clathrates. A charge-balanced Zintl-phase model has been suggested for these compounds with the guest (alkali metal or alkaline earth) donating its charge to the host frame. This model was confirmed by band structure calculations of Na_8Si_{46} [8], K_8Ge_{46} [9] and $Na_2Ba_6Si_{46}$ [10]. Recent experiments however, have raised the question whether the guest is close to being neutral in some cases [11-12]. In order to estimate the validity of the rigid band model, we have carried out x-ray emission measurements of crystalline Si (c-Si), K_8Si_{46} and Na_8Si_{46} and compare these to our calculations.

DISCUSSION OF CALCULATIONS AND MEASUREMENTS

The densities of (occupied electronic) states (DOS) of Si_{46}, Na_8Si_{46} and K_8Si_{46} obtained from FLAPW calculations are shown in Fig. 1. The main features of total and partial density of states (DOS) are very similar for all three compounds. Differences occur mainly in the degree of filling of the energy bands by valence electrons and the energy position with respect to the Fermi level. For Si_{46} the valence band is completely filled and the conduction band is empty giving rise to its insulating or intrinsic semiconducting behavior. In the cases of Na_8Si_{46} and K_8Si_{46} the additional sodium and potassium electrons fill the next energy band and the Fermi level is overlapping the conduction band providing the metallic properties of this doped clathrate. Similar behavior has been observed in calculated band structures of Ge_{46} and K_8Ge_{46} and Na_8Si_{46} and Ba_8Si_{46}. The conduction-band density of states does not show strong modifications upon the inclusion of metal atoms. This is due to weak hybridization between the Si_{46} conduction-band states and Na and K states and indicates that metal-metal and metal-Si interactions are ionic and that Na and K act as electron donors. Therefore alkali metal doping introduces a narrow band labeled as *D* in Fig. 1. This band - directly below the Fermi level - is separated by an energy gap of several eV from the main density of electronic states (features A, B and C) and should give rise to a spectroscopically observable feature. Its origin is in the lowest conduction band in the undoped Si_{46} clathrate. Our calculations also indicate that a significant charge transfer from Na or K to the Si skeleton is

taking place and the rigid band model is a valid model for describing the electronic structure of these clathrates. We define the rigid band as a rigid shift of the Fermi level from the pristine Si_{46} to Na_8Si_{46} when filling empty bands with electrons from the Na atom.

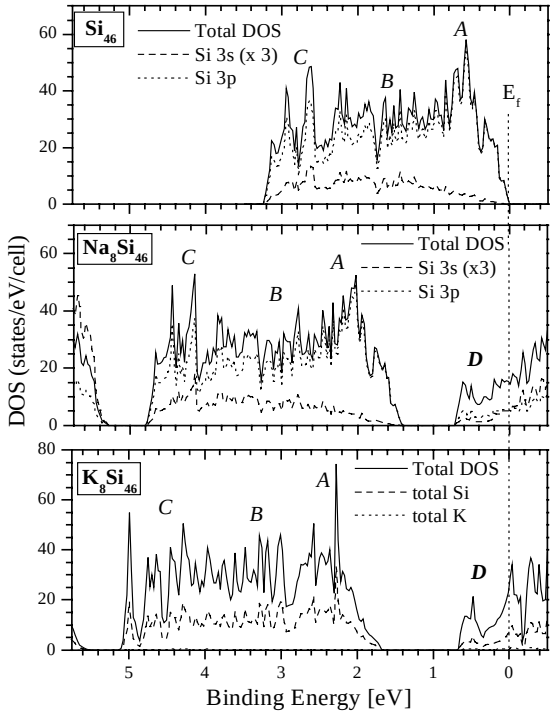

Figure 1. Total and partial density of states (DOS) for Si_{46} and clathrates Na_8Si_{46} and K_8Si_{46}.

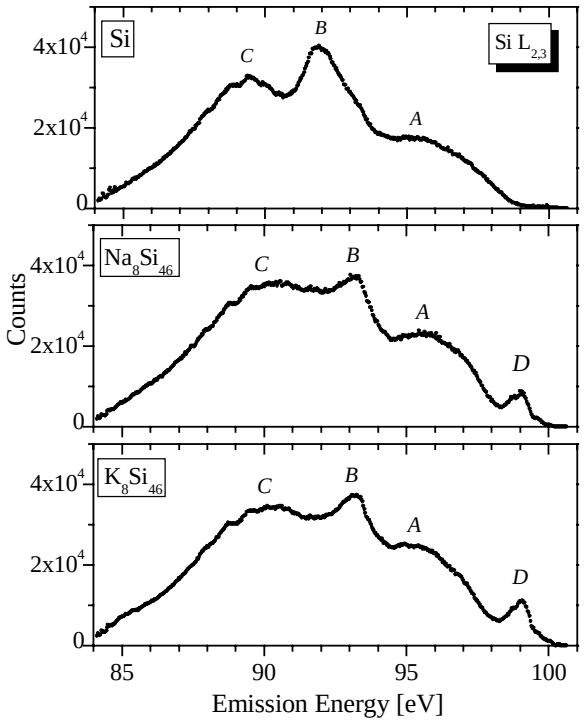

Figure 2. Si $L_{2,3}$ XES of c-Si, Na_8Si_{46} and K_8Si_{46}.

Fig. 2 displays the Si $L_{2,3}$ emission spectra of crystalline silicon (c-Si) and Si-clathrates (Na_8Si_{46} and K_8Si_{46}) as solid dots. Three main features labeled *A*, *B* and *C* are observed in both, crystalline Si and clathrates and are due to transitions from *s, d* and *sd*-like bands, respectively. The feature *D* discussed above has its spectroscopic counterpart in the additional feature that is present at 99 eV and labeled *D*. Feature D is present only in the spectra clathrates. It results from transitions of the lowest conduction band, introduced due to charge-transfer from the metal atoms and it corresponds to feature *D* in Fig. 1. The spectroscopic presence of this band demonstrates good agreement between experiment and density of state calculations and that the rigid band model is a good description for these materials.

This work was supported by Natural Sciences and Engineering Research Council (NSERC), the Russian Foundation for Basic Research (Projects 00-15-96575) and the NATO Collaborative Linkage Grant.

Principal investigator: Alexander Moewes, University of Saskatchewan, Dept. of Physics and Engineering Physics. Email: moewes@usask.ca. Telephone: 306-966-6431.

Electronic structure of CMR compounds investigated by means of XES

K. Küpper[1], B. Schneider[1], S. G. Chiuzbaian[1], M. Matteucci[2] and D. D. Sarma[3]

[1]University of Osnabrück, Department of Physics, Barbarastr. 7, D-49069 Osnabrück, Germany
[2]Institute of Condensed Matter, National Research Council c/o Sincrotone Trieste, Padriciano 99, 1-34012 Trieste, Italy
[3]Solid State and Structural Chemistry Unit, Indian Institute of Science, Bangalore 560012, India

INTRODUCTION

In the last few years the manganese perovskites $La_{1-x}A_xMn_{1-y}TM_yO_3$ (A = Ca, Ba, Sr, TM = Co, Ni, Fe) have been subject to intense experimental and theoretical studies due to the colossal magnetoresistance effect (CMR) [1, 2, 3]. The mother compound $LaMnO_3$ is an A-type antiferromagnetic insulator with orthorhombic crystal structure. We present results of Resonant X-ray emission spectroscopy (RXES) of $LaMnO_3$ performed at at Beamline 8.0.1 equipped with SXF endstation.

Recently the CMR effect in a double perovskite system, Sr_2FeMoO_6, has been discovered [4]. This material shows a strong effect at low magnetic fields and a high ferromagnetic transition temperature ($T_c \approx 420$K) and a half metallic behaviour as predicted on the basis of band structure calculations. In contrast Sr_2FeWO_6 is an antiferromagnetic insulator [5]. Because of the different transport properties of these two materials, it is predicted that an alloy $Sr_2FeMo_xW_{1-x}O_6$ will show a metal-insulator transition (MIT) as a function of x. While in an earlier work the critical concentration was reported to be between $0.4 < x_c < 0.5$ [6], Ray *et. al.* found $x_c \approx 0.25$ [7]. The aim of this work is to investigate the influence of the predicted MIT to the partial density if states. Therefore we recorded RXES data at the L edge of Fe, the M edge of Mo, and the K edge of O of Sr_2FeMoO_6 and $Sr_2FeMo_xW_{1-x}O_6$, respectively.

RESULTS AND DISCUSSION

Sr_2FeMoO_6 and $Sr_2FeMo_{0.6}W_{0.4}O_6$

Figure 1 shows the Fe L-emission spectra taken at indicated excitation energies, for both samples.

We recognise that these spectra for both materials look very similar. One can investigate additionally to the NXES-peak a rather weak elastic peak. At $E_{exc} \approx 720$ eV

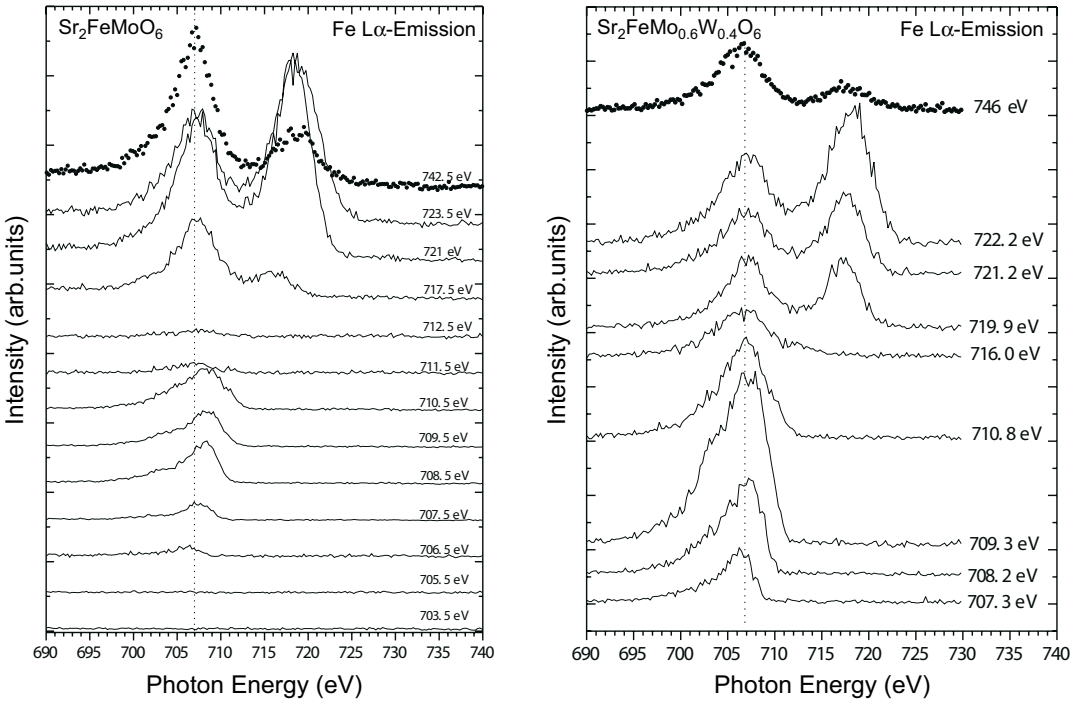

Figure 1: Fe Lα emission spectra of Sr_2FeMoO_6 and $Sr_2FeMo_{0.6}W_{0.4}O_6$

a strong resonance for both samples can be observed. At E_{exc} = 738 eV one observes an emission from the 3d level not only into the $2p_{3/2}$ level but also into the $2p_{1/2}$ level. The intensity ratio of both components is slightly below the expected value of 2. This indicates the presence of Coster-Kronig-transitions. The O Kα-emission spectra (not shown here) show for both materials only a weak energy dependence. The main emission features can be observed at 525.5 eV for both samples. This results are in good agreement with the relusts of Ray *et. al.* [7], the measurements of Fe L-emission of $Sr_2FeMo_{0.6}W_{0.4}O_6$ show no significant difference compared to the recorded spectra of Sr_2FeMoO_6, thus $Sr_2FeMo_{0.6}W_{0.4}O_6$ shows halfmetallic behaviour, although doped with 40 % tungsten on Mo lattice site.

$LaMnO_3$

In figure 2 we present Mn L-emission spectra of $LaMnO_3$. The Mn $L_{2,3}$ emission features are strongly dependent on the excitation energy. At E_{exc} = 642.7 eV a maximum in intensity of three emission peaks around 640 eV is observed. With increasing excitation energy, the intensity of the L_2 emission peaks drops to almost zero when the L_3 emission peak reaches a maximum of intensity around 650 eV. At higher excitation energy the normal x-ray emission takes place. These results are in in further evaluation in order to prepare further measurements on $La_{1-x}A_xMn_{1-y}TM_yO_3$ (A = Ca, Ba, Sr, TM = Co, Ni, Fe)-compounds. These measurements are necessary for a deeper understanding of hybridization in presence of different dopants in different concentrations.

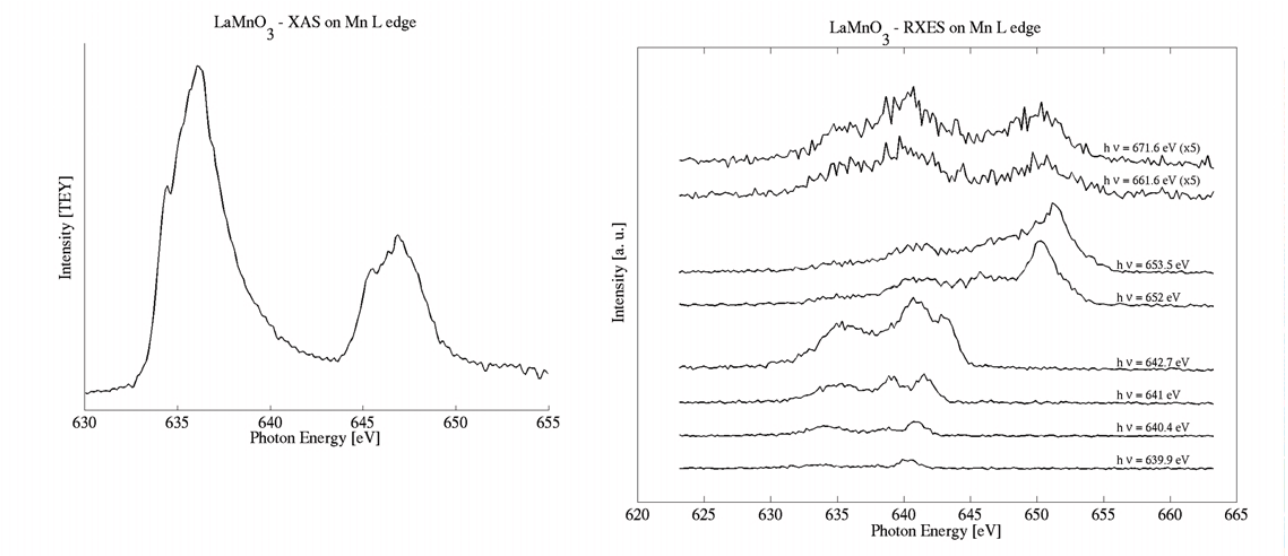

Figure 2: Mn L absorption and emission spectra of $LaMnO_3$

References

[1] A. Millis, Nature, 1998, **392**, 147

[2] M. B. Salamon and M. Jaime, Rev. Mod. Phys., 2001, **73**, 583

[3] I. O. Troyanchuk, M. V. Bushynski, N. V. Pushkarev, H. Szymczak, and K. Bärner, J. Mag. mag. Mat., 2001, **225**, 331

[4] K.-I. Kobayashi, T. Kimura, H. Sawada, K. Tekura, and Y. Tokura, Nature, 1998, **395**, 677

[5] H. Kawanaka, I. Hase, S. Toyama, and Y. Nishihara, Physica B, 2000, **281+282**, 518

[6] T. Nakagawa, K. Yoshikawa, and S. Nomura, J. Phys. Japan, 1969, **27**, 880

[7] S. Ray, A. Kumar, S. Majumdar, E. V. Sampathkumaran, and D. D. Sarma, J. Phys. Cond. Mat., 2001, **13**, 607

This work was partly supported by BMBF (project 05SF8MPA/0)

Principal investigator: apl. Prof. Dr. M. Neumann, University of Osnabrück, Barbarastr. 7, D-49069 Osnabrück, Germany, Email: mneumann@uos.de, Telephone: +49541 969 2668

Electronic Structure of Divalent Hexaborides

J. D. Denlinger[1], G.-H. Gweon[2], J. W. Allen[2] and Z. Fisk[3]
[1]Advanced Light Source, Lawrence Berkeley National Lab, Berkeley, California 94720, USA
[2]Department of Physics, University of Michigan, Ann Arbor, Michigan 48109, USA
[5]NHMFL, Florida State University, Tallahassee, Florida 32306, USA

INTRODUCTION

Great interest in the divalent hexaborides has been generated recently by the discovery of high Curie temperature weak-moment ferromagnetism (FM) in La-doped CaB_6 [1] and by exotic theoretical models to explain the unusual magnetism, *e.g.* that it represents the ground state of a dilute electron gas [2] or of a doped excitonic insulator [3]. The starting point of most thinking about the divalent hexaborides, and central to the excitonic instability model, is the presumed existence of a band overlap between the top of the boron valence states and the bottom of the cation *d*-conduction band at the X-point of the simple cubic Brillouin zone appropriate to these materials. Without such overlap stoichiometric divalent hexaborides would be insulators. Band overlap is predicted by band structure calculations [4] and magneto-oscillatory studies [5] have been interpreted in this semi-metal framework. However, a new quasiparticle band calculation that includes a GW self-energy correction predicts CaB_6 to have an X-point bandgap of 0.8 eV [6].

Our early angle-resolved photoemission spectroscopy (ARPES) studies at the SRC synchrotron of EuB_6 and SrB_6 showed, contrary to the band-overlap picture, an isolated X-point electron pocket separated from the X-point boron valence band maximum by a gap >1 eV. Motivated by the prior theoretical and experimental evidence for bulk band overlap and by certain surface sensitive aspects of the data, we interpreted the observed gap as a property only of the surface region probed in ARPES. The new quasiparticle band calculation provides a theoretical basis for interpreting the X-point bandgap as a bulk property of divalent hexaborides. Reported here are new ARPES measurements of CaB_6 and EuB_6 [7], that provide a more detailed view of the k-dependent electronic structure and variations of the surface chemical potential with cation and time.

EXPERIMENT

Single crystal samples of CaB_6 and EuB_6, grown from an aluminum flux using powders prepared by boro-thermally reducing cation oxides, were cleaved in ultra-high vacuum ($<4\times10^{-11}$ torr) at ≈30K exposing the [001] surface for ARPES measurements at ALS Beamline 10.0.1. The ability to rotate the HERS spectrometer relative to the incident beam polarization allowed for measurement in two different symmetry selection geometries, *i.e.* p- and s-polarization. A total instrumental resolution of ≈40 meV and full angular acceptance of ≈0.2° was employed.

RESULTS

Figures 1(a,b) show the experimentally measured band structure for CaB_6 along Γ-X for the two different p- and s-polarization geometries. The data exhibit strong initial state symmetry selection rule effects. Fig. 1(c) shows a sum of the two polarization data sets with comparison to the GW calculated band structure [6]. Identification of all the calculated bands in the summed data, but not for the individual polarizations, highlights the utility and importance of having this rotational capability of the HERS detector. The bands selected by the s-polarization geometry correspond to the theory bands labeled 2 and 5, both of which have the same symmetry label of Δ_5.

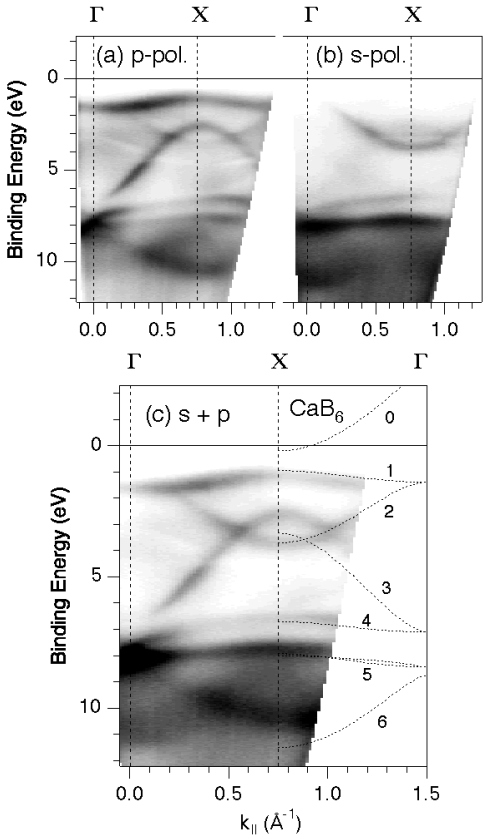

Fig. 1. Comparison of the experimental and theoretical band structures of CaB_6 along Γ-X. The reverse gray scale image of angle-resolved photoelectron intensities is the sum of two data sets with 30 eV s- and p-polarized excitation. Dashed lines are from the quasiparticle GW calculation [6] shifted by 0.45 eV to lower energy.

The qualitative agreement between experiment and theory dispersions in Fig. 1(c), most importantly including the existence of a band gap near E_F, is very striking. The theory bands have been rigidly shifted by 0.45 eV to lower energy for better visual alignment to the experimental data. Quantitative discrepancies, however, are also quite visible, including: *(i)* the size of the band gap near E_F, *(ii)* the overlap between bands 2 and 3, *(iii)* the overall boron-block bandwidth (between bands 1 and 6), and *(iv)* an additional weak broad dispersion at the bottom of the valence band.

This latter counter-dispersing band, 11 eV at Γ to ≈9 eV at X is suggestive of band back-folding resulting from a periodicity doubling. Indeed, low energy electron diffraction (LEED) images of freshly cleaved CaB_6 surfaces exhibit 2×1 surface order. The absence of conduction band intensity (band 0) at E_F for CaB_6 in Fig. 1 implies a >1 eV band gap and insulating behavior. While this result agrees with electron counting for stoichiometric material, it does not agree with bulk Hall transport measurements of electron carriers and dHvA measurement of Fermi surfaces. Also, as noted, earlier ARPES measurements of EuB_6 and SrB_6 both showed X-point electron pockets and ellipsoidal Fermi surface contours, contrary to this CaB_6 data set.

To address these different results for different cations, we present in Fig. 2 ARPES measurements along Γ-X for EuB_6 for the p-polarization geometry. Similar to the CaB_6 data in Fig. 2(a), the Δ_5 symmetry bands (2 and 5) are absent and no states near E_F are observed (see top panels of Fig. 2). However, this surface exhibited a very interesting time dependent behavior, illustrated by Fig. 2(b,c), in which the emergence of a small electron pocket at the X-point (corresponding to band 0 in Fig.1) is observed at ≈4 hours after cleavage of the sample. Accompanying this change at E_F, some additional redistribution of spectral weight in the boron block bands also occurs (illustrated by a comparison of X-point spectra in Fig. 2(c)). In addition, while the surface order before and after the spectral changes in this sample is not known, another important difference between EuB_6 and CaB_6 is the observation of 1×1 versus 2×1 LEED, respectively, performed after the ARPES experiments.

While the mechanism for this temporal change is not yet understood, it is important to note that the existence of the >1 eV X-point gap between bands 0 and 1 does *not* change — only the position of the chemical potential varies. Presumably band bending near the surface either relaxes an insulating surface layer or creates a metallic surface two-dimensional electron gas. The former is implied by bulk transport and dHvA measurements which show n-type carriers and the existence

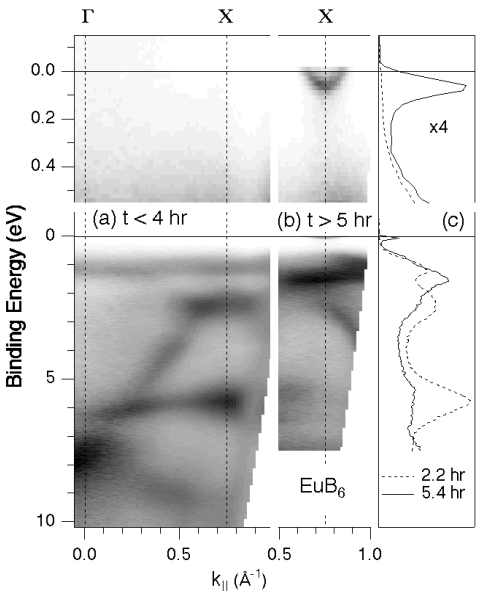

Fig. 2. Time dependent change in the band structure of EuB_6. (a) <4 hours and(b) >5 hours after the initial cleave. The reverse gray scale images are measured with p-polarized 30 eV excitation. (c) Comparison of X-point spectra. Upper panels show an expanded region near E_F.

of small elliptical Fermi surface pockets for the bulk electronic structure. The ability to simultaneously measure the complete band dispersions at the X-point using the angular mode of the Scienta analyzers was crucial to the discovery and monitoring of such time-dependent changes. Complementary bulk-sensitive soft x-ray absorption and emission measurements at the boron K-edge performed at ALS Beamline 8.0 [8] also provide an (angle-integrated) confirmation of the existence of a bulk band gap consistent with the ARPES data.

In summary, the existence of a semiconducting bandgap (rather than a semimetallic band overlap) is observed in the divalent hexaborides, thereby ruling out the excitonic insulator model for the novel FM in La-doped CaB_6. The location of the chemical potential at the bottom of conduction band indicates non-stoichiometric defects contributing excess electrons. The likely defects are boron vacancies, recently shown to carry magnet moments [9], and may be relevant to the novel ferromagnetism discovered in doped and undoped divalent hexaborides .

REFERENCES

1. D. P. Young *et al*, Nature **397**, 412 (1999).
2. D. Ceperley, Nature **397**, 386 (1999); G. Ortiz, M. Harris and P. Ballone, Phys. Rev. Lett. **82**, 5317 (1999).
3. M. E. Zhitomirsky, T. M. Rice, and V. I. Anisimov, Nature **402**, 251(1999); L. Balents and C. M. Varma, Phys. Rev. Lett. **84**, 1264 (2000); V. Barzykin and L. P. Gor'kov, Phys. Rev. Lett. **84**, 2207 (2000).
4. A. Hasegawa and A. Yanase, J. Phys. C, Solid State Phys. **12**, 5431 (1979); S. Massidda, A. Continenza, T. M. D. Pascale, and R. Monnier, Z. Phys. B **102**, 83 (1997).
5. R. G. Goodrich *et al*., Phys. Rev. B **58**, 14896 (1998); M. C. Aronson *et al*., Phys. Rev. B **59**, 4720 (1999).
6. H. J. Tromp *et al*., Phys. Rev. Lett. **87**, 016401 (2001).
7. J. D. Denlinger *et al*., cond-mat/0107429.
8. J. D. Denlinger, G.-H. Gweon, J. W. Allen, A. D. Bianchi and Z. Fisk, cond-mat/0107426; Surface Review and Letters, in press; and ALS Compendium, 2001.
9. R. Monnier and B. Delley, Phys. Rev. Lett. **87**, 157204 (2001).

This work was supported at U. of Michigan by the U.S. Dept. of Energy (DoE) under contract No. DE-FG02-90ER45416 and by the U.S. NSF under grant No. DMR-99-71611.

Principal investigator: Jonathan Denlinger, Advanced Light Source, LBNL. Email: JDDenlinger@lbl.gov. Telephone: 510-486-5648.

Electronic structure of graphite fluorides

E.Z. Kurmaev[1], A. Moewes[2], D.L. Ederer[3], H. Ishii[4], K. Seki[4], M. Yanagihara[5], F.Okino[6], and H. Touhara[6]

[1]Institute of Metal Physics, Russian Academy of Sciences-Ural Division, 620219 Yekaterinburg GSP-170, Russia
[2] Department of Physics and Engineering Physics, University of Saskatchewan, 116 Science Place, Saskatoon, Saskatchewan S7N 5E2, Canada
[3]Department of Physics, Tulane University, New Orleans, LA 70118, USA
[4]Research Center for Materials Science and Department of Chemistry, Graduate School of Science, Nagoya University, Furocho, Chikusa-ku, Nagoya 464-8602, Japan
[5]Research Institute for Scientific Measurements, Tohoku University, Sendai 980-77, Japan
[6]Department of Chemistry, Faculty of Textile Science and Technology, Shinshu University, Ueda 386-8567, Japan

Fluorination of graphite leads to the formation of polycarbon monofluoride $(CF)_n$ and polydicarbon monofluoride $(C_2F)_n$. These compounds are exceptional lubricants under high temperature and high vacuum and quite successful cathodic depolarizers in a high-energy density battery. It is supposed that their structure is layered and altered from graphite by inserting covalently bonded fluorine atoms above and below every hexagon in each layer. According to Ref. 1 the structure of graphite fluorides is an infinite array of *trans*-linked cyclohexane chairs. It also has been suggested that it might be an infinite array of *cis-trans*-linked cyclohexane boats [2]. First principle calculations of the stability of these two configurations have shown that the energetic difference between these two structures is 0.0725 eV/atom in favour of the chair conformation, which is considered now the optimal structure for graphite fluorides [3]. Based on these recently performed *ab-initio* band structure calculations for $(CF)_n$ it has been concluded that carbon atoms have completely lost their aromatic nature [3]. In order to experimentally verify these conclusions regarding the chemical bonding, we have measured carbon and graphite X-ray emission spectra (XES) of $(CF)_n$ and $(C_2F)_n$.

The measurements were performed at Beamline 8.0 using the soft X-ray fluorescence endstation [4]. The samples were excited non-resonantly at 310 eV and 720 eV. Fig. 1 a shows X-ray fluorescence measurements of $(CF)_n$ and $(C_2F)_n$ [5]. Carbon Kα XES of $(CF)_n$ and $(C_2F)_n$ display features labelled *1-5* that are more similar to those of diamond where carbon atom has sp^3 bonding configuration than to graphite (configuration sp^2). Our findings confirm that in $(CF)_n$ and $(C_2F)_n$ all carbon atoms are of sp^3 type and covalently bonding to fluorine. This is in good agreement with results of nuclear magnetic measurements [6] according to which a resonance line is observed in the ^{13}C NMR spectrum of graphite fluoride and attributed to the sp^3 carbon atoms. Fig. 1 b presents fluorine Kα emission measurements of $(CF)_n$ and $(C_2F)_n$. A chemical shift in the F Kα emission spectra of about 0.7 eV takes place with respect to the spectrum of the ionic compound LiF. On the other hand, an increase in line width is observed for F Kα XES of $(CF)_n$ (~3.1 eV) and $(C_2F)_n$ (~3.6 eV) with respect to that of LiF (~2.8 eV). Both effects could be due to an increase in covalency in the chemical bonding. The fluorine spectra therefore also show that fluorine atoms are covalently bonding to carbon atoms.

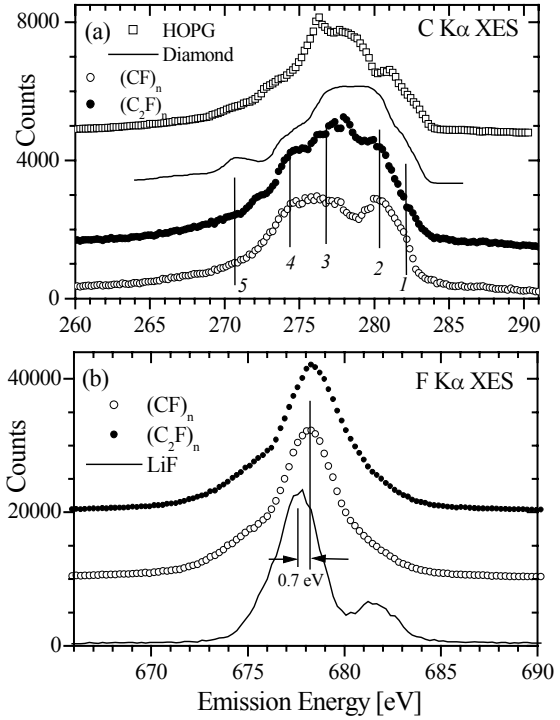

Fig. 1 Carbon (a) and fluorine (b) XES of $(CF)_n$, $(C_2F)_n$ and reference compounds.

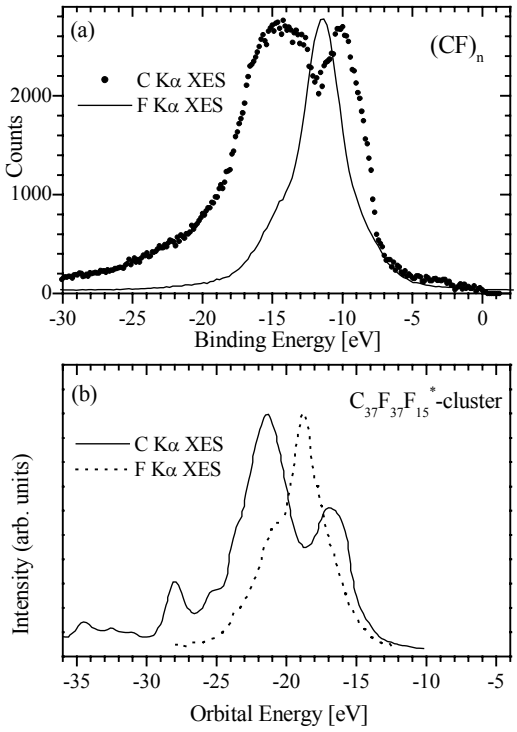

Fig. 2 (a) Experimental carbon and fluorine Kα XES of $(CF)_n$. (b) Theoretical C and F Kα XES of $C_{37}F_{37}F^*_{15}$ cluster.

Fig. 2 shows carbon and fluorine spectra of $(CF)_n$ in the binding energy scale. The emission energies are converted to binding energies using XPS C 1s and F 1s measurements of $(CF)_n$ [$E_{b.e.}$ (C 1s) = 290.4 eV and $E_{b.e.}$ (F 1s) = 689.6 eV. These emission spectra are caused by $2p \rightarrow 1s$ dipole transitions and therefore give a possibility to study the occupied carbon and fluorine 2p-states. Both spectra show a negligible intensity in the vicinity of the Fermi level, which is in agreement with electrical measurements of $(CF)_n$ according to which this material is an insulator. The intensity maximum of fluorine Kα XES occupy some intermediate position between two main peaks of carbon Kα XES of $(CF)_n$. According to the band structure calculations [3], F 2p-states are located at the bottom of the valence band: the F σ band is separated from the bottom of the C σ band by a gap of 8.4 eV at Γ and the F π-bands span a 6.8 eV range below the Fermi level interacting with lower π and upper σ carbon bands. The experiment shows (see Fig. 2) that F 2p-states are located at the middle of the valence band pushing up and down the carbon 2p-subbands. Our findings are more close to results of semi-empirical MO LCAO calculation of electronic structure of $(CF)_n$ [7]. According to these MO LCAO calculations, carbon 2p-states form two subbands originating from σ(C-C), τ*(C-F) and σ(C-C), τ(C-F) orbitals, respectively, divided by ~4.7 eV (Fig. 2b). Fluorine 2p-states are formed by the F 2p lone pair and occupy energy range between carbon 2p-subbands (Fig. 2b). The tails of fluorine 2p-states overlap with carbon 2p-states forming τ*(C-F) and τ(C-F) bonds. This MO LCAO structure is in an agreement with carbon and fluorine Kα XES (see Fig. 2a). The splitting of C Kα XES of $(CF)_n$ is found to be about 4.6 eV and F Kα XES is located exactly in minimum between two peaks of carbon spectrum.

To conclude, we have studied X-ray emission spectra of constituents of $(CF)_n$ and $(C_2F)_n$. We found that carbon atoms are of the sp^3 type and covalently bound to fluorine. Our measurements show that results of band structure calculations based on chair-type structure of $(CF)_n$ are not confirmed. Therefore the crystal structure of graphite fluorides is still not solved and must be refined.

REFERENCES

1. W. Rudorff and G. Rudorff, Z. Anorg. Allg. Chem. 253 (1947) 281.
2. L.B. Ebert, J.I. Brauman, and R.A. Huggins, J. Am. Chem. Soc. 96 (1974) 7841.
3. J.-C. Charlier, X. Gonze and J.-P. Michenaud, Phys. Rev. B 47 (1993) 16162.
4. J.J. Jia, T.A. Callcott, J. Yurkas, A. W.Ellis, F.J. Himpsel , M.G. Samant, J. Stöhr, D.L. Ederer, J.A. Carlisle, E.A. Hudson, L.J. Terminello, D.K. Shuh, and R.C.C. Perera, Rev. Sci. Instrum. 66 (1995) 1394.
5. E.Z. Kurmaev, A. Moewes, D.L. Ederer, H. Ishii, Seki, M. Yanagihara, F.Okino and H. Touhara, Phys. Lett. A 288 (2001) 340.
6. C.A. Wilkie, G.Y. Lin, D.T. Haworth, J. Solid State Chem. 30 (1979) 197.
7. L.G. Bulusheva, A.V. Okotrub, V.N. Mit'kin, V.V. Murakhtanov, L.N. Mazalov, Zh. Struct. Khim. 36 (1995) 630; L.G. Bulusheva and A.V. Okotrub, Rev. Inorg. Chem., 19 (1999) 79.

The Russian Foundation for Basic Research (Project 00-15-96575) and NATO Collaborative Linkage Grant supported this work. Funding by the Natural Sciences and Engineering Research Council (NSERC) is gratefully acknowledged. The Deutsche Forschungsgemeinschaft (Schwerpunktprogramm 1073) funded the work in Augsburg. The Advanced Light Source at Lawrence Berkeley National Laboratory is supported by U.S. Department of Energy (Contract No. DE-AC03-76SF00098).

Principal investigator: Ernst Kurmaev, Institute of Metal Physics, Russian Academy of Sciences-Ural Division, 620219 Yekaterinburg GSP-170, Russia. Email: kurmaev@ifmlrs.uran.ru. Telephone: +7-3432-744183.

Fermi Surface Topology, Bilayer Splitting, and (π,0) dispersion kinks in Bi2212

A. D. Gromko[1],Y.-D. Chuang[1,2], A. V. Fedorov[1,2], J. D. Koralek[1], Y. Aiura[3], Y. Yamaguchi[3], K. Oka[3], Yoichi Ando[4], D. S. Dessau[1]

[1]Department of Physics, University of Colorado, Boulder, CO 80309-0390, USA
[2]Advanced Light Source, Lawrence Berkeley National Lab, Berkeley, CA 94720, USA
[3]National Institute of Advanced Industrial Science and Technology (AIST), AIST Tsukuba Central 2, 1-1-1 Umezono, Tsukuba, Ibaraki 305-8568, JAPAN
[4]Central Research Institute of Electric Power Industry (CRIEPI), 2-11-1 Iwato Kita, Komae, Tokyo 201-8511, JAPAN

INTRODUCTION

There have been many key developments in our understanding of the E vs. **k** band dispersion in $Bi_2Sr_2CaCu_2O_{8+\delta}$ (Bi2212) recently, both in the normal and superconducting states. Earlier work of ours [1] was the first to break tradition and indicate that the Fermi Surface (FS) of Bi2212 was not simply a single hole-like pocket centered around the (π,π) points of the Brillouin zone. In particular, we found that a more electron-like portion of the FS was observable at certain photon energies such as 33 eV, in contrast to the standard hole-like FS, which is observed at photon energies near 20 eV. Papers [2] and [3] dealt with this issue and principally contained data from the ALS. The concept of an electron-like FS portion in Bi2212 was supported by additional measurements made by the Stanford group [4]. This Fermi surface topology issue has evolved into the finding of bilayer split bands in the Bi2212 family [6,7]. This discovery explains the observance of two different FS topologies, and has allowed us to unearth new self-energy effects in the E vs. **k** band dispersion near the critical (π,0) point of the Brillouin zone [8,9].

EXPERIMENT

Experiments were carried out at beamline 10.0.1.1 of the Advanced Light Source, and at beamline 5-4 of the Stanford Synchrotron Radiation Laboratory using Scienta SES 200 electron spectrometers. Experiments were conducted at photon energies of 20, 22, 33, and 47eV. The measurements requiring the highest resolution were carried out with a combined experimental energy resolution of 12meV, and a momentum resolution better than $0.01\pi/a$ (where a is the CuO_2 plane lattice constant) along the entrance slit to the spectrometer. Experiments were carried out with the in-plane component of the photon polarization along the (0,0)-(π,0) direction.

RESULTS AND DISCUSSION

The bilayer splitting effect in Bi2212 is expected to occur due to the intracell c-axis coupling between the two CuO_2 layers per unit cell. However, this had not been previously observed, with most experiments indicating that the coupling was zero [5], a possibility consistent with exotic theories of superconductivity such as those favoring the low-dimensional state necessary for spin-charge separation. Simultaneous to the Stanford group's report [6], we made the first measurements of bilayer splitting in a high temperature superconductor, using overdoped Bi2212 samples [7]. We found the splitting to have a maximum value of approximately 100 meV, to be maximal at the (π,0) point of the Brillouin zone, and to be zero

along the (π,π) nodal direction. The large value of this splitting relative to other parameters such as the value of the superconducting gap, pseudogap, and some of the magnetic energy scales means that this intracell coupling is strong and should be included in any proper description of the electronic structure. This also should be necessary information for understanding why the T_c of the cuprates depends so strongly upon the number of layers per unit cell. Data showing this splitting is contained in figure 1.

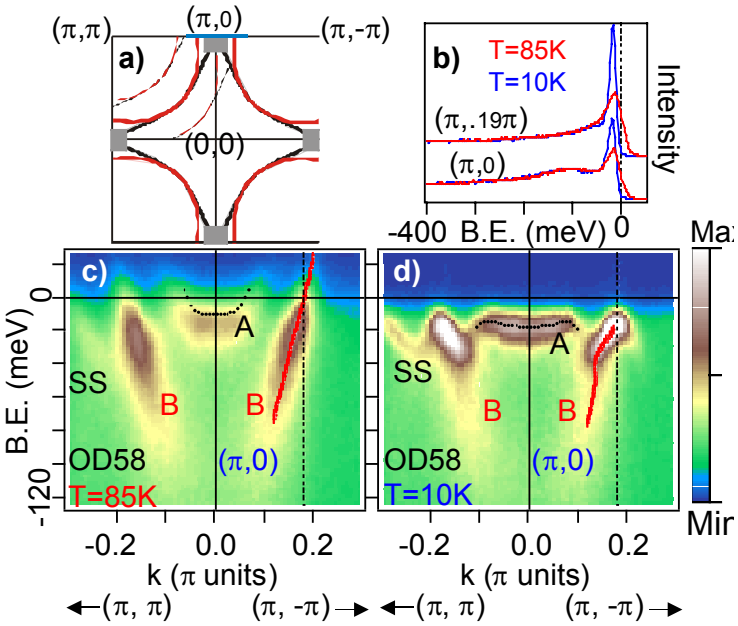

Figure 1. ARPES data in the normal (c) and superconducting state (d) of a T_c=58K overdoped Bi2212 sample, from ref [9]. A and B indicate the antibonding and bonding bands, respectively. The k-space location is along the blue line of panel (a). Panel (b) shows EDCs at two k-space locations.

A later paper of ours made the first extension of the bilayer splitting measurements to optimal and underdoped samples [8]. In these samples, the intrinsic peak broadening is greatly increased, and it is more difficult to separate the contributions of the separate bilayer split bands. By choosing optimal photon energy and polarization conditions we were able to selectively enhance one of the bilayer split bands relative to the other and make an accurate deconvolution. While the decreased c-axis conductivity in underdoped samples led us to expect that the bilayer splitting would be reduced in these samples as well, we found the surprising result that the bilayer splitting energetics are essentially identical for all doping levels [8]. This implies that other effects such as the scattering rate or the opening of the pseudogap must be more relevant to the change in the c-axis conductivity.

The ability to accurately deconvolve the bilayer splitting opened up many more opportunities for research in the critical (π,0) region of the Brillouin zone, where the bilayer splitting is the largest, as well as where the superconducting gap, pseudogap, van-Hove singularity, etc. are all maximal. Earlier measurements had been unknowingly looking at a superposition of the two bands in this region, with misinterpretations arising because of this. For example, there was the very famous peak-dip-hump lineshape at (π,0) observed by many groups in the superconducting state of Bi2212, but not in the normal state. This had been discussed as various types of self-energy effects, including $\alpha^2F(\omega)$ oscillations, coupling to magnetic modes, shake-off effects, etc. Our new data indicates that it is simply an effect of the bilayer splitting [9]. It is present in both the normal and superconducting states (figure 1b), but it was only previously visible in the superconducting state because the broad features present in the normal state pushed the signal below the background.

Even more importantly, the ability to accurately deconvolve the bilayer split bands has allowed us to make the first measurements of a dispersion "kink" near the (π,0) portion of the

Brillouin zone (figure 1d). This result follows up on the pioneering kink studies of cuprates done by the Stanford [10] and other [11,12] groups, except that these previous results were predominantly limited to the nodal region, where the pairing correlations are weakest. We have measured the temperature and momentum dependence of the new $(\pi,0)$ kink on over and optimally doped samples. We find that the kink strength (but not its energy scale) is a strong function of these parameters. In particular, the kink appears just below T_c, existing only in the superconducting state, while the nodal kink is present both above and below T_c. Also, the kink is localized in a small k-space region near $(\pi,0)$, with a momentum dependence that closely matches that of the famous "41 meV" magnetic resonance mode observed in inelastic neutron scattering measurements [13]. We argue that these factors point to a likely connection between the $(\pi,0)$ kink and the magnetic resonance mode, although more work needs to be done to understand the energy scales. If this picture holds together, the kink should be due to electronic coupling to the magnetic resonance and there will be a strong possibility that the pairing of electrons is mediated by this magnetic mode. This should be a very active and important area for future study.

ACKNOWLEDGEMENTS

We acknowledge sample preparation help from M. Varney, beamline support from X.J. Zhou, P. Bogdanov, Z. Hussain and D.H. Liu, and helpful discussions with G. Aeppli, A. Chubukov, C. Kendziora, A. Millis, P. Lee, D. Pines, D. Scalapino, J. Schmallian, Z-X. Shen, and S.C. Zhang. We gratefully acknowledge the help of R. Goldfarb at NIST for the use of the SQUID magnetometer.

REFERENCES

1. Y.-D. Chuang, A. D. Gromko, D. S. Dessau, Y. Aiura, Y. Yamaguchi, K. Oka , A. J. Arko, J. Joyce, H. Eisaki, S.I. Uchida, K. Nakamura, Yoichi Ando, Phys. Rev. Lett. **83** 3717, 1999.
2. A. D. Gromko, Y. -D. Chuang, D. S. Dessau, Y. Aiura, K. Oka, K. Nakamura, Yoichi Ando, cond-mat/0003017.
3. Y.-D. Chuang, A. D. Gromko, D. S. Dessau, K. Nakamura, Yoichi Ando, Physica C **341-348**, 2079 (2000).
4. D.L. Feng et al., cond-mat/9908056; P. Bogdanov et al, cond-mat/0005394.
5. H. Ding et al., Phys. Rev. Lett. **76**, 1533 (1996).
6. D.L. Feng, et al., Phys. Rev. Lett. **86**, 5550 (2001).
7. Y.-D. Chuang, A. D. Gromko, A.Fedorov, Y. Aiura, K. Oka, Yoichi Ando, H. Eisaki, S.I. Uchida, D. S. Dessau, Phys. Rev. Lett. **87**, 117002 (2001).
8. Y.-D. Chuang, A.D. Gromko, A.V. Fedorov, Y. Aiura, K. Oka, Yoichi Ando, D. S. Dessau cond-mat/0107002 (Phys Rev Lett, submitted).
9. A.D. Gromko, A.V. Fedorov, Y.-D. Chuang, J.D. Koralek, Y. Aiura, Y. Yamaguchi, K. Oka, Yoichi Ando, D. S. Dessau (in preparation).
10. A. Lanzara, P. V. Bogdanov, X. J. Zhou, S. A. Kellar, D. L. Feng, E. D. Lu, T. Yoshida, H. Eisaki, A. Fujimori, K. Kishio, J.-I. Shimoyama, T. Noda, S. Uchida, Z.Hussain, Z.-X. Shen, Nature **412**, 510 (2001).
11. A. Kaminski et al., Phys. Rev. Lett. **86**, 1070-1073 (2001).
12. P.D. Johnson et al., Phys. Rev. Lett. **87** 177007 (2001).
13. H. He et al. Phys. Rev. Lett. **86**, 1610-1613 (2001).

This work was supported by the NSF Career-DMR-9985492 and the DOE DE-FG03-00ER45809. ALS and SSRL are operated by the DOE, Office of Basic Energy Sciences.

Principal investigator: Dan Dessau, University of Colorado, Department of Physics, Boulder, CO 80309. Email: dessau@spot.colorado.edu. Telephone: 303-492-1607.

Infrared conductivity of photocarriers in organic molecular crystals

Chris Weber*[1,2], Ch. Kloc[3], Michael Martin[4], J.H. Schoen[3], B. Batlogg[3], Joe Orenstein[1,2]
[1] Department of Physics, University of California, Berkeley, CA 94720
[2] Material Sciences Division, Lawrence Berkeley National Laboratory, Berkeley, CA 94720
[3] Bell Laboratories, Lucent Technologies, Murray Hill, New Jersey 07974-0636
[4] Advanced Light Source Division, Lawrence Berkeley National Laboratory, Berkeley, CA 94720

This project, begun in March of 2001, seeks use infrared spectroscopy to probe the properties of photocarriers in organic molecular crystals. A group at Bell Laboratories has recently succeeded in creating FETs on ultrapure single crystals of pentacene, tetracene, and other "polyacenes" (rigid, rodlike chains of Benzene rings). Carriers injected into these transistors have exhibited metal-insulator transitions, superconductivity, lasing, and the quantum Hall effect (see, e.g., J. H. Schoen, Ch. Kloc, B. Batlogg, *Science* v. 288 p. 2338; *Science* v. 288 p. 656; *Nature* v. 406 p. 702). The goal of our experiment is to photoexcite carriers in these same materials, and to measure the infrared spectrum of these photocarriers.

The apparatus, at ALS beamline 1.4, includes an Argon-ion laser for photoexcitation of charge carriers, a Bruker 66v/S Fourrier-Transform Infrared (FTIR) spectrometer, and a variable-temperature cryostat. The laser allows photoexcitation at energies from 2.4 eV to 3.5 eV. At the UV frequencies, the quantum efficiency of photocarrier generation in pentacene is high, about 30%. The light is coupled to the sample (in the cryostat) by means of an optical fiber. The cryostat allows us to reach temperatures from 5 K to 300 K, and the FTIR spectrometer allows measurement of infrared transmission on the range of at least 100 cm^{-1} to 7800 cm^{-1}.

The basic result of a measurement is a transmission spectrum, $T(\omega)$, either with the sample illuminated with laser light, $T_{on}(\omega)$, or with the sample unilluminared, $T_{off}(\omega)$. From these spectra we determine difference spectra, $\Delta T / T = (T_{on}(\omega) - T_{off}(\omega)) / T_{off}(\omega)$. Our measurements at room temperature on crystals of Tetracene have shown good reproducibility, both in the shape and in the magnitude of the difference spectra. The measurement is sensitive to changes in the transmission of one part in 10^4 or better through most of the spectral range. We have resolved many clear and reproducible features that are an order of magnitude larger than the noise.

Although these results demonstrate that the apparatus is, indeed, able to make the desired measurements, they do not put us particularly close to our scientific goals. Most or all of the features we have seen thus far appear to be due to shifting or broadening of phonon absorptions due to the heating effect of the laser. This result at room temperature is no surprise, as the mobility of carriers in polyacene crystals increases as T^{-2} below room temperature, so that the conduction of the carriers should only become visible at low temperatures. More surprising was the result that tetracene crystals large enough to measure optically will invariably shatter upon cooling below about 180 K (the temperature seems to vary a bit). Pentacene crystals, on the other hand, do not shatter, but also do not seem to be available in sizes large enough for optical measurement. Other

polyacenes have much lower efficiencies of photocarrier generation (due to their having broader bandgaps), and so are not suited to this experiment.

We are now seeking thin-film samples of the polyacenes, as these should survive cooling and should have the large area desirable for infrared measurement. High-quality pentacene films have been shown to display many of the same electronic properties as their single-crystal counterparts (J. H. Schoen, Ch. Kloc, *Applied Physics Letters*, v. 79, p. 4043).

Funding sources: This work and the Advanced Light Source are supported by the Director, Office of Science, Office of Basic Energy Science, Material Science Division, of the United States Department of Energy under contract number DE-AC03-76SF00098 at Lawrence Berkeley National Laboratory.

* To whom correspondence should be addressed:
cpweber@lbl.gov
(510) 486-5879

Investigation of Surface and Bulk Half-metallic Character of Fe_3O_4 by Spin Resolved Photoemission

S. A. Morton (a), G. D. Waddill (a), S. Kim (b), Ivan K. Schuller (b), S. A. Chambers (c) and J. G. Tobin (d)

(a) Department of Physics, U. of Missouri-Rolla, Rolla, MO 65409, USA
(b) Department of Physics, U. of California San Diego, La Jolla, CA 92093, USA
(c) Pacific Northwest National Laboratory, Richland, WA 99392, USA
(d) Lawrence Livermore National Laboratory, Livermore, CA 94550 USA

The existence of a new class of magnetic materials displaying metallic character for one electron spin population and insulating character for the other was first postulated by DeGroot *et al* [1] in 1983 based on theoretical band structure calculations of the ferromagnetic Heusler alloy NiMnSb. Since then such half metallic materials, which by definition posses 100% electron polarization at the Fermi energy have attracted considerable theoretical, experimental, and technological interest as potential pure spin sources for use in spintronic devices [2], data storage applications, and magnetic sensors. In addition to Heusler alloys half metallic character has also been predicted to occur in a wide range of manganites [3], metallic oxides [4], and CMR systems [5]. However, such predictions have proven to be extremely difficult to confirm experimentally [6]. A major factor in this failure has proven to be significant experimental challenges in obtaining a clean stoichiometric surface with a magnetization that is truly representative of the bulk material and thus suitable for further study by magneto-optical or spectroscopic techniques.

In recent experiments at the ALS we have used spin resolved photoemission to study the role that surface reconstruction plays in the observed polarization of the half metallic candidate material magnetite, Fe_3O_4. Magnetite has a structure that is relatively simple in comparison to most other candidate half metals and it can be grown epitaxially using conventional deposition techniques [7], making it one of the strongest candidates for spintronic applications. However previous spin resolved measurements have shown that the polarization at the Fermi edge is only ~40% [8] rather than the anticipated 100%.

By conducting spin resolved depth profile measurements and comparing the results to theoretical band structure calculations we have demonstrated that Fe_3O_4 exhibits a semiconducting non-magnetic surface re-construction which significantly reduces the observed polarization but that, in contrast, the underlying bulk material is in fact very strongly polarized. Indeed, once the effects of this surface reconstruction are taken into account by theoretical models of the polarization an excellent match is obtained between the experimental spin resolved spectra and simulated spectra generated from theoretical spin polarized band structure calculations [9] (fig. 1). Hence our results strongly support the notion that Fe_3O_4 is indeed a half-metallic material suitable for use in a new generation of spintronic devices.

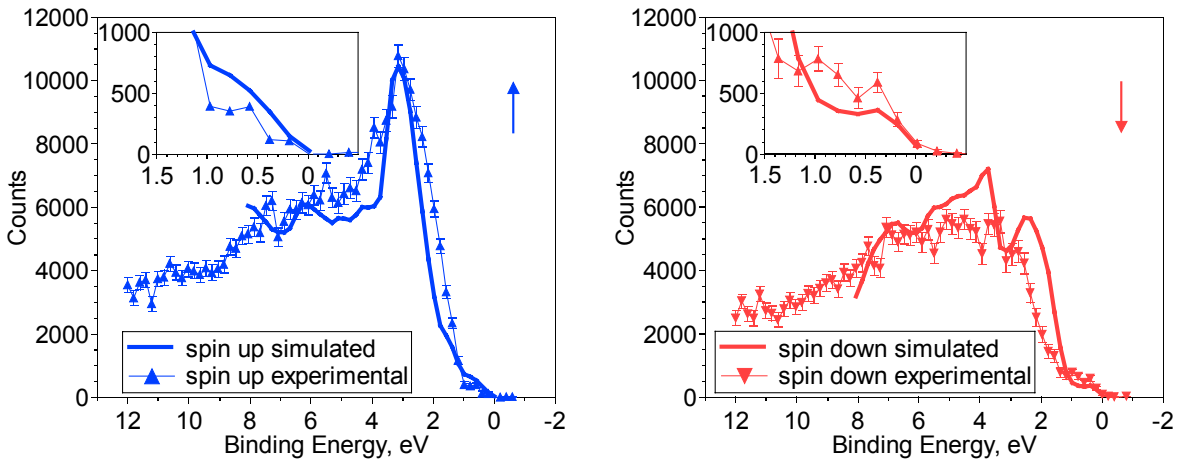

Figure 1

Comparison of experimental spin resolved Fe_3O_4 valence bands with equivalent simulated spectra derived from theoretical calculations that have been corrected to account for the presences of a nonmagnetic surface reconstruction

References

1. R. A. de Groot *et al., Phys. Rev. Lett*. **50,** 2024 (1983).
2. S. A. Wolf, D. Treger, *IEEE Trans. Mag*. **36** 2748 (2000).
3. S. Jin *et al*., *Science* **264,** 413 (1994).
4. Z Zhang, S. Satpathy, *Phys. Rev. B* **44**, 13319 (1991).
5. W. E. Pickett, D. J. Singh, *Phys. Rev. B* **53**, 1146 (1996).
6. K. P. Kamper *et al.*, *Phys. Rev. Lett.* **59** 2788 (1987).
7. S. A. Chambers, S. A. Joyce, *Surf. Sci.* **420,** 111 (1999).
8. S. F. Alvarado *et al*., *Phys. Rev. Lett*. **34,** 319 (1975).
9. S.A. Morton *et al*., *Submitted to Surface Science Letters*

This work was supported by the Director, Office of Energy Research, Office of Basic Energy Sciences, Materials Science Division, of the U.S. Department of Energy under Contract No. # R5-32633.A02. This work was performed under the auspices of the U.S Department of Energy by Lawrence Livermore National Laboratory under contract no. W-7405-Eng-48.

Principal Investigator: Ivan K. Schuller, Department of Physics, University of California San Diego, La Jolla, CA 92093. Phone: (858) 534-2540 fax: (858) 534-0173 Email: ischuller@ucsd.edu

Magnetic Circular Dichroism in the X-ray Absorption Spectra of the CMR Compound, $Yb_{14}MnSb_{11}$

A. P. Holm[1]; S. M. Kauzlarich[1]; S. A. Morton[2]; G. D. Waddill[3];
W. E. Pickett[4]; J. G. Tobin[2]

[1]Department of Chemistry, University of California, Davis, CA 95616.
[2]Lawrence Livermore National Laboratory, Livermore, CA 94550.
[3]Department of Physics, University of Missouri-Rolla, Rolla, MO 65401-0249.
[4]Department of Physics, University of California, Davis, CA 95616.

This work is part of ongoing investigations into the magnetic and electronic properties of the rare-earth transition metal Zintl phases $A_{14}MnPn_{11}$ (A = Eu, Yb; Pn = Sb, Bi) at the Advanced Light Source. We have recently obtained exciting new results from X-ray magnetic circular dichroism (XMCD) investigations of the $Yb_{14}MnSb_{11}$ system. Specifically, we have used XMCD as an element specific probe into the nature of the magnetic moment in this system with the intention of exploring the proposed half-metallic nature of this compound and its related substitutional analogues. Our XMCD measurements indicate that $Yb_{14}MnSb_{11}$ is a half-metallic ferromagnet, and we have submitted our results for publication to Physical Review Letters.

The term half-metallic ferromagnet arises from theoretical predictions made by R.A. de Groot et al based on band structure calculations of the ferromagnetic Heusler alloy NiMnSb.[1] These calculations proposed a new phase of matter that displays separate electronic properties for majority-spin and minority-spin electrons. Specifically, one electron spin population is metallic and the other is insulating. Such a material, (possessing 100% spin polarization of the conduction electron) would hold significant technological potential as a single-spin electron source for spintronic devices, data storage applications, and high efficiency magnetic sensors.[2]

The materials we are studying are new compounds that belong to a class of materials called transition-metal Zintl phases. These compounds are isostructural to $Ca_{14}AlSb_{11}$ and crystallize in the tetragonal space group $I4_1/acd$ (Z = 8). The $Yb_{14}MnSb_{11}$, $Yb_{14}MnBi_{11}$ and $Eu_{14}MnSb_{11}$ analogues are each reported to order ferromagnetically at 56 K, 58 K and 28 K, and 92 K, respectively.[3-6] $Eu_{14}MnBi_{11}$ is an antiferromagnet with a Néel transition at T_N = 32 K.[6] Each of these materials exhibits a large resistance drop associated with their unique magnetic ordering temperature. This behavior is attributed to colossal magnetoresistance effects, and could help support the proposal made by Pickett and Singh of a correlation between half-metallicity and colossal magnetoresistance.[7] These systems are ideal for investigations into the links between magneto-resistance, magnetic moment and half-metallic behavior.

The ability to perform X-ray magnetic circular dichroism experiments on the EPU has allowed us to probe the dichroic characteristics of Mn and Sb in the $Yb_{14}MnSb_{11}$

system during experiments recently performed on beamline 4.0 of the ALS. Figure 1 shows the results from XMCD experiments on the Mn L_{23}, Sb M_{45}, and Yb N_{45} edges of $Yb_{14}MnSb_{11}$. A dramatic dichroism effect is shown in the Mn L_{23} region which is confined to one sub-component of the Mn edge and closely matches theoretical models for Mn^{2+}, d^5 dichroism (Figure 1d). The difference in intensity upon change of helicity is greater than 30%, and is strong evidence of a significant moment being present on the Mn. In contrast, no dichroism was observed in the Yb edges, but a small antialigned moment is present in the Sb M_{45} edges as shown on the left side of Figure 1. This result is surprising because initial models predicted that dichroism would be restricted to the Mn L_{23} region (with no dichroism in the Sb M_{45} region) and that it would be Mn^{3+}, d^4 like in character. However, an ongoing collaboration with theoretical groups in the physics departments of the University of California, Davis and the University of Illinois, Urbana to model the Ca and Ba analogues of this structure type has now produced calculated results consistent with our experimental observations of how the Sb behaves in this system. They argue that the Mn should be in a 2+, d^5 configuration, and the Sb_4 cage surrounding the Mn should have a hole antialigned to the Mn moment giving a total moment of ~4 μ_B/ formula unit. Our experimental results are consistent with these new theoretical results, and in addition, these comparisons of data with theoretical calculations and SQUID magnetometry measurements confirm that $Yb_{14}MnSb_{11}$ is indeed a half-metallic ferromagnet.[8-10]

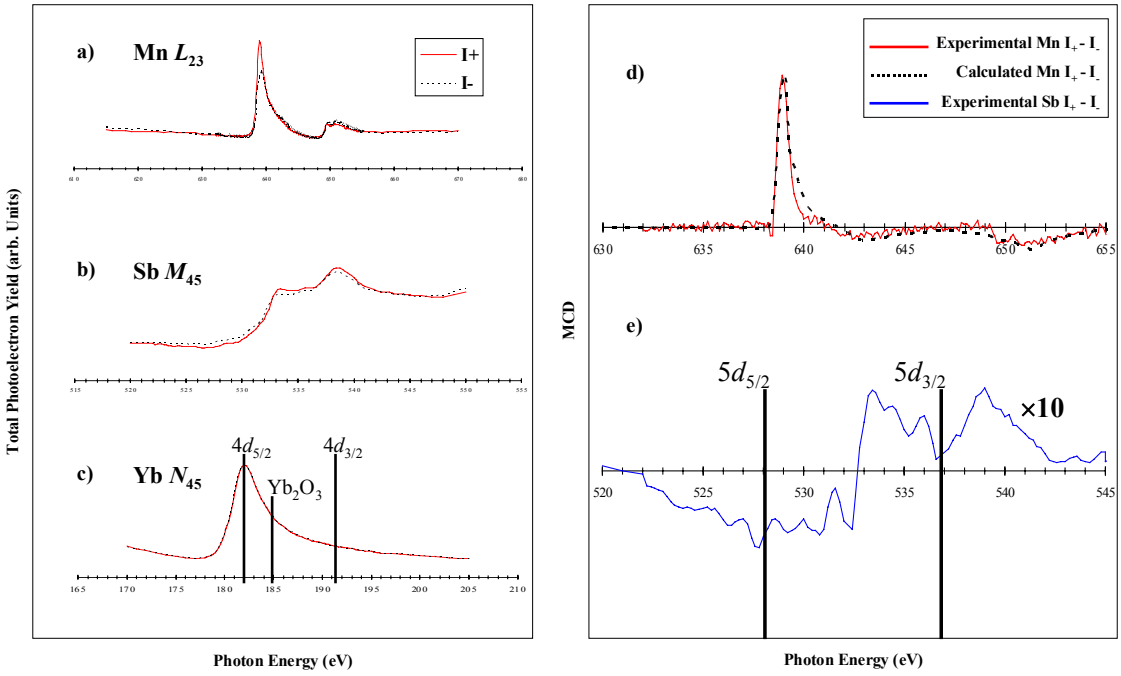

Fig. 1. The raw absorption spectra at plus and minus light polarization for a) Mn L_{23}, b) Sb M_{45}, and c) Yb N_{45} are shown on the left. The MCD spectra for d) the experimental Mn L_{23} denoted by a solid red line and the calculated Mn^{2+}, d^5 L_{23} denoted by a dashed black line, and e) the experimental Sb M_{45} denoted by a solid blue line.[10]

References:

1. de Groot, R. A.; Mueller, F. M.; van Engen, P. G.; Buschow, K. H. J. *Physical Review Letters* **1983**, *50*, 2024 -2027.
2. Prinz, G. A. *Science* **1998**, *282*, 1660 - 1663.
3. Chan, J. Y.; Kauzlarich, S. M.; Klavins, P.; Shelton, R. N.; Webb, D. J. *Chemistry of Materials* **1997**, *9*, 3132-3135.
4. Chan, J. Y.; Olmstead, M. M.; Kauzlarich, S. M.; Webb, D. J. *Chemistry of Materials* **1997**, *10*, 3583 - 3588.
5. Chan, J. Y.; Wang, M. E.; Rehr, A.; Kauzlarich, S. M.; Webb, D. J. *Chemistry of Materials.* **1997**, *9*, 2131 - 2138.
6. Chan, J. Y.; Kauzlarich, S. M.; Klavins, P.; Shelton, R. N.; Webb, D. J. *Physical Review B* **1998**, *57*, 8103 - 8106.
7. Pickett, W. E.; Singh, D. J. *Physical Review B* **1996**, *53*, 1146 - 1160.
8. Sánchez-Portal, D.; Martin, R. M.; Kauzlarich, S. M.; Pickett, W. E. *Physical Review B* **2001**, *Submitted September 31*.
9. van der Laan, G.; Thole, B. T. *Physical Review B* **1991**, *43*, 13401-13411.
10. Holm, A. P.; Kauzlarich, S. M.; Morton, S. A.; Waddill, G. D.; Pickett, W. E.; Tobin, J. G. *Physical Review Letters* **2001**, *Submitted November 26*.

This work was supported by the Director, Office of Energy Research, Office of Basic Energy Sciences, Materials Science Division, of the U.S. Department of Energy under Contract No. # R5-32633.A02. This work was performed under the auspices of the U.S Department of Energy by Lawrence Livermore National Laboratory under contract no. W-7405-Eng-48.

Principal Investigator: Susan M. Kauzlarich, Department of Chemistry, University of California Davis, California 95616. Phone: (530)752-4756 fax: (530)752-8995 Email: smkauzlarich@ucdavis.edu

Multi-Atom Resonant Photoemission Effects from Solid Surfaces and Free Molecules

N. Mannella[1,2], B.S. Mun[1,2], S.-H. Yang[2], A.W. Kay[1,2,#],F.J. Garcia de Abajo[1,3], E. Arenholz[4], A.T. Young[4], Z. Hussain[4], H. Wang[5], O. Hemmers[5], D.W. Lindle[5], M.A. Van Hove[1,2], and C.S. Fadley[1,2]

[1]Dept. of Physics, University of California-Davis, Davis, CA 95616
[2]Materials Sciences Division, Lawrence Berkeley National Laboratory, Berkeley, CA 94720
[3] Centro Mixto CSIC-UPV/EHU, San Sebastian, Spain
[4]Advanced Light Source, Lawrence Berkeley National Laboratory, Berkeley, CA 94720
[5]Dept. of Chemistry, University of Nevada, Las Vegas, NV 89154
[#]Present address: Intel Corporation, Portland, OR

INTRODUCTION

In prior work at the ALS, it has been pointed out that a new type of interatomic resonant photoemission effect exists, and that this effect furthermore has the potential of providing a useful probe of near-neighbor atomic identities, bonding, and magnetism [1-5]. The phenomenon has been termed multi-atom resonant photoemission (MARPE). In measuring this effect, the photoelectron intensity of a given core level from atom "A" (e.g. O 1s from MnO) is monitored while the photon energy is tuned through a strong absorption edge for a core level on another atom "B" in the sample (e.g. the Mn 2p edges in MnO). Initial observations on MnO and other metal oxides appeared to show significant entirely-positive interatomic resonant effects in photoemission of up to 100% [1]. Additional measurements in Auger emission and soft x-ray emission from MnO seemed to confirm that such effects were also present in secondary decay processes as a result of resonant enhancement of the initial O 1s core hole formation [2]. A theoretical model for these effects based on the extension of intraatomic resonant photoemission ideas to the interatomic case was also developed and compared favorably with experiment [3]. Other measurements on transition-metal compounds [6] and an adsorbate-substrate system [7a] seemed to confirm these measurements and analysis.

Subsequently, it has been realized that such experimental measurements require very careful allowance for potential detector non-linearities [4,5,7b], since the observed electron intensities (particularly inelastically scattered backgrounds) change dramatically in going over any core resonance. In particular, the detector used for several of the first MARPE studies [1,2,4-7a], the standard microchannel plate-plus-phosphor-plus-CCD camera incorporated in the Gammadata-Scienta series of electron spectrometers, exhibits not only a typical saturation effect for high countrates, but also a strong quadratic component of counting that goes above linear for low countrates. Thus, spectra obtained in this low-countrate regime, while not exhibiting any kind of saturation effect, can be artificially enhanced in intensity in passing over a core-level resonance. Methods of accurately correcting spectra for these non-linearities have been discussed [4,5,7b, and abstract by Mannella et al. in this 2001 Compendium]. When these effects are allowed for, the magnitude of the effect is reduced and the form is found to change, with the shape usually involving a negative-then-positive swing in intensity reminscent of a Fano profile in form [4,5,7b,8].

We here report more recent experimental results providing further evidence of such interatomic resonant effects in photoemission, for two very different limiting-case types of systems: a cleaved single-crystal oxide-NiO and a free molecule-SF_6. These data are discussed in terms of existing theoretical models for such MARPE effects [3,5], in particular, an x-ray optical (dielectric) approach that well describes the NiO data and a microscopic quantum mechanical model that should be useful in describing the SF_6 data.

EXPERIMENTAL PROCEDURE

The NiO measurements were performed on beamline 4.0.2 and made use of the Advanced Photoelectron Spectrometer/Diffractometer located there. Detector non-linearities were corrected for in all data presented here, using methods described elsewhere [4,5, and abstract in the 2001 Compendium]. A NiO single crystal was cleaved just before insertion into ultrahigh vacuum via a loadlock, then ion bombardment and annealing in oxygen to remove minor surface contaminant levels and assure correct stoichiometry before measurement. The incidence angle of the radiation was varied from grazing values of 5° to much higher values up to 40° (cf. experimental geometry in Figure 1(a)).

The SF_6 measurements were performed on beamline 8.0.1 and made use of a time-of-flight spectrometer described in detail elsewhere [9]. The detectors in this spectrometer are positioned in angle with respect to the incoming radiation and polarization vector such that non-dipole contributions to the angular distributions can be readily measured with high accuracy. For reference, the angular distributions of photoelectrons from a randomly oriented ensemble of free molecules is given by $d\sigma / d\Omega = (\sigma / 4\pi)\{ 1 + \beta P_2(\cos\Theta_e) + [\delta + \gamma \cos^2\Theta_e] \sin\Theta_e \cos\Phi_e \}$, with β the dipole asymmetry parameter and δ and γ the first-order non-dipole parameters (cf. geometry in Figure 2(a), with Φ_e being the azimuthal angle around the polarization vector $\boldsymbol{\varepsilon}$) [9].

EXPERIMENTAL RESULTS AND DISCUSSION

NiO(001): In Figure 1, we show experimental O 1s intensities from NiO as a function of photon energy and for five different x-ray incidence angles. For the lowest incidence angle of 5°, the effect of crossing the Ni 2p absorption resonances is dramatic, yielding a negative-then-positive excursion on crossing $2p_{3/2}$ whose amplitude is 75% of the intensity below the resonance. The magnitudes of these effects decreases as the incidence angle is increased, falling off to about 5% for an incidence angle of 40°.

Also shown in Figure 1 are theoretical curves based on an x-ray optical model of such effects, as discussed previously [5]. The optical constants that are key inputs for this model have been derived from concomitant partial-yield x-ray absorption measurements, with corrections for x-ray incidence angle and secondary electron takeoff angle [4], and subsequent Kramers-Kronig analysis [5]. The resulting theoretical curves are in excellent agreement with experiment for the lowest angle, and the agreement is very good for all other angles as well, although with some overprediction of the amplitudes at the higher angles. Non-zero effects are observed and predicted over the full angle range, in qualitative agreement with prior data for MnO [5]. These data thus disagree with one aspect of an earlier study of NiO by Finazzi et al. [8], in which they did not observe any sort of MARPE effect in O 1s emission from NiO; this lack of any effect appears to be due to measuring with too high an incidence angle and having insufficient statistical accuracy to resolve the small remaining effects seen, e.g. in Figures 2(e)-2(f).

We thus expect such MARPE effects to be observable in photoemission from any solid surface, with strength depending on the relative intensities of the absorption resonances. Furthermore, for homogeneous systems with flat surfaces, the x-ray optical model should provide a reasonably quantitative picture of the observed phenomena. Effects following an x-ray optical analysis have also recently been observed for photoemission from an adsorbate on a metal-N_2/Ni(001) [10]. For more complex cases with, e.g., three-dimensional nanometer-scale heterogeneity, the use of a microscopic model will be more appropriate.

SF_6: In Figure 2, experimental results for SF_6 are summarized. The x-ray absorption coefficient is shown in Figure 2(b), and the S 2p photoemission intensity and its asymmetry parameters were measured as photon energy was scanned across the "A" absorption resonance (corresponding to a F

$1s\ t_{1u}$-to-a^*_{1g} excitation). Although the total S 2p intensity (proportional to σ) does not show a significant change in crossing the resonance (≤few %), the dipole asymmetry parameter β (as shown in Figure 2(b)) exhibits about a 15% excursion in magnitude that is also of the same general form as those in Figure 1. Similar effects are also seen in the parameters δ and γ [11].

Thus, interatomic resonant effects are also seen in this free molecule, and although they are too small to be observed as yet in the total intensity, they are clearly observed in the various asymmetry parameters. No theoretical calculations have as yet been performed for this case, but the x-ray optical model would clearly be inappropriate, and a microscopic approach such as that discussed previously [3,5] is the logical starting point for understanding these effects.

CONCLUSIONS

Multi-atom resonant photoemission effects are found in both the total intensities from homogeneous solid surfaces and adsorbates on such surfaces, for which an x-ray optical model is found to well describe the data, and in the angular distribution asymmetry parameters of a free molecule, for which a microscopic theoretical approach will be necessary. Similar effects in nanoscale structures will lie somewhere between these two cases.

REFERENCES

1. A. Kay, E. Arenholz, B.S. Mun, F.J. Garcia de Abajo, C.S. Fadley, R. Denecke, Z. Hussain, and M.A. Van Hove, *Science* **281**, 679(1998).
2. (a) E. Arenholz, A.W. Kay, C.S. Fadley, M.M. Grush, T.A. Callcott, D.L. Ederer, C. Heske, and Z. Hussain, *Phys. Rev. B* **61**, 7183 (2000); (b) E. Arenholz, A.W. Kay, unpublished results.
3. F.J. Garcia de Abajo, C.S. Fadley, and M.A. Van Hove, *Phys. Rev. Lett*. **82**, 4126 (1999).
4. A.W. Kay, Ph.D. dissertation (University of California-Davis, September, 2000), Chapters 4 and 5.
5. A.W. Kay, F.J. Garcia de Abajo, S.H. Yang, E. Arenholz, B.S. Mun, M.A. Van Hove, Z. Hussain, and C.S. Fadley, Physical Review B **63**, 5119 (2001).
6. A. Kikas, E. Nommiste, R. Ruus, A. Saar, and I. Martinson, Sol. St. Commun. **115**, 275 (2000).
7. (a) M.G. Garnier, N. Witkowski, R. Denecke, D. Nordlund, A. Nilsson, M. Nagasono, and N. Mårtensson, and A. Föhlisch, Maxlab Annual Report for 1999 and private communication correcting this data; (b) D. Nordlund, M. G. Garnier, N. Witowsky, R. Denecke, A. Nilsson, M. Nagasono, N. Mårtensson and A. Föhlisch, Phys. Rev. B **63**, 121402 (2001).
8. M. Finazzi, G. Ghiringhelli, O. Tjernberg, L. Duo, A. Tagliaferri, P. Ohresser, and N. B. Brookes, Phys. Rev. B **62**, R16215 (2000).
9. (a) O. Hemmers et al., Rev. Sci. Instrum. **69**, 3809 (1998); (b) O. Hemmers et al., Phys. Rev. Lett. **87**, 273003 (2001).
10. D. Menzel, W. Wurth, A. Föhlisch, P. Fuelner, S.-H. Yang, and C.S. Fadley, private communication.
11. H. Wang, O. Hemmers, P. Focke, M. M. Sant'Anna, D. Lukic, C. Heske, R. C. C. Perera, I. Sellin, and D. Lindle, to be published.

This work was supported by the U.S. Department of Energy, Office of Science, Office of Basic Energy Sciences, Materials Sciences Division, under Contract No. DE-AC03-76SF00098, and the National Science Foundation.

Principal investigator: N. Mannella, Department of Physics UC Davis, and Materials Sciences Division, Lawrence Berkeley National Laboratory. Email: norman@electron.lbl.gov. Telephone: 510-486-4581

Figure 1. (a) Experimental geometry for measurements on Ni(001). (b)-(f) O 1s intensity as photon energy is scanned through the Ni $2p_{1/2\text{-}3/2}$ absorption resonances. Both experimental data (blue points) and theoretical calculations based on an x-ray optical model (red curves) are shown.

Figure 2. (a) Experimental geometry for measurements on gas-phase SF_6. (b) The x-ray absorption coefficient in the F 1s region as measured by partial electron yield. (c) The dipole asymmetry parameter β as photon energy is scanned through the "A" resonance in (b).

Figure 1.

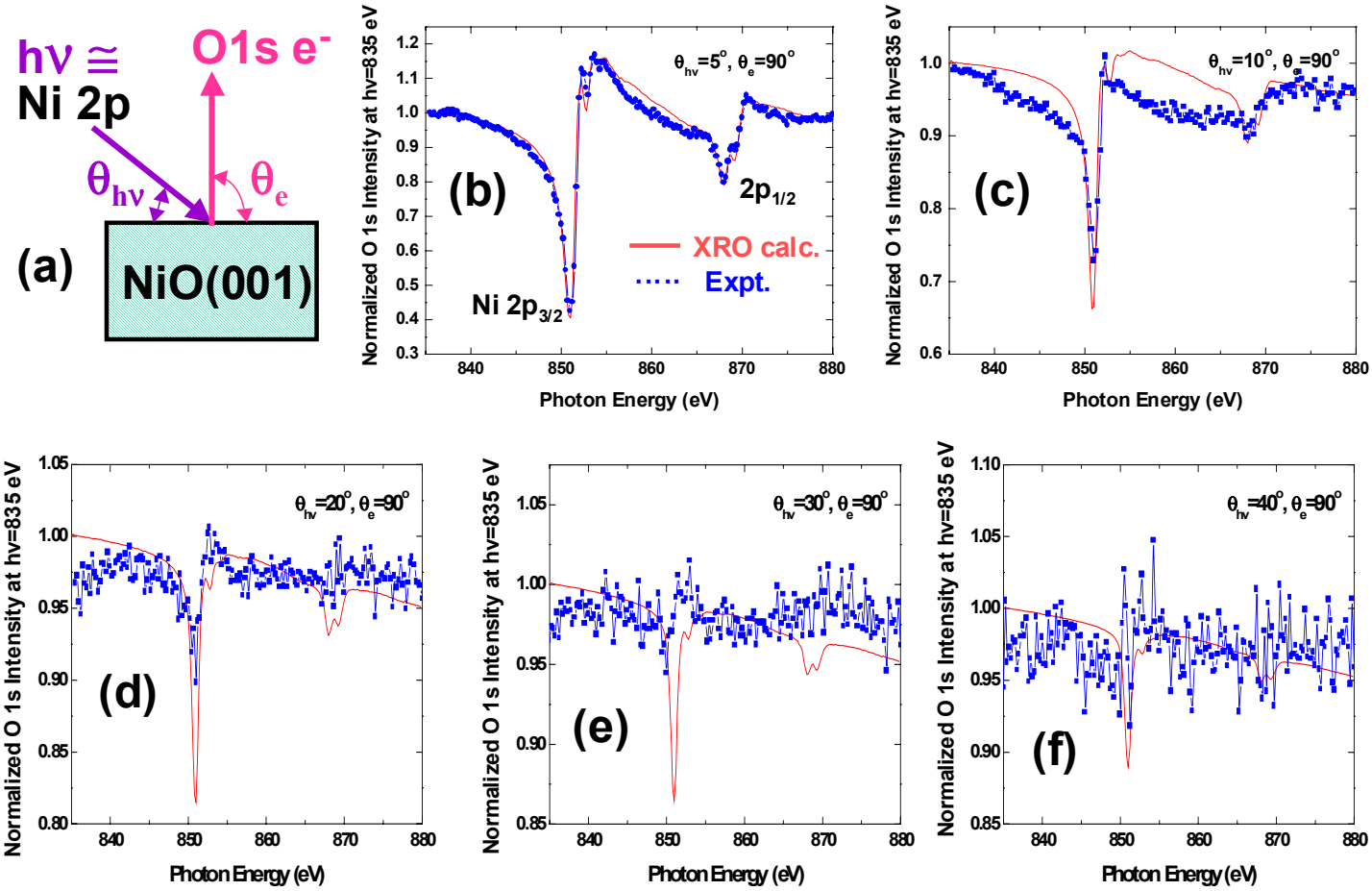

Figure 2.

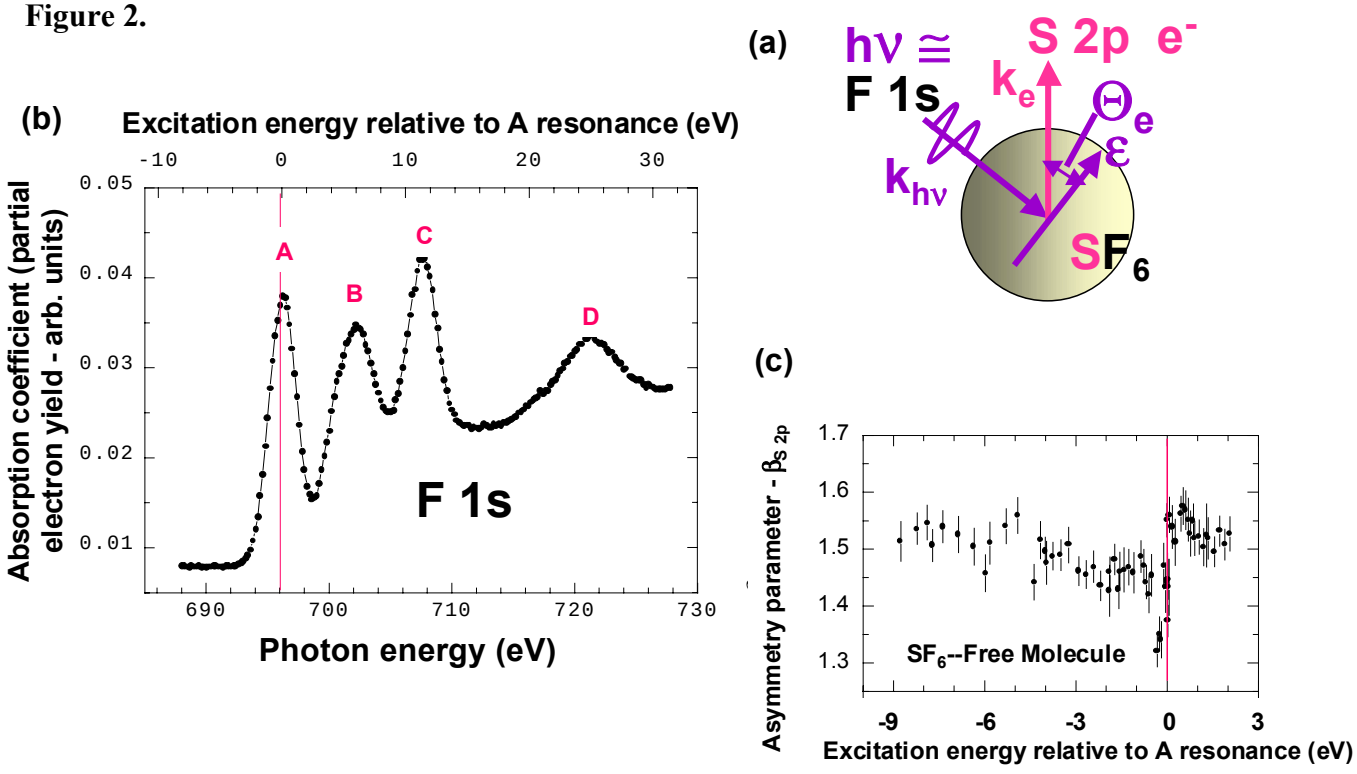

O 1s XAS of H_2O in the solvation shell of monovalent and trivalent ions

L.Å. Näslund[1], Ph. Wernet[2], H. Ogasawara[1], D. Edwards[3], S. Myneni[3] and A. Nilsson[1,2]

[1]Stockholm University, SCFAB, Fysikum, S-106 91 Stockholm, Sweden
[2]SSRL, 2575 Sand Hill Road, MS 69, Menlo Park, CA94025, USA
[3]Department of Geosciences, Princeton University, Princeton, NJ 08544, USA

INTRODUCTION

Earlier experiments with the Soft X-ray Endstation for Environmental Research (SXEER) have shown that pure liquid water consists of three different species of water molecules - symmetric (SYM), acceptor asymmetric (A-ASYM), and donator asymmetric (D-ASYM) [1]. By dissolving Potassium Chloride or Aluminum Chloride we introduce a fourth type of water species - water molecules in the solvation shell of the dissolved ions. X-ray Absorption Spectroscopy at the oxygen K-edge (O 1s XAS) gives the information of Oxygen p-character and hence the local geometric arrangement around the probed oxygen atom. In this report we will show some of the XAS spectra we have obtained at beamline 8.0.

O 1s XAS OF WATER WITH DISSOLVED KCl AND $AlCl_3$

If we dissolve Potassium Chloride (KCl) into water, the water molecules will form a solvation shell around each Potassium- and Chloride ion. These water molecules will have a different electronic structure than a water molecule in the bulk water. We can actual say that we have a fourth water species. Figure 1 is showing a XAS spectrum at the oxygen edge of water with dissolved KCl. We can see changes in two energy ranges. The pre-edge at 535 eV has higher intensity and has a shoulder at 534.3 eV. This is probably due to changes in the distribution of D-ASYM water species in the bulk water. The higher intensity at 537.0 eV can be explained by water molecules in the solvation shell of K^+ ion. Preliminary calculations are supporting the experimental data.

Comparing water dissolved KCl with water dissolved Aluminum Chloride ($AlCl_3$) can give some input to the interpretation. An O 1s XAS spectrum of water with dissolved $AlCl_3$ is shown in figure 2. As in dissolved KCl there is a shoulder at 534.3 eV. For water with dissolved $AlCl_3$ the shoulder is more distinct and indicates that the feature at 535 eV is a double peak. However, the interpretation is the same as in the case of dissolved KCl - there are changes in the distribution of D-ASYM water species in the bulk. At higher energy the O 1s XAS spectrum of water with dissolved $AlCl_3$ is showing higher intensity than pure water. If we compare the spectrum of water dissolved $AlCl_3$ with water dissolved KCl we can see that water dissolved $AlCl_3$ have lower intensity at 537.0 eV and higher intensity at 540.5 eV. This can be explained by differences in the electronic structure of water molecules in the solvation shell of trivalent ions from that of monovalent ions. Preliminary calculations show that the fourth water species, water molecules in the solvation shell of the Al^{3+} ion, is giving higher intensity in a different energy range than the water molecules in the solvation shell of the K^+ ion.

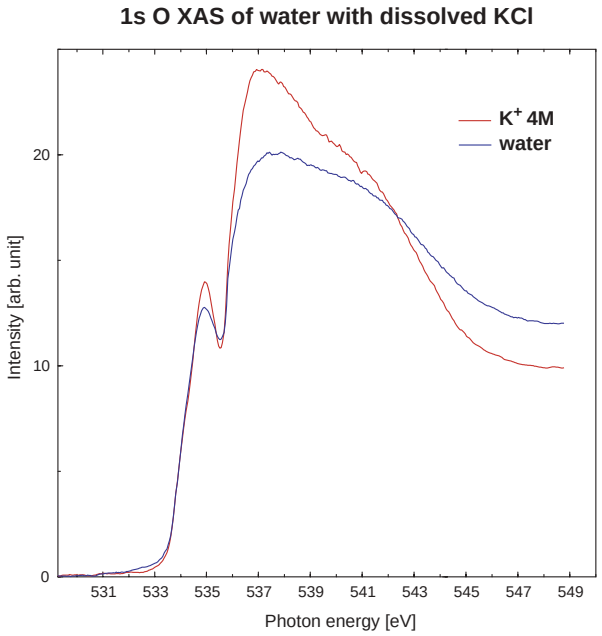

Figure 1. Oxygen 1s XAS of water with dissolved Potassium Chloride (KCl) compared to pure water. The spectrum of water with dissolved KCl has a shoulder at 534.3 eV. It is easier seen in figure 2.

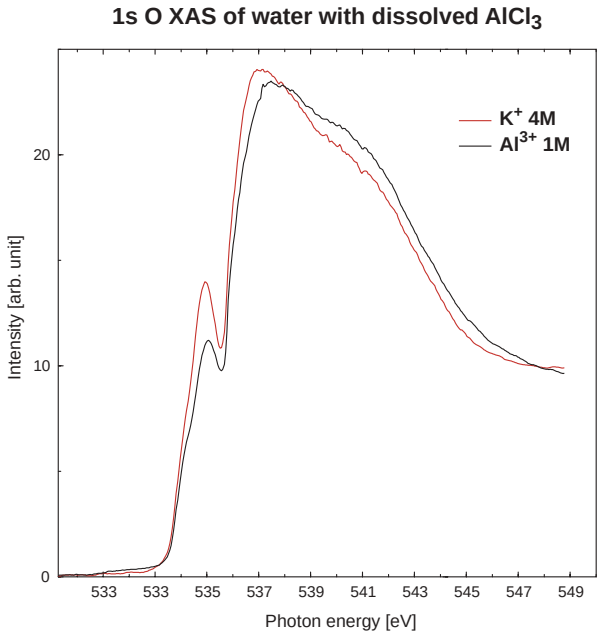

Figure 2. Oxygen 1s XAS of water with dissolved Aluminum Chloride ($AlCl_3$) compared to water with dissolved Potassium Chloride (KCl).

CONCLUSION

We have shown that O 1s XAS is sensitive enough to resolve the electronic structure of water molecules in a solvation shell of an ion. As an example we have presented differences in the O 1s XAS spectrum between pure liquid water, water with dissolved KCl and water with dissolved $AlCl_3$. The distribution of the D-ASYM water species in bulk water is changing when KCl or $AlCl_3$ is dissolved in the water. Further investigation will tell how the distribution is changed.

ACKNOWLEDGMENTS

M. Cavalleri and L.G.M Pettersson at Fysikum, University of Stockholm have done the preliminary calculations and are involved in the analyzing of the data collected at Beamline 8.0.

REFERENCES

1. S. Myneni, Y. Luo, L.Å. Näslund, M. Cavalleri, L. Ojamäe, H. Ogasawara, A. Pelmenschikov, Ph. Wernet, P. Väterlein, C. Heske, Z. Hussain, L.G.M. Pettersson, and A. Nilsson, *Journal of Physics: Condensed Matter, In press*

This work is supported by the Basic Energy Sciences (Geosciences, Department of Energy, USA), the Swedish Royal Academy of Science (KVA), and the Göran Gustafssons Foundation for Research in Natural Science and Medicine.

Principal investigator: S. Myneni, Department of Geosciences, Princeton University, Princeton, NJ 08544, USA. Email: smyneni@Princeton.EDU. Telephone: 609-258 5848.

Partial Density of States of B-2*p* in AlB_2 type Compounds

J. Nakamura,[1] K. Kuroki,[1] N. Yamada,[1] T.A. Callcott,[2] D.E. Ederer,[3]
J.D. Denlinger[4] and R.C.C. Perera[5]

[1]Department of Applied Physics and Chemistry, The University of Electro-Communications, Chofu, Tokyo 182-8585, Japan

[2]Department of Physics, University of Tennessee, Knoxville, TN 37996

[3]Department of Physics, Tulane University, New Orleans, LA 70118

[4]Advanced Light Source, Ernest Orlando Lawrence Berkeley National Laboratory, University of California, Berkeley, CA 94720

[5]Center for X-ray Optics, Ernest Orlando Lawrence Berkeley National Laboratory, University of California, Berkeley, CA 94720

Since the discovery of superconductivity in MgB_2 with a transition temperature, T_c, of 39 K by Nagamatsu *et al.*,[1] large number of researches from experimental[2-5] and theoretical point[6-12] of view have been performed on this compound and on a series of isostructural diborides. Although there are many experimental results that suggest holes in B-2*p*σ band with a strong electron-phonon coupling play important roles in the superconductivity of MgB_2, the reason for the high value of T_c is not clear.

In order to clarify the mechanism of high T_c superconductivity in MgB_2, it is important to investigate the difference in the electronic states between MgB_2 and other isostructural diborides. In the present study, we present X-ray emission (XES) and absorption spectra (XAS) near the boron (B) *K* edge in MB_2 (*M*=Mg, Al, Ta and Nb). AlB_2 and TaB_2 are not superconductors and a superconductivity in NbB_2 is controversial now. XAS was measured by both the total fluorescence yield (TFY) and the total electron yield (TEY) measurements at the same time. The reason we choose boron is because the band calculations for MgB_2 indicate that the bands near the Fermi energy are mainly composed from boron 2*p* orbitals.

The commercial specimens from Rare-Metallic Co. characterized by powder X-ray diffraction and dc-magnetization measurements, were used as samples of MB_2 (*M*=Mg, Al, Ta and Nb). The dc magnetization measurements indicate that the superconducting transition temperature of about 38 K for MgB_2 sample, and no superconducting transition for TaB_2, NbB_2 and AlB_2 above 1.8 K. The soft X-ray emission and absorption spectroscopies were performed at BL-8.0.1 of Advanced Light Source (ALS) in LBNL. In order to calibrate energy, XAS by TEY were also measured at the well calibrated beam line BL- 6.3.2 of the ALS.

Figure 1(a) shows XES (○) and XAS (●) of MgB_2. The sharp decrease of XES and XAS at about 186.3 eV is attributed to the Fermi energy measured from 1*s* core level. The solid line in Fig. 1(b) is the boron PDOS obtained from a band structure calculation[10], where we have taken into account the effect of the instrumental resolution by gaussian broadening. The intensities of experimental XES and XAS in Fig. 1(a) are scaled to the theoretical PDOS in the energy region, $E \leq 182$ eV for XES and $187 \text{ eV} \leq E \leq 191$ eV for XAS. The sum of the experimental XES and XAS are also plotted in Fig. 1(b). It can be seen that the overall feature of both XES and XAS, including the existence of a large PDOS around the Fermi energy, are remarkably well reproduced by the band structure calculation, enabling us to attribute each observed structure to *p*π and/or *p*σ states. Namely, the existence of peaks A and B, which is consistent with recent studies[3], are characteristic of bonding *p*σ states. The region C in the energy range from 187 to 191 eV is attributed to the *p*π states. A sharp peak D at about 192 eV in XAS is reported to be a resonance peak of *p*π* state[3], and also corresponds to antibonding

$p\sigma^*$ state predicted by a band calculation. Thus peak D contains both the $p\sigma^*$ and resonance state of $p\pi^*$ states.

Figure 1(c) shows XES and XAS of AlB_2. The intensity of XES is normalized so that the area intensity coincides with that for MgB_2 below E_F, while the intensity of XAS is scaled so that the intensity in the high energy region, $E \geq 198$ eV, coincides with that for MgB_2. In the high energy region, XAS shows no strong characteristic peaks. A broad tail of XES below 183 eV is similar to that of MgB_2, but the value of E_F shifts to be 187.5 eV. The form of XES of AlB_2 is broad compared to that of MgB_2. Figure 1(d) shows experimental PDOS derived from the sum of XES and XAS. A dip is observed at about 188 eV near the Fermi energy, indicating that the B-2*p* PDOS around the Fermi energy is drastically reduced compared to that in MgB_2. This is the major difference between MgB_2 and AlB_2.

This difference can be understood from results of the band calculation for AlB_2.[12] Namely, there are several factors that make the boron 2*p* PDOS around the Fermi level in AlB_2 much smaller than in MgB_2. First of all, the bonding σ bands, whose tops are located above the Fermi level in MgB_2, are fully filled in AlB_2. Secondly, the Fermi level is located at a point where the top of the bonding and bottom of the antibonding π bands touch with each other at the *K* point. If the system were purely two-dimensional, this would be a point where the DOS vanishes linearly as a function of energy. Although the π band is three dimensional, the above two-dimensional property remains because the system is anisotropic.

The difference between MgB_2 and AlB_2 can qualitatively be understood within a simple rigid band model, namely by simply shifting the Fermi energy as mentioned above. To be more precise, there are some quantitative differences, whose origin seems to lie beyond a rigid band picture. Namely, in AlB_2, the intensity of XAS just above the dip is larger than that in MgB_2, while the intensity of peaks A and D is suppressed. Looking again into the band calculation results, these features may be attributed to the increase of three dimensionality in AlB_2.

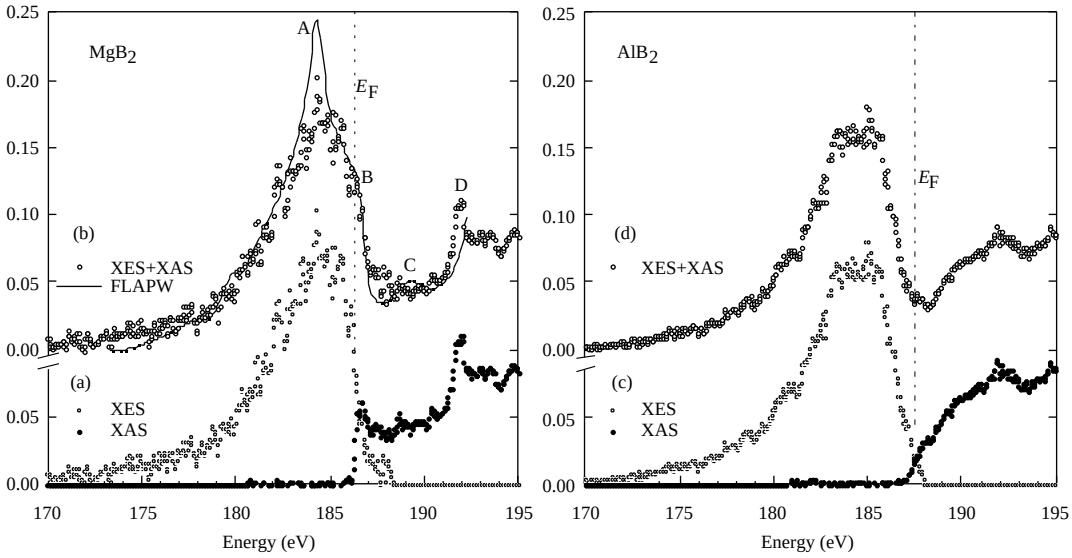

Fig.1 (a) The observed XES (○) and XAS (●) spectra of MgB_2. (b) The sum of XES and XAS (□) and the theoretical PDOS (solid line) derived from FLAPW method broadened with experimental resolution. (c) The observed XES (○) and XAS (●) spectra of AlB_2. (d) The sum of XES and XAS (□).

The XES and XAS of TaB_2 and NbB_2 are similar to those for AlB_2 except for a shift in

the Fermi energy up to 188.6 eV, owing to a larger band filling compared with AlB_2. The B-2*p* PDOS at the Fermi energy of TaB_2 is similar to that for AlB_2, so if TaB_2 is indeed superconducting, the difference between these two compounds should lie elsewhere. In NbB_2 compound, the Fermi energy is almost the same as that of TaB_2, but a considerable amount of DOS below the Fermi energy is observed. In both compounds, TaB_2 and NbB_2, band calculation suggests a strong hybridization between B-2$p\pi$ and Ta-5*d* or Nb-4*d* electrons. The characters of the states near the Fermi energy in TaB_2 and NbB_2 cannot be identified from the present results.

To summarize, the most characteristic feature in MgB_2 as compared to other related materials is the large B-2*p* PDOS around the Fermi level. Since this is partially attributed to the existence of the $p\sigma$ bonding band at the Fermi level, one may be tempted to consider that the $p\sigma$ band plays a crucial role in the occurrence of superconductivity in MgB_2.[8] This is indeed probable, but is not necessarily the case because the $p\pi$ band filling is also different between MgB_2 and other materials as mentioned above, which should result in a large difference in the shape of the $p\pi$ band Fermi surfaces. Let us note that the shape of the Fermi surfaces can play an essential role in the occurrence of superconductivity. For example, in those mechanisms that exploit nesting between the Fermi surfaces of bonding and antibonding π bands, the shape of the Fermi surfaces (namely the π band filling) is crucial. We believe that further studies are necessary to clarify this point.

This work was supported by a Grant in Aid for Science Research from the Ministry of Education, Scinece, and Culture, Japan, and published in Phys. Rev. B.[18]

REFERENCES

[1] J. Nagamatsu et al.: Nature (London) **410**, (2001) 63.
[2] Z. Kurmaev et al.: cond-mat/0103487.
[3] T.A. Callcott et al.: Phys. Rev. B**64**, 132504 (2001)
[4] S.L. Bud'ko et al.: Phys. Rev. Lett. **86**, 1877 (2001).
[5] H. Schmidt et al.: Phys. Rev. B **63**, 220504 (2001).
[6] J. Kortus et al.: Phys. Rev. Lett. **86**, 4656 (2001).
[7] M. Imada, J. Phys. Soc. Jpn. **70**, 1218 (2001).
[8] K. Yamaji, J. Phys. Soc. Jpn. **70**, 1476 (2001).
[9] K. D. Belashchenko et al.: Phys. Rev. B **64**, 092503 (2001)
[10] G. Satta et al.: Phys. Rev. B **64**, 104507 (2001)
[11] J.M. An and W. E. Pickett, Phys. Rev. Lett. **86**, 4366 (2001).
[12] S. Suzuki et al.: J. Phys. Soc. Jpn. **70**, 1206 (2001).
[13] D. Kaczorowski et al.: cond-mat/0103571.
[14] V.A. Gasparov et al.: cond-mat/0104323.
[15] A.S. Cooper et al.: Proc. Nat. Acad. Sci. **67**, 313 (1970).
[16] J. Akimitsu et al., Abstract for 2001 Annual meeting of Physical Society of Japan, Vol 3. p.533.
[17] L. Leyarovskaya and E. Leyarovski, J. Less Common Met. **67**, 249 (1979).
[18] J. Nakamura et al., Phys. Rev. B **64**, 174504 (2001).

Email: jin@pc.uec.ac.jp.

Polarization-dependent soft-x-ray absorption of highly oriented ZnO microrod-array

J.-H. Guo[1], L. Vayssieres[2], C. Persson[2], R. Ahuja[2], B. Johansson[2], and J. Nordgren[2]
[1]Advanced Light Source, Lawrence Berkeley National Laboratory, Berkeley, CA 94720
[2]Department of Physics, Uppsala University, Box 530, S-75121 Uppsala, Sweden

Zinc oxide represents an important basic material (II-VI semiconductor) due to its low cost, wide bandgap as well as its electrical, optoelectronic and luminescent properties. ZnO is of importance for fundamental research as well as relevant for various fields of industrial and high technological applications. Recently, a low threshold lasing action has been observed at room temperature in highly oriented ZnO nanorod arrays. From a fundamental point of view, it is crucial to probe and understand the electronic structure of such novel materials to tailor their physical properties as well as developing novel and improved devices. A novel approach to materials chemistry has been developed which contributed to the fabrication of purpose-built nano/microparticulate thin films from aqueous solution[1]. Such well-defined and well-ordered materials should contribute to reach required enhanced fundamental knowledge of the relation between structure and physical properties.

Here we report a polarization-dependent x-ray absorption spectroscopy (XAS) study performed at synchrotron radiation facility on highly oriented ZnO microrods. The experiments were performed on BL7.0.1 at the ALS[2]. The x-ray absorption spectra were measured by recording the total electron yield while scanning the photon energy over the O *1s*-edge region at a resolution of 0.2 eV. The XAS experiments were carried out on two different (isotropic and anisotropic) homogeneous and crystalline zincite ZnO (wurtzite) thin film samples, i.e. ZnO spheres, which consist of monodisperse spherical particles of 150 nm in diameter, and ZnO microrods consisting of monodisperse, anisotropic and highly oriented crystallites grown along the c-axis and perpendicular to a transparent conducting glass substrate (F-SnO2)\cite{Vayssieres01a}. The microrods of 10 μm in length and 1.5 μm in width are oriented normal to the substrate surface.

The polarization-dependent x-ray absorption measurements are shown in Figure 1. The variations in the spectral shape continue up to 30 eV above the absorption threshold. The resolved absorption features are indicated as a_1-a_8. Prior to a_1, no polarization-dependence is observed in x-ray absorption spectra for either sample. However at higher photon energies, strong anisotropic effects are observed for the ZnO microrods (bottom spectra). Measuring at grazing incidence geometry, i.e. incidence angle $\theta = 10$ degrees, where the absorption features a_3, a_5, and a_8 are stronger, the excitation to the state along the *c*-axis of the wurtzite structure is enhanced. At normal incidence geometry, i.e. $\theta = 90$ degrees, where the absorption features a_2, a_4, and a_7 are stronger, the excitation to the in-plane state is enhanced. No significant change is observed for the isotropic samples of ZnO consisting of spherical particles as a function of the polarization angle. However, all the absorption features are averaged out and observed in the

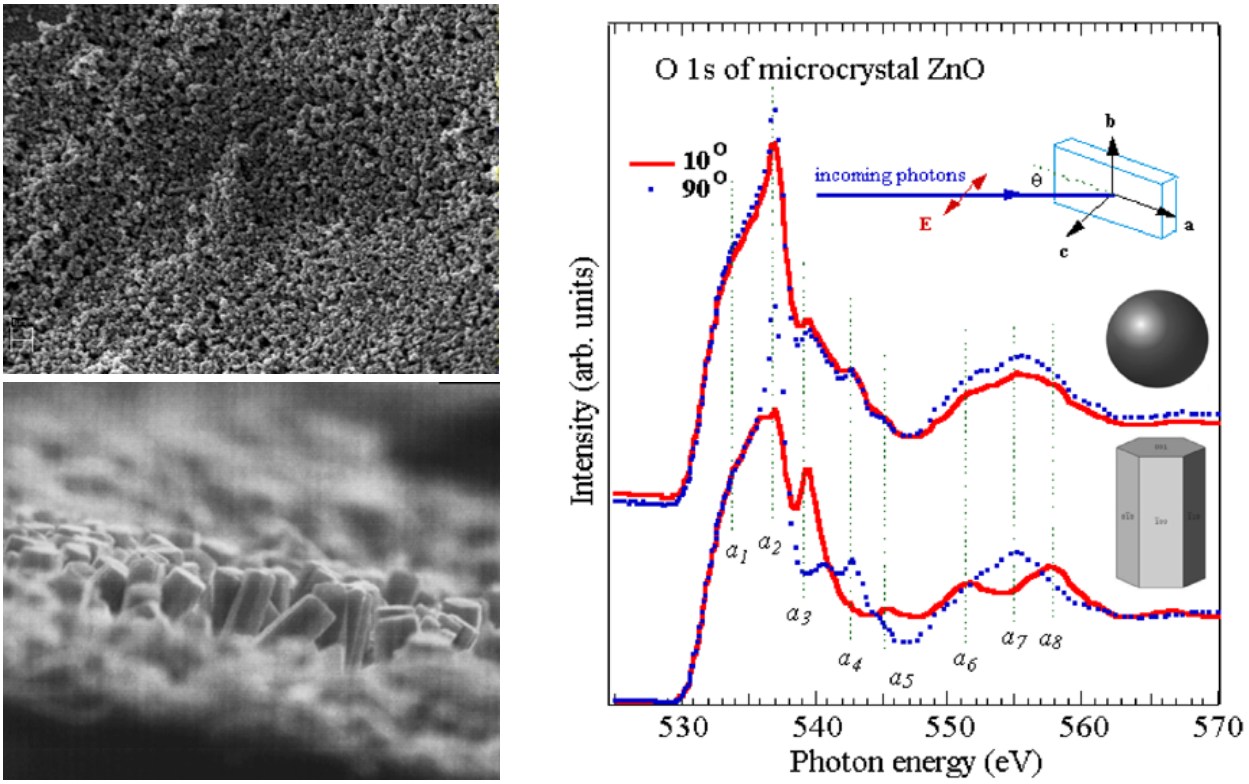

Fig. 1. Polarization-dependent x-ray absorption measurements.

XAS spectra measured with either geometrical detection. The experimental findings suggest a strong correlation between the electronic structure and the geometrical structure of the crystalline ZnO arrays. Such results demonstrate that designing materials with the appropriate morphology and orientation, i.*e purpose-built* materials, enables to reach better fundamental understanding of nano/microscale materials and their physical properties. Probing the orbital symmetry of oxygen and resolving its contribution to the conduction band of this important large band-gap II-VI semiconductor is of crucial importance for the understanding of its optoelectronic properties.

References:

1. L. Vayssieres, A. Hagfeldt and S. E. Lindquist, Pure Appl. Chem. **72**, 47 (2000).
2. T. Warwick, P. Heimann, D. Mossessian, W. McKinney and H. Padmore, Rev. Sci. Instrum. **66**, 2037 (1995).

This work was supported by the Swedish Natural Science Research Council (NFR), Council for Engineering Sciences (TFR), and the Göran Gustafsson Foundation for Research in Natural Science and Medicine (GGS). Department of Energy Materials Sciences Division Contract DE-AC03-76SF00098.

Principal investigator: Jinghua Guo, Advanced Light Source, LBNL. E-mail: jguo@lbl.gov.
Telephone: 510-495-2230.

Quantum confinement observed in α-Fe_2O_3 nanorod-array

J.-H. Guo[1], L. Vayssieres[2], C. Såthe[2], S. M. Butorin[2], and J. Nordgren[2]
[1]Advanced Light Source, Lawrence Berkeley National Laboratory, Berkeley, CA 94720
[2]Department of Physics, Uppsala University, Box 530, S-75121 Uppsala, Sweden

Resonant inelastic x-ray scattering (RIXS) has been applied to the studies of *dd* excitations in MnO and $SrCuO_2Cl_2$ [1,2]. The lowest-lying electronic excitations can be studied most directly by charge neutral spectroscopies, such as electron energy-loss spectroscopy (EELS) and optical absorption. The dd excitations in transition metal compounds are dipole forbidden and therefore very faint in optical spectroscopy.

α-Fe_2O_3 is an antiferromagnetic charge transfer insulator with a bandgap of 2.1 eV. Hematite crystallises in the trigonal system, rhombohedral R-3c group. The crystal structure is the corundum type (Al_2O_3) and can be described as a hexagonal close packed layering of oxygen with 6-fold co-ordinated iron ions yielding to face and edge-sharing octahedra. In an octahedral symmetry, a d^5-configuration is found to have well-separated dd-excitations. Optical absorption spectroscopy of α-Fe_2O_3 has revealed many transitions ranging from infrared to ultraviolet.

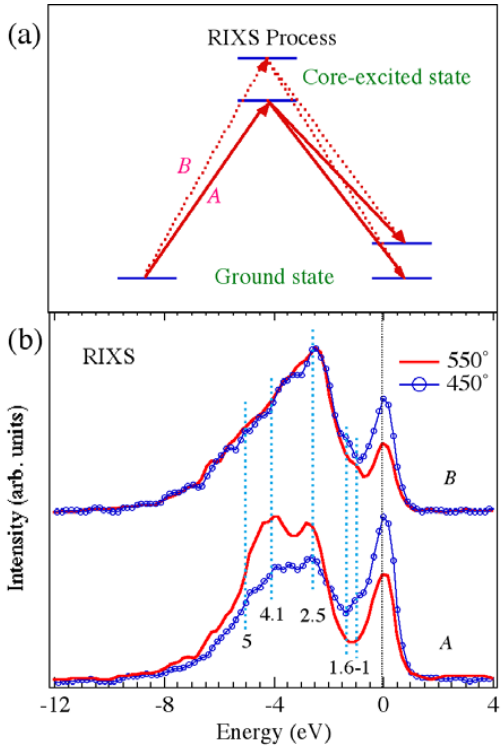

Using the RIXS process, we probed specifically the *dd* excitations in α-Fe_2O_3 by transition sequence $2p^63d^5 \rightarrow 2p^53d^6 \rightarrow 2p^63d^5$. These *dd* transitions become fully allowed, and their intensity can be more easily calculated than that in optical spectroscopy and EELS.

The experiments were performed at beamline 7.0.1 [5] at Advanced Light Source, Lawrence Berkeley National Laboratory. The photon energy resolution was set to 0.2 eV for x-ray absorption spectroscopy (XAS) measurement. The resonant x-ray Raman scattering was measured using a grazing-incidence grating spectrometer [6]. The resolution of both monochromator and fluorescence spectrometer in RIXS measurement was set to 0.5 eV.

The measurements were done on synthetic α-Fe_2O_3 nanorods grown by Controlled Aqueous Chemical Growth [7]. The samples investigated in this letter are thin films, which consist of 3D crystalline array of hematite nanorods bundles of 50 nm in diameter and 500 nm in length perpendicularly oriented onto the substrate. Each bundle was found to consist of self-assembled nanorod of 3-5 nm in diameter. The samples were prepared by

heteronucleation growth and thermodynamic stabilization of akaganeite (β-FeOOH) in solution at 90˚C onto the substrate and subsequently heated in air to 550˚C to allow the crystal phase transition to hematite (α-Fe_2O_3) as confirmed by XRD.

In the resonant inelastic x-ray scattering process, final states probed via such a channel, which are related to eigenvalues of the ground state Hamiltonian. The core-hole lifetime is not a limit on the resolution in this spectroscopy [2]. According to the many-body picture, an energy of a photon, scattered on a certain low-energy excitation, should change by the same amount as a change in an excitation energy of the incident beam (see the decay route of core-excitation *B* versus that of *A* in Fig. 1a). Thus, the RIXS features have constant energy losses and follow the elastic peak.

The RIXS spectra at the Fe *L*-edge of α-Fe_2O_3 nanorods were recorded and shown in Fig.1. A few energy-loss features are clearly resolved. The low energy excitations, such as the strong dd and charge-transfer excitations, are identified in the region from 1 to 5 eV. The 1-eV and 1.6-eV energy-loss features originate from multiple excitation transitions. The 2.5-eV excitation corresponds to the bandgap transition, which is significantly larger than the 2.1-eV-bandgap of single-crystal hematite.

References:

1. S. M. Butorin, J.-H. Guo, M. Magnuson, P. Kuiper, and J. Nordgren, Phys. Rev. B **54**, 4405 (1996).
2. P. Kuiper, J.-H. Guo, C. Såthe, L.-C. Duda, J. Nordgren, J. J. M. Pothuizen, F. M. F. de Groot, and G. A. Sawatzky, Phys. Rev. Lett. **80**, 5204 (1998).
3. L. A. Marusak, R. Messier, and W. B. White, J. Phys. Chem. Solids **41**, 981 (1980).
4. L.-C. Duda, J. Nordgren, G. Dräger, S. Bocharov, Th. Kirchner, J. Electr. Spectros. and Related Phenom. **110-111**, 275 (2000).
5. T. Warwick, P. Heimann, D. Mossessian, W. McKinney and H. Padmore, Rev. Sci. Instrum. **66**, 2037 (1995).
6. J. Nordgren, G. Bray, S. Cramm, R. Nyholm, J. E. Rubensson, and N. Wassdahl, Rev. Sci. Instr. **60**, 1690 (1989).
7. L. Vayssieres, H. Beermann, S.-E. Lindquist, and A. Hagfeldt, Chem. Mater. (in press, 2000).

This work was supported by the Swedish Natural Science Research Council (NFR), Council for Engineering Sciences (TFR), and the Göran Gustafsson Foundation for Research in Natural Science and Medicine (GGS). Department of Energy Materials Sciences Division Contract DE-AC03-76SF00098.

Principal investigator: Jinghua Guo, Advanced Light Source, LBNL. E-mail: jguo@lbl.gov. Telephone: 510-495-2230.

Soft X-Ray Emission and Absorption Spectra in the Si *L* Region of Polysilanes

Y. Muramatsu[1], M. Fujino[2], E. M. Gullikson[3] and R. C. C. Perera[3]
[1]*Japan Atomic Energy Research Institute, Sayo-gun, Hyogo 679-5148, Japan*
[2]*NTT Basic Research Laboratories, Atsugi, Kanagawa 243-0198, Japan*
[3]*CXRO, Lawrence Berkeley National Laboratory, Berkeley, California 94720, USA*

Substituted polysilanes, (SiRR')n, have attracted significant attention because of their unique electronic properties. Their characteristic electronic nature arises from band edge structures which are composed of valence and conduction bands from σ and σ* bands, respectively, which differ from the electronic structure of polyacetylene. To further understand their electronic properties, we have measured the Si *L* x-ray emission spectra of a number of polysilanes with alkyl and phenyl substituents. In addition, their x-ray absorption spectra have also been measured to obtain information regarding unoccupied electronic orbitals.

Chemically synthesized polysilanes, $(SiR_2)n$, where R indicates substitution with a methyl (Me; CH_3), ethyl (Et; C_2H_5), propyl (Pr; n-C_3H_7), butyl (Bu; n-C_4H_9), pentyl (Pe; n-C_5H_{11}) or phenyl (Ph; C_6H_5) group, were used for spectroscopic measurements. Soft x-ray emission spectra in the Si *L* region were measured using a grating x-ray spectrometer installed in the undulator beamline, BL-8.0.1. The photon energy of the monochromatized incident beam was tuned to about 130 eV to effectively excite Si2p-electrons while preventing multiple ionizations. Total-electron-yield (TEY) x-ray absorption spectra were obtained by monitoring sample photocurrent in BL-6.3.2. Measured x-ray emission and absorption spectra were analyzed using discrete variational (DV)-Xα molecular orbital calculations.

Figure 1 shows soft x-ray emission and absorption spectra in the Si *L* region of both the polysilanes and the reference compounds, Si and SiO_2. In the emission spectra, polysilane spectral features exhibited similar structures; a main peak near 90 eV, and high-energy and low-energy shoulders clearly differ from those of the Si and SiO_2 references. In absorption spectra, alkyl-substituted polysilanes exhibit a threshold energy of 101 eV, while the Ph-substituted polysilane exhibits a slightly lower threshold energy. In the fine-structure at the thresholds of polysilanes, a pre-edge peak is observed near 101 eV and an intense peak is seen at 102 eV for the Ph-substituted polysilane. No such pre-edge or intense peaks, however, are observed in the spectra of alkyl-substituted samples. From spectral analysis using DV-Xα molecular orbital calculations Si *L* x-ray emission spectra, which include a main peak with high- and low-energy shoulders, are explained by the summed DOS spectra of occupied Si3s and Si3d orbitals hybridized with Si3p, C2s and C2p orbitals. X-ray absorption spectra are also qualitatively explained by the summed DOS spectra of unoccupied Si3s and Si3d orbitals. In both x-ray emission and absorption spectra, little difference is observed among alkyl-substituted polysilanes. It is therefore confirmed that the length of alkyl substituents has little effect on the electronic structure of the Si backbone. X-ray spectral features of the Ph-substituted polysilane, however, slightly differ from alkyl-substituted features. This is explained by the difference in hybridization of Si and C orbitals between sp^2-C atoms in phenyl substituents and sp^3-C atoms in alkyl ones.

We thank Dr. J. Denlinger of the Lawrence Berkeley National Laboratory for his help and support in performing x-ray emission measurements. This work has been supported by the Hyogo Science and Technology Association and the US Department of Energy under contract No. DE-AC03-76SF00098.

Principal Investigator: Yasuji Muramatsu, Japan Atomic Energy Research Institute. Email: murama@spring8.or.jp. Telephone: +81-791-58-2601.

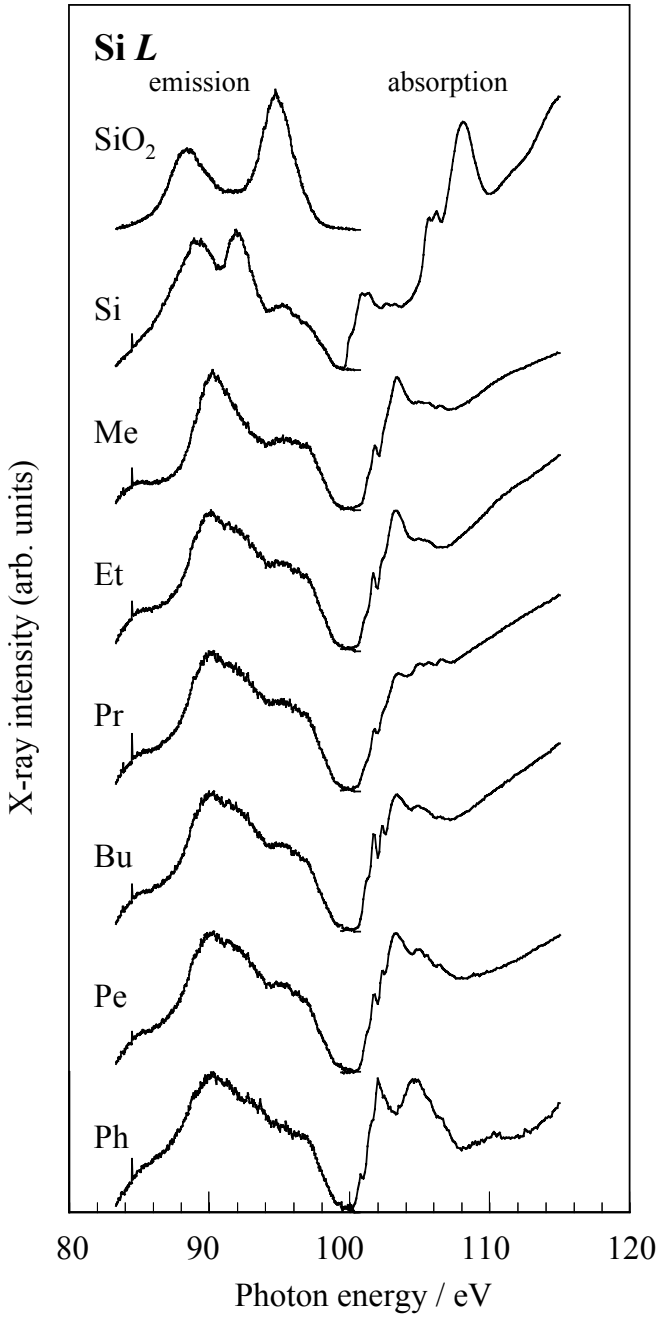

Figure 1 Soft x-ray emission and TEY x-ray absorption spectra in the Si *L* region of the polysilanes, $(SiR_2)n$, and Si and SiO_2 reference compounds. Substituents in the polysilanes, R, are denoted by Me (CH_3), Et (C_2H_5), Pr (n-C_3H_7), Bu (n-C_4H_9), Pe (n-C_5H_{11}), and Ph (C_6H_5).

Soft X-ray emission spectroscopy of the liquid-solid interface between water and a $Cu(In,Ga)(S,Se)_2$ thin film solar cell absorber

C. Heske[1], U. Groh[1], O. Fuchs[1], L. Weinhardt[1], E. Umbach[1], Ch.-H. Fischer[2], Th. Schedel-Niedrig[2], M.Ch. Lux-Steiner[2], S. Zweigart[3], F. Karg[3], J.D. Denlinger[4], B. Rude[4], C. Andrus[5], and F. Powell[5]

[1]Experimentelle Physik II, Universität Würzburg, Am Hubland, D-97074 Würzburg, Germany
[2]Hahn-Meitner-Institut, Glienicker Str. 100, D-14109 Berlin, Germany
[3]Siemens & Shell Solar GmbH, SSSG T, Otto-Hahn-Ring 6, D-81739 München, Germany
[4]Advanced Light Source, 1 Cyclotron Rd., Berkeley, CA 94720
[5]Luxel Corp., 515 Tucker Ave., Friday Harbor, WA 98250

INTRODUCTION

The development of experimental methods to probe the properties of liquid-solid interfaces is one of the fundamental issues for understanding a multitude of natural and technological processes involving liquids. Up to date, however, very few experiments have been performed to learn about the electronic structure, particularly if an atom-specific point of view is desired. While in surface science such information can easily be derived from photoelectron spectroscopy, this approach is not viable for the study of liquid-solid interfaces due to the limited information depth of PES. Thus, the necessity to probe "through" a liquid (or solid) layer calls for photon-in-photon-out experiments. The soft X-ray regime, however, which is the most suitable to study core and valence states of light elements, has not yet been explored, mostly due to the high attenuation of soft X-rays in matter. In this report we demonstrate that soft X-ray emission spectroscopy (XES) can be used to investigate the chemical and electronic properties of particular atoms at liquid-solid interfaces, in this case the water–$Cu(In,Ga)(S,Se)_2$ interface. Furthermore, we will show that, with XES, it is possible to monitor interfacial chemical reactions with high spectral resolution *in-situ*.

MATERIAL SYSTEM

$Cu(In,Ga)(S,Se)_2$ (CISSe) is widely used as an absorber material in thin film solar cells, and conversion efficiencies up to 18.8 % have been achieved [1]. Apart from being a model system for the present investigation, the water–CISSe interface is of large importance for two reasons. First, a complete CISSe solar cell is comprised of several thin film layers, including the CISSe absorber layer and a thin (approx. 20 nm) CdS buffer deposited in a chemical *bath* deposition process. The CdS/CISSe interface plays one of the central roles in understanding the electronic structure of the devices. Hence, the possibility to study liquid-solid interfaces *in-situ* allows the monitoring of the substrate, the growing film, and the interface formation process from a spectroscopic point of view. Secondly, one of the main issues on the way to a complete industrial product is the control of humidity impact on the electronic cell properties. The investigation of the relevant water–solid interfaces is expected to shed light on the chemical and electronic changes induced by the humidity on an accelerated time scale.

EXPERIMENTAL

High-resolution soft X-ray emission spectroscopy was performed at beamline 8.0 utilizing the SXF endstation. Beamline 8.0 allows experiments with an excitation photon flux of about 4 x

10^{15} photons/sec near the sulfur $L_{2,3}$ edge. Thin films of CISSe were prepared in a rapid thermal process of elemental precursor layers on Mo-coated soda-lime glass in a sulfur-containing environment. The experiments were performed in ultra-high vacuum (UHV) utilizing suitably designed stainless steel liquid cells, which were glued to the CISSe sample surface with a UHV-compatible epoxy. In the design of the liquid cells, a channel of 1.3 μm of liquid water was created between the CISSe surface and a 1 μm-thick polyimide (PI) window. After hardening of the epoxy (approx. 24 hours), the complete assembly was transferred into UHV for experiments. Reference experiments were also conducted on "bare" CISSe films as well as on PI/Vacuum/CISSe sandwich structures.

RESULTS

Fig. 1 presents a set of sulfur $L_{2,3}$ emission spectra obtained by excitation well above the absorption edge ($h\nu$ = 200 eV). The bottom spectrum was obtained from the "bare" CISSe film surface, i.e., taken directly from the solar cell production line. Peak (1) stems from the emission of sulfur atoms bound in a sulfide environment, and is due to photons emitted by filling S 2p core holes with S 3s electrons [2]. Peaks (2) are associated with the same electronic transition, but for sulfur atoms bound to oxygen. In the present case, the absence of an additional peak around 161.1 eV indicates that at most two oxygen atoms are bound to each probed sulfur atom. The broad peak (3) is due to Cu 3d states in the upper valence band of CISSe and, because of the local nature of the excitation, is indicative of sulfur-copper bonds. In short, the spectral features of the sulfur XES spectrum give a wealth of detailed information about the local chemical bond of the sulfur atoms, which can now be used to monitor interfacial processes.

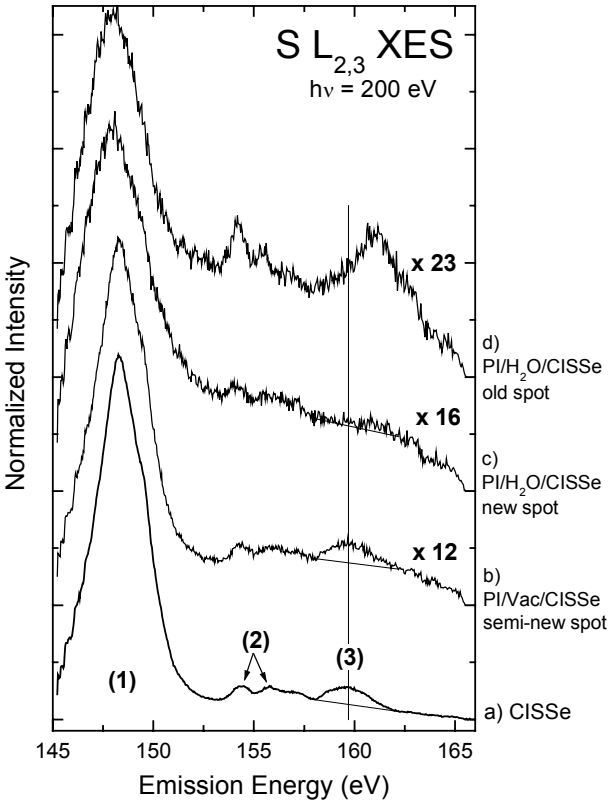

Figure 1. S $L_{2,3}$ X-ray emission spectra of a $Cu(In,Ga)(S,Se)_2$ (CISSe) thin film solar cell absorber film (a) taken from the production process, (b) seen through a 1 μm polyimide (PI) window, and under an additional 1.3 μm water layer (c: new sample spot, d: old sample spot). Samples "under water" show a reduced intensity of the S-Cu-bond and, after X-ray exposure, a sulfate formation.

As indicated in Fig. 1 by the magnification factors at the right hand side, the observed signal intensity is reduced by both the PI window as well as the liquid water layer. These attenuation factors indicate the necessity to use high-flux excitation from a third generation synchrotron source. Note that the PI window is damaged by extended exposure to X-rays. Thus, the transmission decreases as a function of exposure within the probed area, and hence the "age" of the spot also factors into the signal attenuation. The "age" of the different spectra is given on the right-hand side of Fig. 1. A closer inspection of spectra a) and b) reveals that no changes are observed for the PI/Vacuum/CISSe sample (as expected). However, we find a reduction of the intensity associated with sulfur-copper

bonds (peak 3) due to the 24 hour storage "under water" (spectrum c). An even more pronounced spectral change is observed after exposure to X-rays (30 min, spectrum d). Based on the strong S 3d-related emission at 161.1 eV, this spectral change is interpreted as a sulfate formation at the water/CISSe interface.

Apart from a detailed look at the chemical and electronic environment of sulfur atoms, also the Na K_α emission line proves to be a helpful tool to monitor the interfacial reaction at the water/CISSe interface. Na-assisted growth has been shown to substantially improve the efficiency of the CISSe solar cells. Until today, the impact of the Na has not been fully clarified, mostly because several enhancing mechanisms have been proposed and because, due to the complexity of the system, these different mechanisms are not easily separable. An established model by Kronik et al. [3] suggests an interaction of sodium and oxygen at the CISe surface. Nevertheless, apart from a co-adsorption study in ultra-high vacuum [4], no direct experimental evidence of a chemical interaction between sodium and oxygen has yet been reported. Such a direct correlation can now be derived from a simultaneous recording of Cu L_α and Na K_α XES spectra. As expected, we find a small Na signal on the CISSe surface, which does not change in intensity for the PI/Vacuum/CISSe sample. Also, the 24-hour storage under water only leads to a small increase. In contrast, when exposing the sample to the soft X-ray beam, we find a dramatic increase of the Na content at the interface in the course of time, in parallel with the above-discussed surface oxidation (sulfate formation). Apparently, the possibility to form a sulfate species attracts Na atoms from the CISSe film towards the surface. Here, the original driving force could be the X-ray-induced creation of O^{2-} and/or OH^- ions, which then react with the CISSe surface and alter the free energy, such that Na atoms diffuse to the water/CISSe interface. Also the opposite process, namely that the X-ray excitation attracts Na atoms to the surface (e.g., by sample heating), which then act as a catalyst for the surface oxidation, appears possible. Future studies utilizing mini-cells with integrated thermocouples will have to clarify which one of the two scenarios holds true.

In summary, we have presented an experimental investigation of a sulfate formation at the water/CISSe interface. The findings demonstrate that there is a direct correlation between oxidation and sodium enrichment at the interface. The demonstrated general approach of utilizing X-ray emission spectroscopy to study chemical reactions in-situ can be extended to many other liquid-solid interfaces and also lends itself to the study of liquids and solutions as well.

REFERENCES

1. M. A. Green, K. Emery, D. L. King, S. Igari, and W. Warta, Solar Cell Efficiency Tables (Version 17); Progr. Photovolt. Res. Appl. **9**, 49 (2001).
2. C. Heske, U. Groh, O. Fuchs, E. Umbach, N. Franco, C. Bostedt, L.J. Terminello, R.C.C. Perera, K.H. Hallmeier, A. Preobrajenski, R. Szargan, S. Zweigart, W. Riedl, and F. Karg, phys.stat.sol. (a) **187**, 13 (2001).
3. L. Kronik, D. Cahen, and H.W. Schock, Adv. Materials **10**, 31 (1998).
4. C. Heske, G. Richter, Zhonghui Chen, R. Fink, E. Umbach, W. Riedl, and F. Karg, J. Appl. Phys. **82**, 2411 (1997).

This work was supported by the german ministries BMBF (FKZ 01SF007) and BMWI (FKZ 0329889, FKZ 0329218C), as well as the DFG through SFB 410, TP B3.

Principal investigator: Clemens Heske, Eberhard Umbach, Experimentelle Physik II, University of Würzburg, Germany. Email: heske@physik.uni-wuerzburg.de. Telephone: ++49-931-888-5127.

Soft X-ray Probe of Bulk Bandgaps in Divalent Hexaborides

J. D. Denlinger[1], J. W. Allen[2] and Z. Fisk[3]
[1]Advanced Light Source, Lawrence Berkeley National Lab, Berkeley, California 94720, USA
[2]Department of Physics, University of Michigan, Ann Arbor, Michigan 48109, USA
[3]NHMFL, Florida State University, Tallahassee, Florida 32306, USA

INTRODUCTION

The discovery of weak itinerant ferromagnetism in certain divalent hexaborides [1] provides strong motivation to determine the underlying electronic structure giving rise to the metallic carriers. One possibility predicted by LDA band calculations [2] and supported by the interpretation given to magneto-oscillatory studies [3] is a semi-metallic band overlap at the X-point of the cubic Brillouin zone, the absence of which would render stoichiometric material to be insulating. Several theoretical discussions of excitonic insulator origins of the novel ferromagnetism [4] presume the existence of such an overlap. However, a recent quasiparticle band calculation [5] that includes a GW self energy correction, instead predicts CaB_6 to be a semiconductor with a 0.8 eV band gap at the X-point.

Such an X-point band gap (>1 eV) is observed in angle resolved photoemission (ARPES) of CaB_6, SrB_6 and EuB_6 [6] providing strong experimental proof of this new semiconducting model for the divalent hexaborides. Reported here are bulk sensitive soft x-ray emission and absorption data (SXE and XAS, respectively) that provide additional proof of the existence of this semiconducting bandgap complementary to the k-dependent band structure information revealed by ARPES. Also consistent with ARPES, the SXE/XAS measurements imply that the chemical potential is at the bottom of the conduction band indicating the presence of excess electrons arising from nonstoichiometric defects. This situation would be consistent with a picture in which the novel magnetic moments in divalent hexaborides are carried by boron vacancies [7]

EXPERIMENT

Single crystal hexaboride samples were grown from an aluminum flux using powders prepared by boro-thermally reducing cation oxides. Soft x-ray emission and absorption experiments were performed at the ALS Beamline 8.0.1 using the Tennessee/Tulane grating spectrometer. The experimental emission and absorption spectral resolutions were ≈0.35 eV and ≈0.1 eV, respectively. SXE at and above the B K-edge threshold, is used as a probe of the occupied boron 2p partial density of states. X-ray absorption, a probe of the unoccupied states, was measured both with total electron yield (TEY) as a function of photon energy and also with partial fluorescence yield (PFY) with the detection window covering the entire valence band emission. Differences between TEY and PFY signals arise from differing attenuation lengths and the experimental geometry which was set to 60° incidence excitation and 30° grazing emission relative to the sample surface. Absolute PFY energies were calibrated to published TEY spectra of the hexaborides [8] and SXE spectra were calibrated to the excitation energy using an elastic scattering peak in the emission spectra.

RESULTS

Fig. 1 shows a representative data set of soft x-ray emission and absorption at the boron K-edge for the divalent hexaborides. Data very similar to that shown here for CaB_6 was also obtained for SrB_6, EuB_6, and YbB_6. Fig. 1(a) compares the two methods of measuring x-ray absorption, TEY and PFY. TEY, a measurement of the sample current, exhibits a sharp peak at ≈194 eV corresponding to a well-known B 1s→2p π^* transition [8] which in part arises from surface layer

oxidation of the air-cleaved sample. Also the absolute TEY signal exhibits a high background (removed in Fig. 1(a)) with declining slope due to the presence of lower energy absorption edges. In contrast, the PFY signal, a measure of valence emission intensities integrated over the energy window shown in Fig. 1(b), does not exhibit the sharp TEY absorption peak due to a greater bulk emission sensitivity. Also the valence band PFY signal inherently has zero pre-threshold intensity and hence is preferred over TEY for careful measurement of the threshold region. The PFY spectrum for CaB_6 shows a weak step-like threshold onset at 188.0 eV (highlighted in the logarithmic scale inset to Fig. 1(a)). We interpret the half-step intensity of this threshold onset in the PFY spectrum as the energy position of the chemical potential in the conduction band.

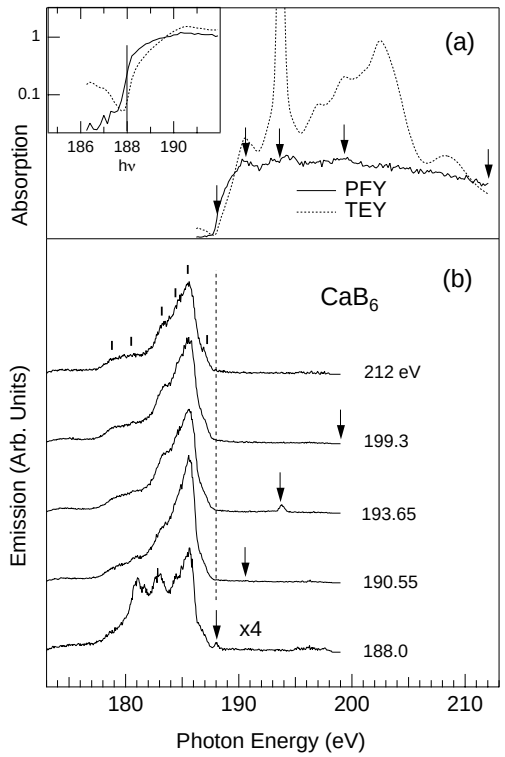

Figure 1. Soft x-ray absorption (TEY, PFY) and emission (SXE) boron K-edge data set for CaB_6. Arrows and values indicate the excitation energies. The logarithmic intensity scale of the inset highlights the step intensity onset of the PFY signal with comparison to the TEY threshold.

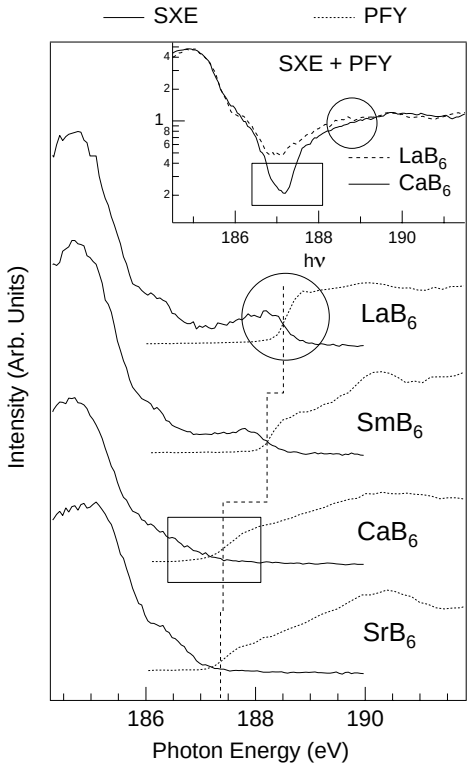

Figure 2. B K-edge SXE and PFY spectra for various hexaborides. The dashed line indicates the half-height energy position of the PFY threshold. Inset: Logarithmic intensity scale comparison of the total DOS, i.e. sum of emission and absorption, for CaB_6 and LaB_6 with the valence band edge of the DOS aligned.

Valence band emission spectra, shown in Fig. 1(b) were acquired at selected photon energies indicated by arrows in Fig. 1. An elastic peak present in the emission spectra is resonantly enhanced at the B 1s→2p absorption peak and is used for calibration of the SXE energy scale to that of TEY and PFY spectra. Excitation at the selected peaks in the PFY/TEY spectra and far above threshold show similar valence band emission profiles with small variations in the relative intensities of at least six discernable peaks and shoulders. Threshold excitation on the other hand produces much larger variation in the relative intensities (and energies) of the different valence emission peaks (discussed in the next section). The elastic peak is also observed to be enhanced at threshold, thus providing a distinct marker for the location of E_F. The non-threshold SXE spectra, on the other hand, exhibit a strong non-metallic decay of intensity approaching E_F and no distinct onset, in contrast to the PFY spectrum.

Fig. 2 shows a comparison of SXE/PFY spectra for two divalent hexaborides SrB_6 and CaB_6, and for mixed-valent SmB_6 and trivalent LaB_6, which contain 0.6 and 1 conduction electrons/formula unit, respectively. The PFY spectra have been normalized to have the same intensity far above threshold, while the SXE spectra have been normalized to have the same maximum amplitude. The overall PFY intensities were then scaled so that the SXE and PFY intensities for LaB_6 match at threshold. Within experimental resolution, a common SXE/PFY threshold occurs for SmB_6 and for LaB_6, as expected for simple metals. The increases in photon energy and intensity of the thresholds of SmB_6 and LaB_6 relative to the divalent systems and to each other are consistent with their differing conduction band fillings. In great contrast, for the divalent hexaborides, the strong decay of SXE intensity to its threshold and the weak PFY intensity at its threshold preclude the two spectra having a common onset.

The inset to Fig. 2 presents a more detailed comparison of CaB_6 and LaB_6 in which the SXE and PFY spectra have been summed and can be discussed as the boron partial DOS. In addition the LaB_6 spectrum has been shifted +0.3 eV, after summing, to align its valence band (185-186.5 eV) to that of CaB_6. The key motivation for this comparison is that apart from band filling, LDA calculations predict nearly identical total DOS for the divalent and trivalent systems. For LaB_6 the emission and absorption spectra meet smoothly so that the crossover place entirely disappears upon summing (see circles), whereas for CaB_6 a distinct dip remains over $\approx$1 eV around 187 eV (see rectangles). This distinct discrepancy immediately tells us that the band structures in the vicinity of the boron valence band maximum for CaB_6 and LaB_6 are different. The interpretation of this bulk-sensitive measurement as a band gap in the divalent hexaborides is strongly supported by the k-dependent view from ARPES which shows a >1 eV band gap in CaB_6 at the X-point in contrast to a 0.2 eV *overlap* of the same two bands in LaB_6 [9]. Additional analyses of the overall boron DOS bandwidth and energy centroid, and of threshold-excited SXE spectra provide complementary evidence of the bulk divalent band gap [10].

REFERENCES

1. D. P. Young *et al*, Nature **397**, 412 (1999); P. Vonlanthen *et al*, Phys. Rev. B **62**, 10076 (2000); H. R. Ott *et al*, Physica B **281-2**, 423 (2000); T. Terashima *et al*, J. Phys. Soc. Jpn. **69**, 2423 (2000).
2. A. Hasegawa and A. Yanase, J. Phys. C, Solid State Phys. **12**, 5431 (1979); S. Massidda, A. Continenza, T. M. D. Pascale, and R. Monnier, Z. Phys. B **102**, 83 (1997).
3. R. G. Goodrich *et al*., Phys. Rev. B **58**, 14896 (1998); M. C. Aronson *et al*., Phys. Rev. B **59**, 4720 (1999).
4. M. E. Zhitomirsky, T. M. Rice, and V. I. Anisimov, Nature **402**, 251(1999); L. Balents and C. M. Varma, Phys. Rev. Lett. **84**, 1264 (2000); V. Barzykin and L. P. Gor'kov, Phys. Rev. Lett. **84**, 2207 (2000).
5. H. J. Tromp *et al*., Phys. Rev. Lett. **87**, 016401 (2001).
6. J. D. Denlinger *et al*., cond-mat/0107429; and ALS Compendium, 2001.
7. R. Monnier and B. Delley, Phys. Rev. Lett. **87**, 157204 (2001).
8. J. J. Jia *et al*., J. Electron Spectrosc. Related Phenom. **80**, 509 (1996).
9. S.-K. Mo *et al*., cond-mat/0107203.
10. J. D. Denlinger, G.-H. Gweon, J. W. Allen, A. D. Bianchi and Z. Fisk, cond-mat/0107426; Surf. Rev. and Lett., in press.

This work was supported at U. of Michigan by the U.S. Dept. of Energy (DoE) under contract No. DE-FG02-90ER45416 and by the U.S. NSF under grant No. DMR-99-71611.

Principal investigator: Jonathan Denlinger, Advanced Light Source, LBNL. Email: JDDenlinger@lbl.gov. Telephone: 510-486-5648.

Soft X-Ray Spectroscopy of Noble Gas Atoms Doped in Solid Matrices

Y. Muramatsu[1], and R. C. C. Perera[2]

[1]*Japan Atomic Energy Research Institute, Sayo-gun, Hyogo 679-5148, Japan*

[2]*CXRO, Lawrence Berkeley National Laboratory, Berkeley, California 94720, USA*

We have measured the soft x-ray emission and absorption spectra of noble-gas atoms doped in carbon, silicon and metal substrates, to investigate their chemical states in solid matrices. Argon or neon ion beams were directed into the solid matrices of highly oriented pyrolytic graphite (HOPG), Si(111), SiO_2, Ti, Cr, Ni and Cu with an acceleration voltage of 5 kV. Soft x-ray emission and absorption spectra in the Ar *L* and Ne *K* regions of Ar- and Ne-doped samples were measured using a grating x-ray spectrometer installed in the undulator beamline, BL-8.0.1. Figure 1 shows the Ar *L* x-ray emission spectra of Ar-doped Si(111) measured with excitation energies of (a) 399.6 eV and (b) 256.6 eV. The subtracted spectrum of (a) – (b), clearly indicates that peak structures are observed on the higher-energy sides of both $L\alpha$ and $L\beta$ peaks arising from 399.6-eV excitation. These peak structures may be due to multiple ionizations. Figure 2 shows the Ar *L* x-ray emission spectra of Ar-doped Si(111), HOPG, Ti and Cu measured with 256.6-eV excitation. Peak widths of $L\alpha$ and $L\beta$ peaks in the Ar *L* x-ray emission spectra from Ti and Cu matrices are broader than that of the Si(111) and HOPG matrices. A similar peak broadness was also observed in the Ne *K* x-ray emission spectra of Ne-doped metal matrices. Such peak broadness may be explained by the formation of noble gas bubbles in the metals. To further explain peak broadness in the spectra, molecular orbital calculations are currently in progress. We thank Dr. J. Denlinger of the Lawrence Berkeley National Laboratory for his help and support in performing x-ray emission measurements. This work has been supported by the Hyogo Science and Technology Association and the US Department of Energy under contract No. DE-AC03-76SF00098. Principal Investigator: Yasuji Muramatsu, Japan Atomic Energy Research Institute. Email: murama@spring8.or.jp. Telephone: +81-791-58-2601.

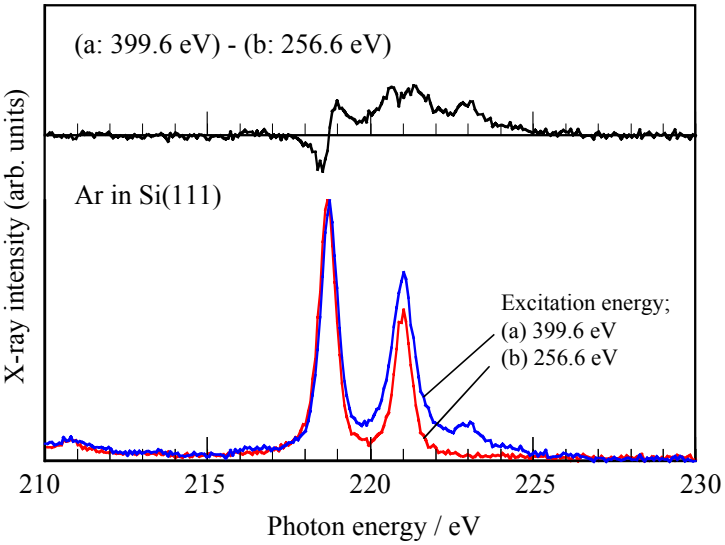

Figure 1 Ar *L* x-ray emission spectra of Ar-doped Si(111) with excitation energies of (a) 399.6 eV and (b) 256.6 eV. Upper panel shows the subtracted spectrum, (a) – (b).

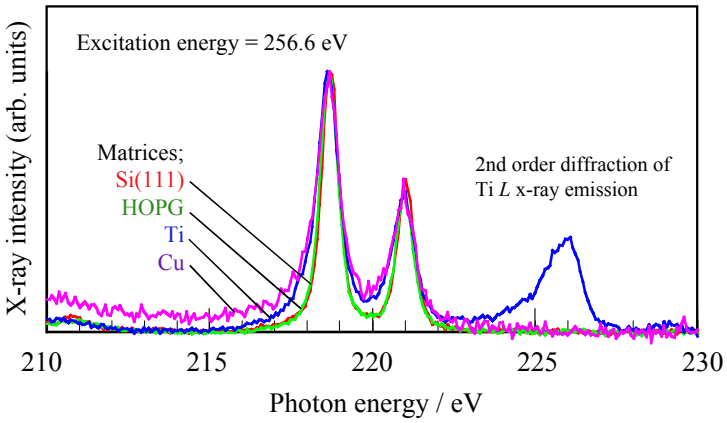

Figure 2 Ar *L* x-ray emission spectra of Ar-doped Si(111), HOPG, Ti, and Cu matrices. Excitation energy was tuned to 256.6 eV.

Spectroscopic observation of polaron-lattice band structure in the conducting polymer polyaniline

E.Z. Kurmaev[1], M.I. Katsnelson[1], A. Moewes[2], M. Magnuson[3], J.-H. Guo[3], S.M. Butorin[3], J. Nordgren[3], D.L. Ederer[4], and M. Iwami[5]

[1]Institute of Metal Physics, Russian Academy of Sciences-Ural Division, 620219 Yekaterinburg GSP-170, Russia
[2]University of Saskatchewan, Department of Physics and Engineering Physics, Saskatoon, SK S7N 5E2, Canada
[3]Department of Physics, Uppsala University, Uppsala, P.O. Box 530, S-75 121, Sweden
[4]Department of Physics, Tulane University, New Orleans, LA 70118, USA
[5]Research Laboratory for Surface Science, Okayama University, Okayama 700-8530, Japan

Interest in polyanilines has been reinforced by the discovery of their high electrical conductivity observed in doped phases, giving rise to a new class of conducting polymers. Polyaniline can be prepared in three major forms that differ in the degree of oxidation *y* (the ratio of amine nitrogens over the total number of nitrogen atoms). For the fully reduced leucoemeraldine base (LEB) *y* is one, the half-oxidized emeraldine base (EB) *y* is 0.5 and for fully oxidized pernigraniline base (PNB) *y* is 0. Polyaniline is an insulator in each of these forms with a band gap of 3.6 eV for LEB and EB and about 1.4 eV for PNB. The polymers can also exist in the corresponding protonated (salt) forms but only emeraldine salt (ES) is highly electrically conductive in this case. The largest conductivity reported to date is about 400 S/cm [1], which is 14 orders of magnitude higher than for the insulating emeraldine base form. Protonation does not change the electronic concentration and a local distortion of the chemical bonds is giving rise to conductivity of the polymer. These distortions are commonly referred to as either a polaron (storing the extra positive charge when only one nitrogen is protonated) or a bipolaron (in the case that both imine nitrogens are protonated). In order to explain the conductive state of ES two models have been proposed. A regular distribution of polarons leaves the electronic band half-filled or the random bipolaron structure leads to the formation of extended electronic states at the Fermi energy. There is no direct spectroscopic evidence to date regarding the electronic structure of ES, which is essential for selecting the adequate picture.

We have studied the differences in the electronic structure of protonated and undoped polyemeraldine by means of soft x-ray emission spectroscopy (XES). Our findings support the application of the polaronic-metal model for highly conducting polymers.

The experiments were carried out at Beamlines 7.0 and 8.0.1 at the Advanced Light Source at the Lawrence Berkeley National Laboratory employing the Uppsala University [3] and University of Tennessee at Knoxville [4] endstations. Photons with energies well above the carbon K-edge (300 eV) and well above the nitrogen K-edge (412-430 eV) were delivered to the sample. The X-ray fluorescence spectrometer provides an energy resolution of 0.30 eV and 0.65 eV for the carbon and nitrogen measurements, respectively. For our measurements we have chosen the basic form of undoped and protonated polyemeraldine. The doped samples were prepared by protonation with 60% camphorsulphonic acid (CSA). The protonation with H^+ adds holes to the imine groups around the quinoid ring.

Figure 1 shows carbon Kα emission spectra (2p→1s transition) of undoped and protonated emeraldine converted to the binding energy scale [5]. The spectra are normalized to the same peak height in the intensity maximum. The intensity of the C Kα emission in the vicinity of the Fermi level E_F is clearly increased for the protonated emeraldine compared to the undoped sample. This finite density of states at the Fermi level evidences the metallicity of the doped phase. The same tendency of higher spectral intensity in the vicinity of the Fermi level for protonated polyemeraldine with respect to the undoped phase is observed in N Kα XES though these measurements have been performed with less energy resolution (due to the higher emission energy) and lower count rate than the carbon data, the latter being due to the smaller content of nitrogen atoms in polyaniline. Protonating increases the finite density of states near the Fermi level and the origin of the increase is the formation of the polaron band. In the case of the bipolaron band structure no finite density of states is expected near E_F. Recently, an extremely small finite density of states for protonated emeraldine has been observed in photoemission measurements [6]. The authors do not indicate the level of protonation and in a protonation of too low concentration could lead to such effect.

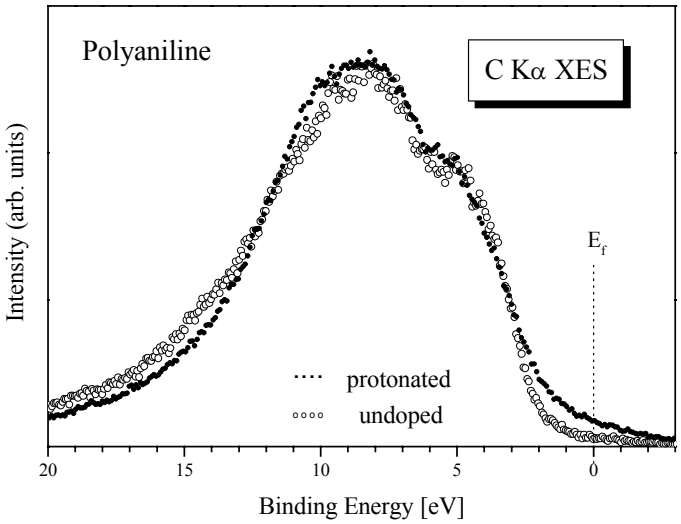

Figure 1 Carbon Kα XES of undoped and protonated polyemeraldine displayed on the binding energy scale.

To summarize, we have observed a finite density of states in protonated emeraldine in the vicinity of the Fermi level using soft X-ray emission measurements. This direct observation is in a full agreement with band structure calculations for the polaron lattice and therefore supports a polaronic-metal model for conducting polymers.

REFERENCES

1. M. Reghu, Y. Cao, D. Moses, and A.J. Heeger, Phys. Rev. B **47**, 1758 (1993).
2. S. Stafström, J.L. Bredas, A.J. Epstein, H.S. Woo, D.B. Tanner, W.S. Huang, and A.G. MacDiarmid, Phys. Rev. Lett. **59**, 1464 (1987).
3. J. Nordgren, G. Bray, S. Gramm, R. Nyholm, J.-E. Rubensson, and N. Wassdahl, Rev. Sci. Instrum. **60**, 1690 (1989).
4. J.J. Jia, T.A. Callcott, J. Yurkas, A. W.Ellis, F.J. Himpsel , M.G. Samant, J. Stöhr, D.L. Ederer, J.A. Carlisle, E.A. Hudson, L.J. Terminello, D.K. Shuh, and R.C.C. Perera, Rev. Sci. Instrum. 66 (1995) 1394.
5. E.Z. Kurmaev, M.I. Katsnelson, A. Moewes, M. Magnuson, J.-H. Guo, S.M. Butorin, J. Nordgren, D.L. Ederer and M. Iwami, J. Phys: Condens. Matter 13 (2001) 3907.
6. H.Sakamoto, M. Itow, N. Kachi, T. Kawahara, K. Mizoguchi, H. Ishii, T. Miyahara, K. Yoshioka, S. Masubuchi, S. Kazama, T. Matsushita, A. Sekiyama and S. Suga, J. Electr. Spectr. Relat. Phenom. **92**, 159 (1998).

This work was supported by the Russian State Program on Superconductivity, the Russian Science Foundation for Fundamental Research (Projects 00-15-96575 and 99-03-32503), the Swedish National Science Research Council (NFR), the Goran Gustavsson Foundation for Research in Natural Sciences and Medicine, NSF Grants DMR-901 7997 and DMR-9420425, the DOE EPSCOR and the Louisiana Education Quality Special Fund (DOE-LEQSF (1993-95-03)). The ALS, Lawrence Berkeley National Laboratory is supported by the U.S. Department of Energy under Contract No. DE-AC03-76SF 00098.

Principal investigator: Ernst Kurmaev, Institute of Metal Physics, Russian Academy of Sciences-Ural Division, 620219 Yekaterinburg GSP-170, Russia. Email: kurmaev@ifmlrs.uran.ru. Telephone: +7-3432-744183.

Spin-resolved electronic structure studies of ultrathin films of Fe on singular and vicinal GaAs

M. Spangenberg[1], E.A. Seddon[1], E.M.M. McCash[2], T. Shen[3],
S.A. Morton[4], D. Waddill[5] and J. Tobin[4]

[1]CLRC Daresbury Laboratory, Keckwick Lane, Daresbury, Cheshire, UK
[2]Department of Chemistry, University of York, Heslington, York, UK
[3]Joule Physics Laboratory, University of Salford, Salford, Greater Manchester, UK
[4]Lawrence Livermore National Laboratory, 7000 East Ave., Livermore, CA 94550
[5]Department of Physics, University of Missouri-Rolla, Rolla, MO 65409

Recently, there has been considerable interest in the study of spin injection at ferromagnetic semiconductor heterojunctions and ferromagnetic metal – semiconductor contacts[1,2,3,4]. Studies of n-type semiconductors have demonstrated spin-coherent transport over large distances[5] and the persistence of spin coherence over a sizeable time scale[6]. Clearly such investigations have been stimulated by the potential of the development of 'spintronics', electronic devices utilising the information of the electron spin states. To understand and improve the magnetic properties of ultrathin Fe films on GaAs has been the aim of many research groups over recent years. The interest in this system has both technological and fundamental scientific motivations. Technologically, Fe on GaAs may serve to realize spin electronic devices. From a fundamental science point of view, Fe on GaAs serves as a prototype for studies of the interplay between the crystalline structure and morphology of an ultrathin film, its electronic structure and the long range magnetic order it exhibits.

In contrast to the attention given to Fe on variously prepared GaAs substrates, the magnetism of Fe on vicinal GaAs substrates has received scant attention. This in spite of the fact that films grown on vicinal substrates present a number of advantages and opportunities. For example, they are known to exhibit enhanced structural homogeneity, surface diffusion tends to follow well mapped patterns (the quasi-periodicity has been exploited to produce quantum wires) and there is an additional degree of control of the film growth beyond those associated with temperature and substrate surface composition[7].

In a preliminary combined spin-polarized secondary electron spectroscopy, photoelectron spectroscopy and LEED study (carried out on the SRS, Daresbury Laboratory) of the remanent magnetic properties of Fe on singular and vicinal (3° offset) GaAs we have shown both that the various magnetic phases formed are dependant upon the Ga to As surface composition of the substrate and that they evolve in characteristic (but not well understood) ways with Fe overlayer thickness[8]. A remarkable feature in this system, which illustrates the importance of the Fe overlayer/substrate interaction, is the magnetic anisotropy; the easy axis of the Fe films on Ga-terminated substrates is perpendicular to that for As-terminated substrates[9,10].

These measurements were followed up with combined spin-resolved photoemission and magnetic linear dichroism experiments on Fe deposited on vicinal (offcut by 3º and 6º) or singular GaAs substrates on Beamline 7 at the ALS in collaboration with Elaine Seddon of CCLRC Daresbury Laboratory, Dan Waddill of The University of Missouri-Rolla and James Tobin Of Lawrence Livermore National Laboratory. The GaAs(100) substrates were available for film deposition at room temperature after substrate decapping *in-situ* (by thermal annealing),

at the ALS. By mounting both singular and vicinal GaAs substrates on the same sample tile the same growth conditions applied for both films facilitating direct comparison. The surface quality was monitored using LEED. The following data were obtained, high resolution spin-integrated valence bands, the spin-resolved valence bands and their energy dispersion, the film thickness dependence of the spin-resolved valence bands, magnetic linear dichroism data on the Fe3p and Fe2p core levels at a variety of photon energies.

The experiments, which were performed with Dr. Simon Morton and Dr. Jim Tobin in November of 2000 have produced considerable amount of interesting results. The significant differences in the spin-resolved valence bands between *ca.*20 Å thick Fe films on singular and vicinal (3º) GaAs are illustrated in Fig.1. As the terrace width is *ca.*55 Å the spectral differences are not due to step-localized features.

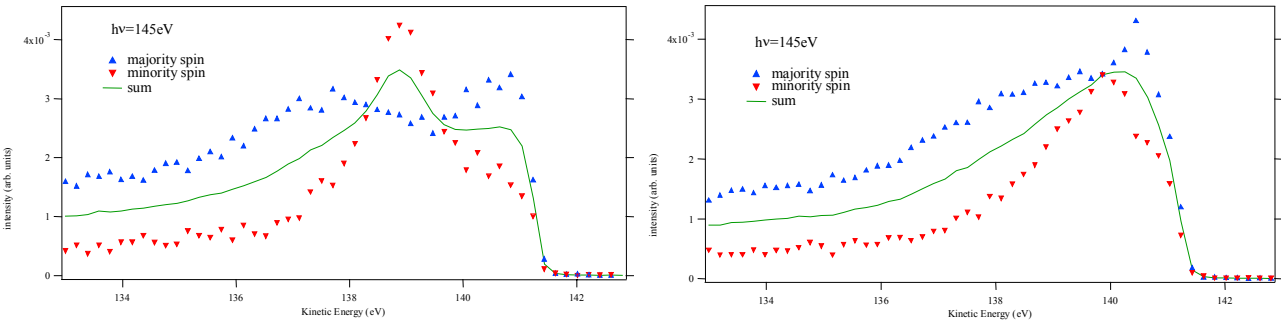

Figure 1
Spin-resolved valence band photoemission results for Fe on singular GaAs (left) and Fe on vicinal (3º) GaAs (right).

Other interesting results include the following. At low film thicknesses, Fe deposited on singular substrates was found to have a lower Curie temperature than Fe on vicinal substrates. Fe deposited on singular substrates reveals a larger energy dispersion of the spin-resolved valence bands than Fe on vicinal substrates. Only marginal differences can be seen between the spin-resolved valence bands of Fe deposited on 3º stepped GaAs substrates and Fe deposited on 6º stepped GaAs substrates. Also, in contrast to the valence band studies, the linear magnetic dichroism results obtained for these samples are very similar.

Further experiments at ALS during oct 2001 enabled us to obtain considerably more interesting results. Whilst the detailed analysis of the results is still underway, Fig.2 shows a large contrast of the valence band spectra of Fe versus incident photon energy between that on a singular and a vicinal substrate. The strong feature on the left in Fig.2 was found to be sensitive to the thickness of the Fe layer and the origin of which is still not yet clear at the present stage.

In summary, the experiments at the ALS have been extremely rewarding. They have answered some questions, clarified our thinking on others and raised yet other questions for which we have no answers at the moment. The run has, however, shown that further access to the ALS is needed to fully understand this fundamental and technologically important system.

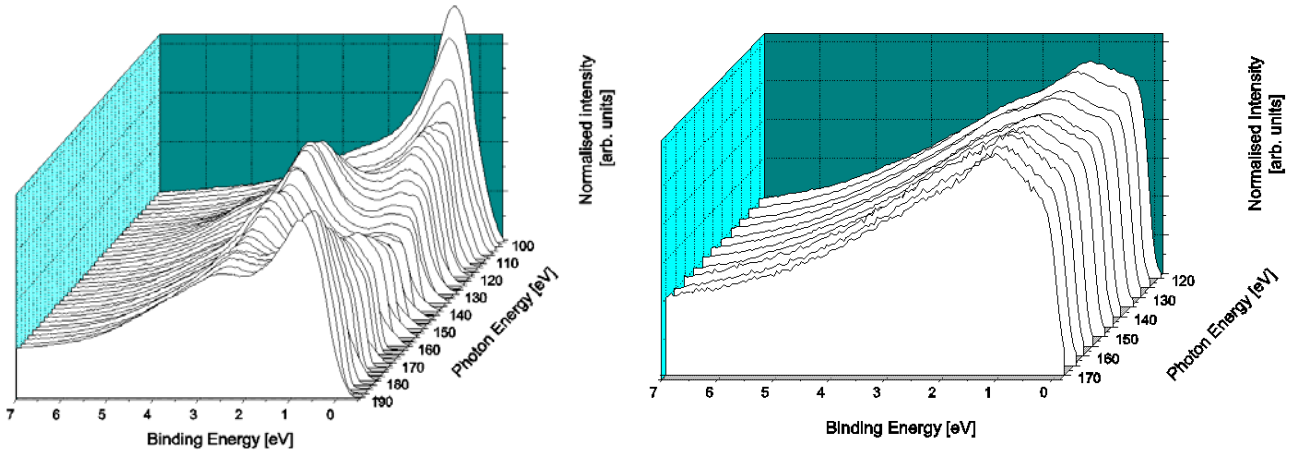

Figure 2.
Valence band spectra of Fe, normalised to the secondary electron tails, versus photon energy for films on singular substrate (left) and on 6 degree vicinal substrate (right).

References:

[1] Malajovich I., Berry J.J., Samarth N. and Awschalom D.D., Nature 411, 770 (2001)
[2] Ohno Y., Young D.K., Beschoten B., Matsukura F., Ohno H. and Awschalom D.D., Nature 402, 790 (1999)
[3] Filip A.T., Hoving B.H., Jedema F.J., van Wees B.J., Dutta B. and Borghs S., Phys. Rev. B 62, 9996 (2000)
[4] Hammar P.R., Bennett B.R., Yang M.Y. and Johnson M., Phys. Rev. Lett. 83, 203 (1999)
[5] Kikkawa J.M. and Awschalom D.D., Nature 397, 139 (1999)
[6] Kikkawa J.M. and Awschalom D.D., Phys. Rev. Lett. 80, 4313 (1998)
[7] Joyce B. A., Neave J. H., Zhang J., Vvedensky D. D., Clarke S., Hugill K.J., Shithara T. and Myers-Beaghton A.K., Semicond. Sci. Technol., **5** 1147 (1990). Kawamura T., Maruta J. and Ishii A., J. Appl. Phys., **39** (7B) 4376 (2000). Gaines J.M., Petroff P.M., Kroemer H., Simes R.J., Geels R.S. and English J.H., J. Vac. Sci. Technol., **B6** 1373 (1998).
[8] Zhang T., Spangenberg M., Greig D., Takahashi N., Shen T-H., Matthew J.A.D., Cornelius S. M., Rendall M. and Seddon, E.A., Appl. Phys. Letters, **78** 961 (2001)
[9] Kneedler E. M., Jonker B. T., Thibado P. M., Wagner R. J., Shanabrook B. V., and Whitman L., J. Phys. Rev. B, **56** 8163 (1997).
[10] Gester M., Daboo C., Hicken R. J., Gray S. J., Ercole A., and Bland J. A. C., J. Appl. Physics **80** 347 (1996).

This work was supported by the Director, Office of Energy Research, Office of Basic Energy Sciences, Materials Science Division, of the U.S. Department of Energy under Contract No. # R5-32633.A02. This work was performed under the auspices of the U.S Department of Energy by Lawrence Livermore National Laboratory under contract no. W-7405-Eng-48. Experiments were carried out at the Spectromicroscopy Facility (Beamline 7.0) at the Advanced Light Source, built and supported by the Office of Basic Energy Science, U.S. Department of Energy.

Principal investigator: E. A. Seddon, CCLRC Daresbury Laboratory, Daresbury, Warrington Cheshire, WA4 4AD, UK, Email: e.a.seddon@dl.ac.uk, Telephone: +44 1925 603245, fax +44 1925 693124

VUV Photoionization of Superfluid Liquid Helium Droplets at the ALS

Darcy S. Peterka[1,2], Lionel Poisson[1], Albrecht Lindinger[1], Musahid Ahmed[2], and Daniel Neumark[1,2]

[1]College of Chemistry,
University of California, Berkeley, California 94720, USA
[2]Chemical Sciences Division, Ernest Orlando Lawrence Berkeley National Laboratory,
University of California, Berkeley, California 94720, USA

INTRODUCTION

Helium droplets have many interesting properties. They are very cold - evaporative cooling reduces the temperature to 380 milliKelvin. At these temperatures, the droplets are superfluid, and the electronic interactions between the He atoms can be described neither by He pair-potentials, nor by mean field theories. For an accurate description, quantum many body effects must be considered[1]. The complex interactions in the droplets will not affect only electronic excitations -relaxation processes will be altered as well. We have begun an in depth study of theses processes near the helium atomic ionization threshold.

EXPERIMENTAL

The droplets were produced in a supersonic expansion using a 5 mm diameter nozzle aperture at typical He pressures of 15-50 bar and source temperatures of 11-18 K. The source conditions provided droplets with $\langle N \rangle = 10^4$ He atoms. The source chamber is pumped by a 3,200 l/s magnetically levitated turbo pump that is able to maintain a source pressure chamber of 10^{-4} with 60 bar, 13 K operation. The main chamber is evacuated by two magnetically suspended turbo pumps (Seiko Seike STP 600 and STP 400) backed by an oil-free scroll pump, providing 1000 l/s of pumping which keep the main chamber in the 10^{-7}'s during the experiment. VUV radiation from a 10 cm period undulator at the Advanced Light Source was dispersed by a 600 line/mm tungsten coated grating in a 3-m, normal incidence, off plane Eagle monochromator (McPherson). The endstation is schematically illustrated in the inset figure. The VUV light then ionized the droplets on the axis of a TOF spectrometer. The generated photoelectrons then struck a 40-mm-diameter dual multi-channel plate (MCP), which is coupled to a phosphor screen (Galileo 3040FM) yielding positional information. The electron optics were biased to achieve "Velocity Map" conditions[2]. A photomultiplier tube monitored the light from the phosphor screen, allowing for total ion yield measurements. The recorded images are 2-dimensional projections of the 3-dimensional recoiling product electron sphere. Axial symmetry is maintained around the polarization axis, allowing reconstruction of the images using conventional inverse Abel transform techniques. The droplet beam was also detected by a residual gas analyzer (SRS RGA 200), which was mounted in the main chamber along the droplet propagation axis.

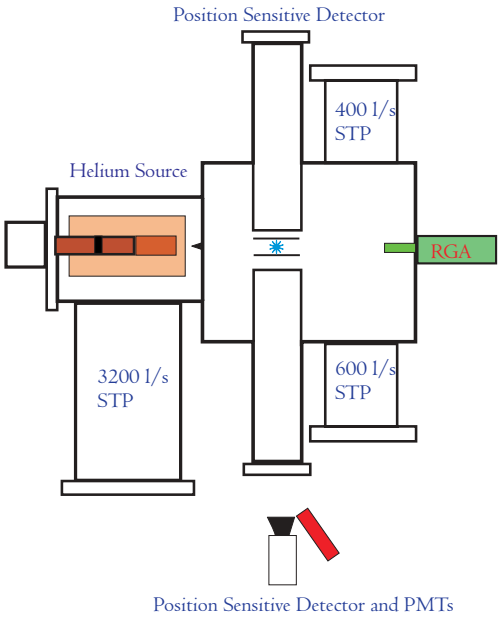

RESULTS and DISCUSSION

A photoelectron yield spectrum is shown to the right. The figure shows signal with the cryostat off - helium atoms only, the cryostat on - atoms and droplets, and the difference between the two. Also indicated in the figure are the atomic helium singlet *np* Rydberg energies converging the the helium ionization energy, 24.587 eV. Immediately one sees that the droplets ionization potential is suppressed relative to the atom.

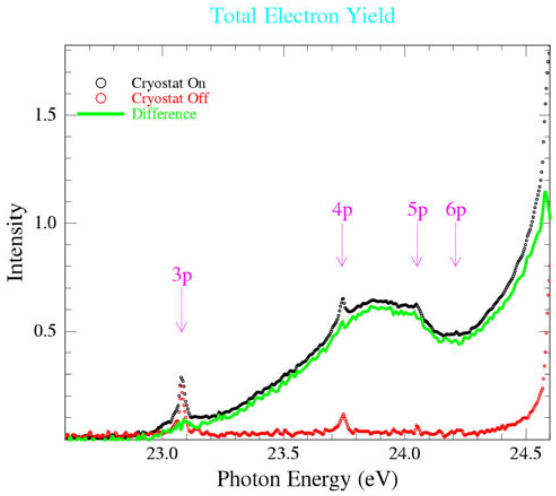

The ionization process is mediated by the formation of He_2^+ which is bound by 2.35 eV relative to $He + He^+$. The photon energy required to access the minimum of the He_2^+ curve is ~22.2 eV. That the threshold for droplet ionization occurs ~.8eV above this is telling of the excitation process. In the droplets, the average distance between He atoms is ~3.6 Å. This is near the asymptotes of the He_2^* dimer potentials [3], thus it is expected that the excitations have significant atomic character. Using the atomic excitations as the zero order states of the droplets, we see the optically allowed excitation to He (3p) ^1P state is the first state of sufficient energy to allow for the production of He_2^+. Our ionization onset is slightly below that of the atomic He (3p) ^1P state (23.08 eV), this could result from a combination of factors. In the droplet, multibody effects can perturb both the energy and symmetry of the states and couple states of differing angular momentum. [4]

Examination of the photoelectrons lets us probe the photoionization process in more detail. The electron leaves the droplet with near zero kinetic energy (< 10 meV), with an isotropic angular distribution. The isotropic distribution contrasts with the dipole allowed excitation, which with linearly polarized light would have a cos^2 character. The electron angular and energy distributions change very little with with large changes in photon energy (23-24.5 eV). This implies that the excitation process is distinct from the ionization process, and is indirect.

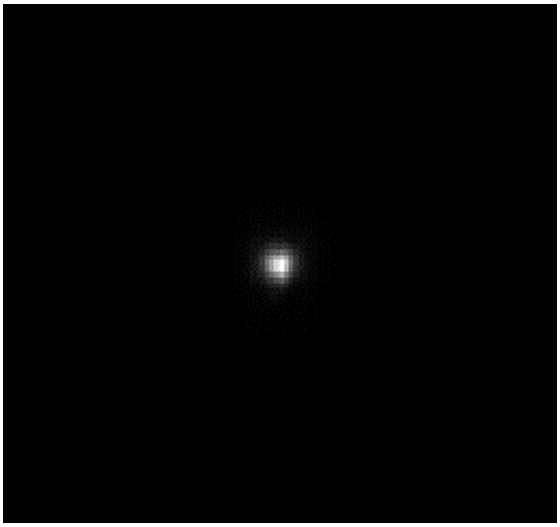

Photoelectron image following droplet excitation at 24 eV . The angular distribution is isotropic, and the electrons have near zero kinetic energy (small image radius)

The initial excitation process generates essentially excited helium atoms in the droplets. These can relax via fluorescence, the dominant process [5], or they can feel the influence of neighboring atoms in the droplet, leading to the formation on He_2^*. Because the poor coupling of He_2^* vibrational modes to those of the droplets, significant energy remains in the He_2^*[6]. These states are energetically degenerate with $He_2^+ + e^-$. We believe this results in vibrational autoionization of the He_2*, and the subsequent generation of low kinetic energy electrons.

CONCLUSIONS

The first dispersed photoelectron spectra from the ionization of helium droplets have been collected, giving insight into the ionization process in liquid helium droplets. The isotropic, near zero energy electrons implicate an indirect ionization process. Ionization below the atomic He threshold results from autoionization of $He_2^*(He_n)$ states. Further work is underway to examine the relaxation of the vibrationally excited He_2^+ remaining in the droplet, and processes occurring above the He atom threshold.

ACKNOWLEDGMENTS

DSP thanks the NSF for fellowship support

REFERENCES

1. F. Dalfovo and S. Stringari, *J. Chem. Phys.*, **115**, 22, (2001)
2. A.T.J. Eppink and D. Parker, *Rev. Sci. Instrum*., **68**, 3755, (1997)
3. J.A. Hornbeck and J.P. Molnar, Phys. Rev., **84**, 62 (1951)
4. K. von Haeften, T. Laarmann, H. Wabnitz, and T. Möller, *Phys. Rev. Lett*., **87**, 15 (2001)
5. Fröchtenicht, U. Henne, J.P. Toennies, A. Ding, M. Fieber-Erdmann, and T. Drewello, *J. Chem. Phys*, **104**, 7 (1996R. Fröchtenicht, U. Henne, J.P. Toennies, A. Ding, M. Fieber-Erdmann, and T. Drewello, *J. Chem. Phys*, **104**, 7 (1996)
6. B.E. Callicoatt. K. Förde, L.F. Jung, T. Ruchti, and K.C. Janda, *J. Chem. Phys.*, **109**, 23 (1998)

This work was supported by the Director, Office of Sciences, Office of Basic Energy Sciences, Chemical Sciences Division, of the U.S. Department of Energy under Contract No. DE-AC03-76SF00098.

Contact Person: Darcy S Peterka, Chemical Dynamics Group, Chemical Sciences Division, Ernest Orlando Lawrence Berkeley National Laboratory. Email: DSPeterka@lbl.gov. Telephone: 510-495-2207

XANES Spectroscopy of Ti and V Centers Grafted onto Mesoporous Sieves: Preliminary Results

W. Lin, D. Bruehwiler, and H. Frei

Physical Biosciences Division, Lawrence Berkeley National Laboratory, Berkeley, CA 94720

INTRODUCTION

Photochemical synthesis of a fuel by reduction of CO_2 using visible light as energy source and H_2O as electron source is one of the most attractive, yet unrealized goals in solar energy to fuel conversion. Photosynthesis of methanol for large scale use in fuel cells is considered a promising option for the replacement of fossil fuel combustion as a means of power generation. We are exploring photochemistry at the gas-solid interface of transition metal molecular sieves as a method for CO_2 conversion to methanol. A most critical aspect of this task is the reliable characterization of the framework of grafted metal centers in these materials, and the verification of the structural integrity of the photoreactor under use. X-ray absorption techniques, especially EXAFS (Extended X-Ray Absorption Fine Structure) and XANES (X-Ray Absorption Near Edge Structure) spectroscopy are the best tools for this type of solids. Based on earlier pre-edge X-ray absorption characterization of Ti silicalite materials at ALS beamline 9.3.1, we have recently been able to establish for the first time some of the key intermediates of carbon oxide reduction and H_2O_2 interaction in this molecular sieve.[1-3]

In an effort to push the redox response of the metal centers from the UV towards visible photon energies, we are exploring the possibility of incorporating visible light-absorbing multinuclear assemblies into molecular sieves. A first step in the synthesis of such assemblies is the introduction of an anchor metal into the material in the form of a framework or grafted center. We have prepared grafted and framework Ti and V centers in mesoporous silicate sieves and have begun structural characterization of the materials by pre-edge absorption spectroscopy.

RESULTS

Using a specially designed sample holder for recording spectra of up to 12 molecular sieve samples in the form of pressed wafers in transmission or fluorescence mode, we have begun to record framework and grafted TiMCM41 and VMCM41 materials synthesized in our laboratory. As described by F. Schlachter in the ALS 2001 Compendium paper " Beamline 9.3.1: Monochromator Upgrade", the beam stability has been greatly improved since our earlier measurements. The new performance allows us to conduct reproducible scans over an energy range of several hundred eV, as demonstrated in Figure 1 by a 500 eV scan covering the Ti K-edge and the Ba L_3-edge of $BaTiO_3$. The spectrum shows the result of a single scan. The sample was a pressed wafer (diameter 1 cm, thickness 100 micron) of $BaTiO_3$ crystallites embedded in a silicate matrix. The measurement was conducted in transmission mode using a Si photodiode detector (Hamamatsu model S2744-08).

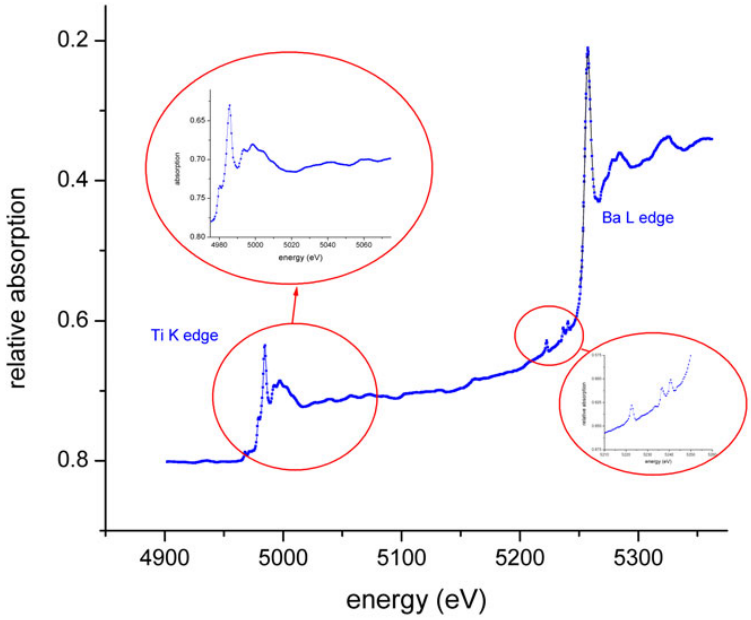

Figure 1. X-ray-absorption spectrum of crystalline barium titanate.

Figure 2a shows the absorption spectrum of framework TiMCM41 sieve in which 1 percent of the Si atoms are isomorphically substituted by Ti. Since the framework sites are tetrahedrally coordinated by oxygen, Ti in such sites gives rise to a sharp 1s-3d transition (A_1-T_2 component) absorbing around 4970 eV. By contrast, any extraframework TiO_2 clusters would feature octahedrally coordinated Ti that only contributes to the K-edge absorption but not to the pre-edge peak (optically forbidden). Figure 2a shows that the intensity of the 1s-3d peak relative to the height of the plateau between K-edge and the onset of the extended region is greater than 0.7. This is indicative of 100 percent framework substitution of the Ti, with no extraframework Ti oxide clusters present in the pores.

Similarly, the pre-edge peak of the grafted TiMCM41 spectrum shown in trace b of Figure 2 indicates that at least 90 percent of the Ti is in tetrahedral coordination. Diffuse reflectance UV and transmission FT-IR spectra of the material imply that the tetrahedrally coordinated Ti centers are tripodal (Si-O)TiOH moieties, i.e., the Ti is covalently anchored to three Si centers on the surface of the pore. Next, measurements will be conducted on recently prepared grafted VMCM materials.

These preliminary measurements establish the high degree of covalent anchoring of Ti as isolated centers in our mesoporous silicate materials. The quality of the single scan results displayed in Figure 1 and 2 shows that the recent monochromator upgrade at beamline 9.3.1 opens up routine XANES and EXAFS measurements up to energies of 5500 eV.

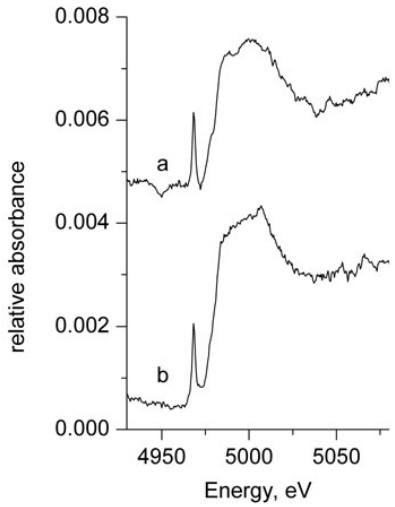

Figure 2. XANES spectrum of framework-substituted Ti-MCM41 (a), and grafted Ti-MCM41 (b).

REFERENCES

1. N. Ulagappan and H. Frei, "Mechanistic Study of CO_2 Photoreduction in TS-1 Molecular Sieve". *J. Phys. Chem. A* **104**, 7834 (2000).
2. Y.H. Yeom and H. Frei, "Photoactivation of CO in Ti Silicalite Molecular Sieve". *J. Phys. Chem. A* **105**, 5334 (2001).
3. W. Lin and H. Frei, "Photochemical and FT-IR Probing of the Active Site of Hydrogen Peroxide in Ti Silicalite Sieve". *J. Am. Chem. Soc*., submitted.

This work was supported by the Director, Office of Science, of the U.S. Department of Energy under Contract No. DE-AC03-76SF00098. The authors thank Fred Schlachter for assistance in the experiments.

Principal Investigator: Heinz Frei, Physical Biosciences Division, Lawrence Berkeley National Laboratory. E-mail: HMFrei@lbl.gov Telephone: 510-486-4325

X-ray Absorption and Emission Spectroscopy at the Nitrogen K-Edge in Dilute $GaAs_{1-x}N_x$

M. Adamcyk[1], A. Ballestad[1], A. Moewes[2], E. Nodwell[1], T. Tiedje[1], S. Tixier[1]

[1]Advanced Materials and Process Engineering Laboratory,
Department of Physics and Astronomy, University of British Columbia,
Vancouver, B.C. V6T 1Z4, Canada
[2]Department of Physics and Engineering Physics,
University of Saskatchewan, Saskatoon, Sask. S7N 5E2, Canada

$GaAs_{1-x}N_x$ and $In_yGa_{1-y}As_{1-x}N_x$ alloys containing a few percent nitrogen have attracted attention in recent years due to their potential use in 1.3 micron emitters on GaAs substrates. The incorporation of nitrogen at low concentrations in these III/V materials results in a large band gap bowing parameter and a sharp decrease of the band gap with increasing nitrogen [1]. A wide range of lattice constants can be obtained by varying the N content. For example $In_{0.3}Ga_{0.7}As_{0.98}N_{0.02}$ quantum wells are pseudomorphic to GaAs and emit at 1.3 micron. In the present work, we have studied the density of states in the valence and conduction bands of dilute $GaAs_{1-x}N_x$ using soft x-ray emission and absorption at the nitrogen K-edge. The emission spectrum is compared to a tight binding band structure calculation for the electronic structure of $GaAs_{1-x}N_x$.

The $GaAs_{1-x}N_x$ samples were grown by Molecular Beam Epitaxy (MBE) at a substrate temperature in the 500-600°C range using a RF plasma source for the dissociation of molecular nitrogen. The nitrogen content ranged from 0.02% to 2%. Nitrogen concentrations were obtained using X-ray diffraction and SIMS. The samples were cleaved in two pieces; one piece was annealed at 850° for 1 min. Nitrogen K-edge absorption and emission spectra were measured at beamline 8.0.1. The absorption spectra were obtained in the fluorescence yield mode. The emission spectra were measured using a 600 lines/mm diffraction grating providing an energy resolution of 0.8eV (FWHM) as determined from the scattered primary beam.

Emission and absorption spectra at the nitrogen K-edge are shown in Fig. 1 for a $GaAs_{1-x}N_x$ sample with a 2% N content, together with calculated nitrogen 2p density of states. The emission spectrum (lower spectrum in the figure) was excited at a photon energy of 402.1 eV corresponding to the peak absorption in the upper spectrum in Fig. 1. The small peak at 402.1 eV in the emission spectrum is the elastically scattered excitation radiation which is not completely rejected by the soft x-ray spectrometer. This peak serves as an energy calibration for the emission spectrometer. The emission and absorption spectra show a band gap of about 1 eV in agreement with optical measurements.

Absorption at the nitrogen K-edge probes the unoccupied density of states in the conduction band with p-symmetry at the nitrogen sites. The spectrum shows a strong

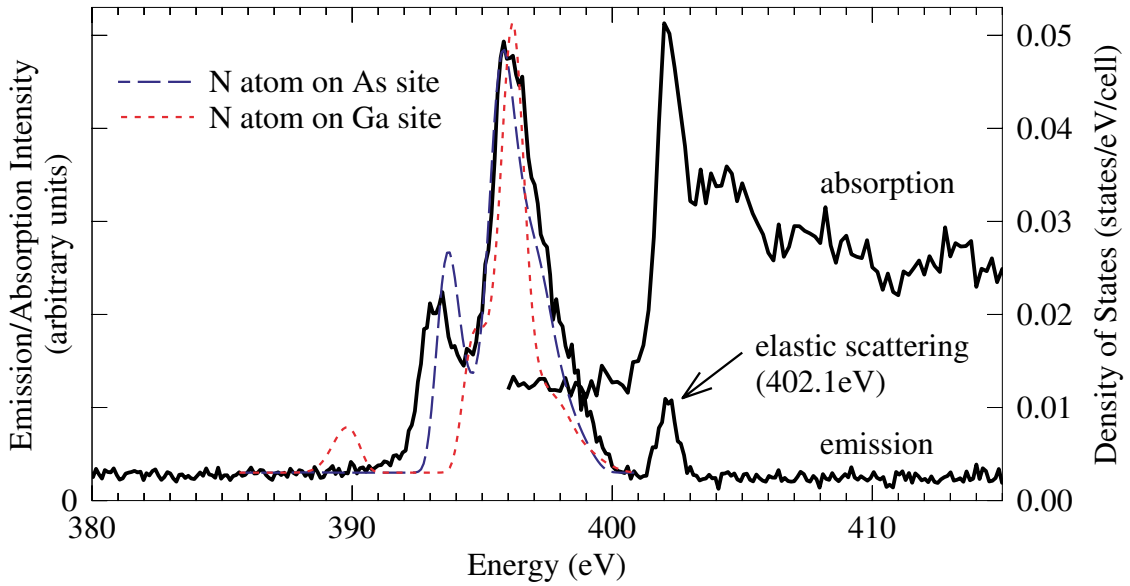

Figure 1: Emission and absorption curves for $GaAs_{1-x}N_x$ with 2% N and calculated local DOS on the Nitrogen 2P state. Orthogonal (random) noise of 0.003 states/eV/cell has been added to the calculated spectra. The origin of the energy scale in the calculations is arbitrary.

excitonic type peak just above the bottom of the conduction band which we attribute to the well known nitrogen resonance in the conduction band. The shape of the absorption spectrum was independent of the nitrogen content.

The emission spectrum in Fig. 1 at the nitrogen K-edge is due to transitions from valence band states on nitrogen sites with p-symmetry to the nitrogen 1s core hole. The spectrum has two peaks located at 393.2 eV and 396.1 eV. No changes in the shape of the spectrum were observed as a function of nitrogen content in the 0.02% - 2% range. Similarly no changes were observed with annealing at 850°C. Annealing is expected to substantially reduce the number of nitrogen interstitials. The absence of a change in the emission spectrum with annealing suggests that the fraction of interstitial nitrogen is low. Emission spectra were measured as a function of excitation energy through the absorption edge and no resonant effects were observed in the soft x-ray emission.

Emission spectra were calculated in a tight binding model in which a single nitrogen atom is located on a Ga or an As site in a 2x2x2 supercell containing 64 atoms. The model spectra are the p-projected densities of states on the nitrogen atom. The energies for the atomic orbitals and interatomic overlap matrix elements for the Ga and As 4s and 4p orbitals were taken from Harrison [2]. The energy level for the nitrogen 2p orbital was taken to be an adjustable parameter and was used to fit the experimental spectrum. The spectra were convolved with a 0.8 eV Gaussian window in accordance with the experimental resolution. The lifetime broadening of the emission band is ignored. A best fit was obtained with the nitrogen 2p orbital energy ϵ_p equal to -8.5 eV which compares with the -11.47 eV recommended by Harrison. For $\epsilon_p <$ -9.5 eV the nitrogen 2p orbital forms a bound state in the valence band and the shape of the emission spectrum changes. The good agreement with the experimental data in Fig. 1 suggests that there is

no nitrogen p-like bound state in the valence band. When the nitrogen is located on a Ga site a deep bound state is obtained in the model as indicated by the peak in the dotted curve in Fig. 1 at 389.8 eV. The good fit with the calculated spectrum for nitrogen on the As site suggests that most of the nitrogen is on the group V site, as expected. No emission was detected from the lower part of the GaAs valence band, which is dominated by As 4s, in good agreement with the model.

Acknowledgments

We thank Tony Van Buuren for his help and the Natural Sciences and Engineering Research Council of Canada (NSERC) for financial support.

References

[1] S.-H. Wei and A. Zunger, Phys. Rev. Lett. **76**, 664 (1996).

[2] W.A. Harrison, *Electronic Structure and the Properties of Solids* (Dover, New York, 1989).

Principal investigator: E. Nodwell, Advanced Materials and Process Engineering Laboratory, University of British Columbia, Vancouver, B.C. V6T 1Z4, Canada. Email: nodwell@physics.ubc.ca. Telephone: 604-822-5425.

X-RAY ABSORPTION STUDIES OF THE cBN COMPOSITES WITH DIFFERENT BONDING PHASES

E. Benko[a], K. Lawniczak-Jablonska[b], P. Nachimuthu[c], I. N. Demchenko[b], E. Piskorska[b], P. Klimczyk[a], R.C.C Perera[c], A. Włochowicz[d], A. Benko[e], T. L. Barr[e]

[a]*Institute of Metal Cutting, Wroclawska 37A Str., 30-011 Cracow, Poland*
[b]*Institute of Physics Polish Academy of Science, Al. Lotnikow 32/46, 02-668 Warsaw, Poland*
[c]*Center for X-ray Optics, Lawrence Berkeley National Laboratory, University of California –Berkeley, Berkeley, California 94720*
[d]*University of Bielsko Biała , Willowa 2 Str., 43-309 Bielsko-Biała*
[e]*Materials Department and Laboratory for Surface Studies, University of Wisconsin-Milwaukee, Milwaukee, WI 53201, USA*

The cBN composites are widely used in various applications because of their excellent wear and corrosion resistance and their thermal and electronic properties. In order to obtain composition materials with optimal properties and using economic and safe for environment technology it is important to recognize chemical reactions occurring at boron nitride during formation of bonding phase. Titanium and their compounds are most commonly used as binders in sintering technology. We present the results of studies of cBN composites with addition of TiN and TiC ceramics to form a bonding phase. The wider class of additions is under investigation.

From thermodynamical calculations it follows that in the temperature range from 1000 to 1400^0C TiC and TiN react with cBN forming in the case of TiC two new phases (TiB_2 and $TiC_{0.8}N_{0.2}$) and only TiB_2 phase in the case TiN addition.

Composites were prepared by high pressure (9GPa) hot pressing (1750^oC) and the samples were subsequently heat treated at 1000 and 1400^oC for 1 hour in vacuum $3*10^{-3}$ Pa. Sinters of cBN-TiN/TiC before and after heat treatment were characterised using transmission electron microscopy and X-ray absorption technique.

RESULTS AND DISCUSSION

TEM studies of the microstructure in cBN sintered with TiN and heated up to 1400 ^{o}C

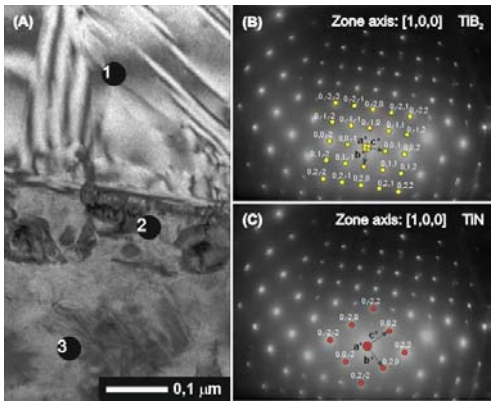

The microstructure of cBN sintered with TiN is compact. Analysis of the electron diffraction (Fig.1, B and C) allowed to conclude that the fine crystallites at the boundary show the TiB_2 phase (B) whereas the bigger grains inside the TiN phase (C). The cBN/TiC compact looks the same like cBN/TiN. But in some places the electron diffraction pattern indicates on the presence of the triple Ti(BC) compound.

Fig.1. Boundary between the two fine-crystalline area of cBN/TiN composite (A) and electron diffraction pattern from the point 2 (B) and 3 (C).

X-ray absorption study

X-ray absorption measurements were carried out at the Advanced Light Source of Lawrence Berkeley National Laboratory (beamline 6.3.2) and at the HASYLAB in Hamburg. (beamline A1). As an example are presented XANES at the Ti K-edge of cBN/TiN (Fig.2) and

Ti $L_{2,3}$-edge (Fig.3) from cBN - TiC/TiN.

Spectra show formation of the TiB_2 new phase after heating to 1300^0C, without heat treatment TiB_2 was not formed (Fig.2). The formed TiB_2 phase is not ideal, it can have defects and inclusions of other phases. The possibility of the foreign phases addition was check (upper curves) and conclusion can be drown that addition to the TiB_2 phase up to 30% of TiN phase does not improve the agreement between modelled and observed phase. In composites without heat treatment the inclusions of up to 20% TiC and 10% TiB_2 cannot be excluded.

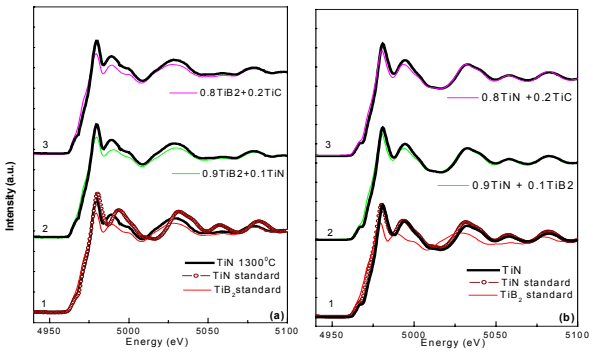

Fig. 2. The Ti K - edges of the cBN/TiN and reference samples heated up to 1300^0C (a) and cBN/TiN without heat treatment (b).

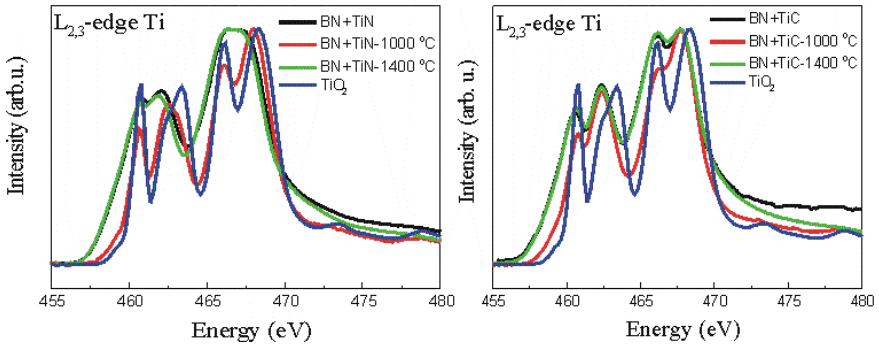

Fig.3. Ti $L_{2,3}$ x-ray absorption edge spectra of cBN/TiN and cBN/TiC composites before and after heat treatment and TiO_2 as reference.

The pick structure in Fig.3 shows formation of TiO_2 like phase in the cBN-TiN/TiC composites. It was proved that the temperature of 1000^0C was not high enough to avoid the oxidation of the composite grains, the heat treatment up to 1400^0C prevent the oxidation of grains.

Conclusion

X ray absorption measurements provide a clear spectroscopic signature of TiB_2 formation in the cBN-TiN/TiC composites. There was proved that the temperature of 1000^0C was not high enough to avoid the oxidation of the composite grains, therefore the heat treatment is necessary. The formed TiB_2 phase is not free from the defects but we do not observed foreign phase inclusion after heating.
From the analysis of the edge shape one can conclude on the chemical processes and optimise of the BN-TiC/TiN composites heat treatment procedure.

Acknowledgements
This study is based on the work sponsored by Polish State Committee for Scientific Research (Grant No 7T08D 014 17) and SPUB (Grant No-M/DESY/P-03/ DZ-213/2000) and IHP-Contract HPRI-CT-1999-00040 of the European Commission.

Principal investigator: Krystyna Lawniczak-Jablonska, Institute of Physics, Polish Academy of Sciences. Telephone: 48 22 8436034. Email: jablo@ifpan.edu.pl.

X-ray emission spectra and electronic structure of charge transfer salts

E. Z. Kurmaev[1], A. Moewes[2], U. Schwingenschlögl[3], R. Claessen[3], M. I. Katsnelson[1], H. Kobayashi[4], S. Kagoshima[5], Y. Misaki[6], D.L. Ederer[7], K. Endo[8], and M. Yanagihara[9]

[1]Institute of Metal Physics, Russian Academy of Sciences-Ural Division, 620219 Yekaterinburg GSP-170, Russia
[2] Department of Physics and Engineering Physics, University of Saskatchewan, 116 Science Place, Saskatoon, Saskatchewan S7N 5E2, Canada
[3] Experimentalphysik II, Universität Augsburg, D-86135 Augsburg, Germany
[4]Institute for Molecular Science, Okazaki 444, Japan
[5] Department of Basic Science, University of Tokyo, Komaba 3-8-1, Meguro, Tokyo 153-8902, Japan
[6]Department of Molecular Engineering, Graduate School of Engineering, Kyoto University Yoshida, Sakyo-ku, Kyoto 606-8501, Japan
[7]Department of Physics, Tulane University, New Orleans, LA 70118, USA
[8]Department of Chemistry, Faculty of Science, Kanazawa University, Kakuma-machi, Kanazawa, 920-1192 Japan
[9]Research Institute for Scientific Measurements, Tohoku University, Sendai 980-77, Japan

Charge transfer salts formed by linear chains of organic molecules BETS (bis(ethylenediteho)tetraselenafulvalene), BEDT-TTF (bis(ethylenediteho)-tetrathiafulvalene) and TMTSF (tetramethyltetraselenafulvalen) display a rich variety of electronic properties from magnetic insulators to superconductors depending on the nature of the donors or acceptors and their location in the crystal structure. Low-dimensionality of charge transfer salts is of special interest due to the theoretical suggestion that the normal state of these systems may be unusual. It has been shown that one-dimensional conductors are not Fermi liquids like normal metals, but Luttinger or Luttinger-Emery liquids with distinct different physical properties. High-resolution angle-resolved photoemission spectra (ARPES) have shown a strong suppression of quasiparticle states near the chemical potential [1]. On the other hand a decrease in photoemission intensity near the Fermi level may result from extrinsic changes in the electronic structure at the surface, reconstruction, off-stoichiometry, or degradation. Additional measurements using bulk sensitive spectral techniques such as X-ray emission spectroscopy are necessary to verify the validity of observations resulting from photoemission experiments.

We report soft x-ray fluorescence measurements for the charge transfer salts $(TMTSF)_2PF_6$, $(BETS)_2FeBr_4$ and (CPDT-STF)(TCNQ), carried out at Beamline 8.0 of the Advanced Light Source. Nonresonant carbon Kα (2p→1s transition) X-ray emission spectra (XES) were recorded employing the soft X-ray fluorescence endstation [2]. Photons with an energy of 300 eV, well above the carbon K-edge, were used for excitation. The carbon Kα spectra were obtained with an energy resolution of 0.3-0.4 eV.

Fig. 1 displays the carbon Kα soft x-ray emission spectra (XES) [3]. A two-peak structure (labeled *a*, *b*) is found for all compounds. The same energy separation of peaks *a* and *b* in C Kα (~2.8 eV) XES is found for all charge transfer salts indicating that the same structure of carbon π-states in the valence band is present in all spectra. Such low-energy subbands have been found in X-ray emission spectra of compounds and are attributed to ns-states of non-metal atoms. Therefore this subband can stem from the hybridization of carbon 2p-states of the BEDT-TTF molecule and 2s states of the oxalate layer $[(H_3O)Fe(C_2O_4)_3]$ or from the nitrogen in benzonitrile

C_6H_5CN, which is due to hybridization between carbon π-metal electrons of donor (BEDT-TTF)-molecule and s-states of anion. The presence of an additional subband in carbon Kα XES evidences strong cation-anion interaction in $(BEDT\text{-}TTF)_4[(H_3O)Fe(C_2O_4)_3]C_5H_5N$.

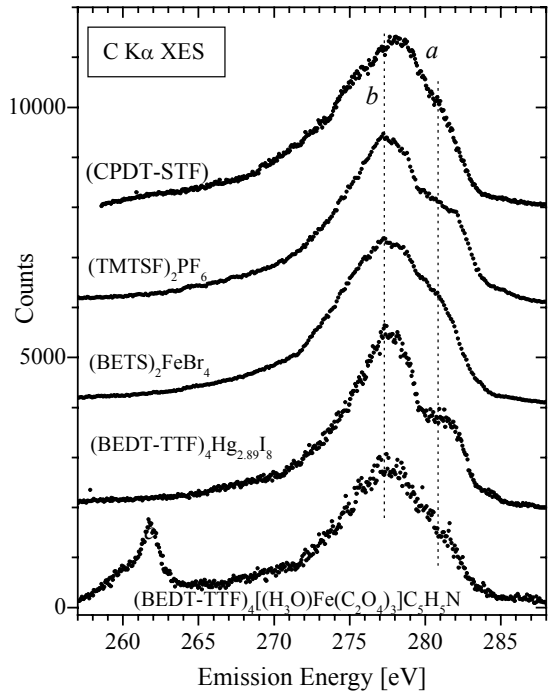

Fig. 1 C Kα XES of charge transfer salts in the entire valence-band region

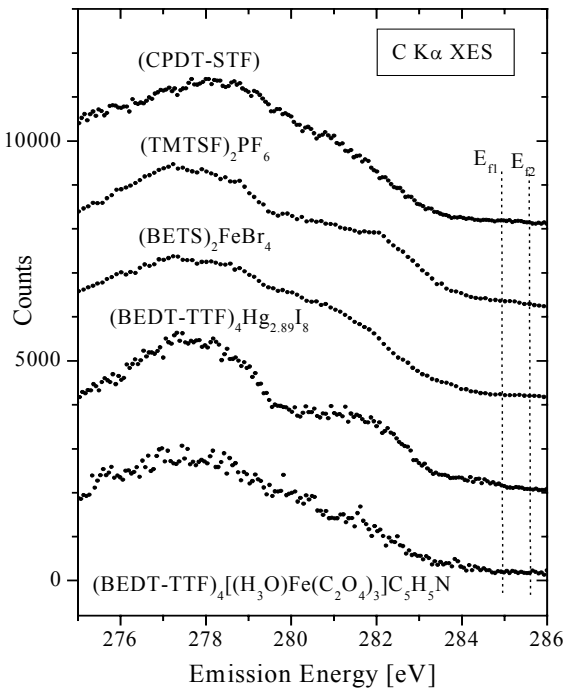

Fig. 2 C Kα XES in the vicinity of the Fermi level.

In order to examine the behavior of the carbon emission features near the Fermi level, one would need XPS binding energies of the C 1s core levels. Unfortunately such measurements have been performed, up to now, only for few charge transfer salts [3]. The binding energies vary between 0.2 and 0.7 eV, allowing us to estimate the position of the Fermi level in the carbon Kα spectra displayed. Fig. 2 shows carbon Kα XES in the vicinity of the Fermi level. For carbon C Kα XES two Fermi level positions are indicated (E_{f1} and E_{f2}) which correspond to the lower and higher C 1s binding energies, respectively. All spectra show almost linear tails in the vicinity of the Fermi level (extending towards higher emission energies) and a suppression of the spectral weight at E_f. This pseudogap as well as the absence of a Fermi edge is incompatible with the usual spectroscopic behavior of normal 3D metals, which display Fermi-edges.

Our observations are in contrast to the conventional Fermi liquid picture of a metal where quasiparticle bands cross the Fermi level. We conclude that non-Fermi liquid features are observed in X-ray emission spectra of charge transfer salts. At the same time we point out that the decrease in spectral weight in the XES spectra stretches over almost 2 eV, which seems unreasonably large for Luttinger liquids. This value is even larger than the conduction bandwidths derived for organic CT salts (0.5 to 1 eV). This problem also exists in the non-Fermi liquid interpretation of the photoemission spectra.

REFERENCES

1. F. Zwick, M. Grioni, G. Margaritondo, V. Vescoli, L. Degiorgi, B. Alavi, and G. Gruner, Solid State Commun. 113 (2000) 179.
2. J.J. Jia, T.A. Callcott, J. Yurkas, A. W.Ellis, F.J. Himpsel , M.G. Samant, J. Stöhr, D.L. Ederer, J.A. Carlisle, E.A. Hudson, L.J. Terminello, D.K. Shuh, and R.C.C. Perera, *Rev. Sci. Instrum*. 66 (1995) 1394.
3. E. Z. Kurmaev, A. Moewes, U. Schwingenschlögl, R. Claessen, M. I. Katsnelson, H. Kobayashi, S. Kagoshima, Y. Misaki, D.L. Ederer, K. Endo, and M. Yanagihara, Phys. Rev. B 64 (2001) 233107.

The Russian Foundation for Basic Research (Project 00-15-96575) and NATO Collaborative Linkage Grant supported this work. Funding by the Natural Sciences and Engineering Research Council (NSERC) is gratefully acknowledged. The Deutsche Forschungsgemeinschaft (Schwerpunktprogramm 1073) funded the work in Augsburg.

Principal investigator: Ernst Kurmaev, Institute of Metal Physics, Russian Academy of Sciences-Ural Division, 620219 Yekaterinburg GSP-170, Russia. Email: kurmaev@ifmlrs.uran.ru. Telephone: +7-3432-744183.

X-ray transitions for studying the electronic structure of 5d metals

E.Z. Kurmaev[1], A. Moewes[2], Z. Pchelkina[1], I. Nekrasov[1], T.A. Callcott[3], and D.L. Ederer[4]

[1]Institute of Metal Physics, Russian Academy of Sciences-Ural Division, 620219 Yekaterinburg GSP-170, Russia

[2] Department of Physics and Engineering Physics, University of Saskatchewan, 116 Science Place, Saskatoon, Saskatchewan S7N 5E2, Canada

[3]University of Tennessee, Knoxville, Tennessee 37996, USA

[4]Department of Physics, Tulane University, New Orleans, LA 70118, USA

Transition metals of the 5d-series, their alloys and compounds are used in a wide range of applications. Unfortunately the direct study of their electronic structure by means of soft X-ray emission spectroscopy is limited due to the absence of suitable X-ray transitions. According to XPS measurements [1], the 5d transition elements (from Hf to Au) have $4p_{1/2,3/2}$ ($N_{2,3}$) core levels in the binding energy region of 380-643 eV. The X-ray emission bands of these metals, arising from the electric dipole transitions between the 5d valence electrons and 4p core level vacancies ($5d \rightarrow 4p_{3/2,1/2}$ transition) can be used for studying the occupied density of 5d-states (DOS). Due to the presence of strong competing radiationless transitions, these spectra are not listed in systematic studies of soft X-ray emission bands of 5d-transition metals [2, 3]. Due to the inherently low fluorescence yield of the ultra-soft x-ray emission process, we utilized the high brightness available at Lawrence Berkeley National Laboratory's Advanced Light Source for the measurements of fluorescence $N_{2,3}$ X-ray emission spectra (XES) of 5d metals. The spectra were taken at Beamline 8.0, employing the soft x-ray fluorescence endstation [4]. Photons with an energy of 399-490 eV, were used for excitation. All measurements reported here were made with a 100-micrometer entrance slit for the spectrometer.

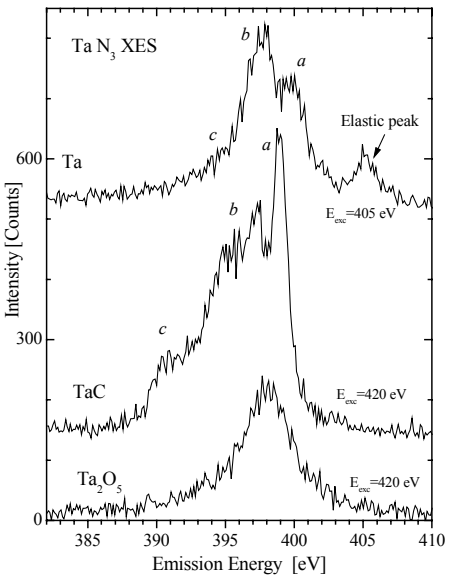

Fig. 1 (a) Ta N_3 XES of Ta, TaC and Ta_2O_5.

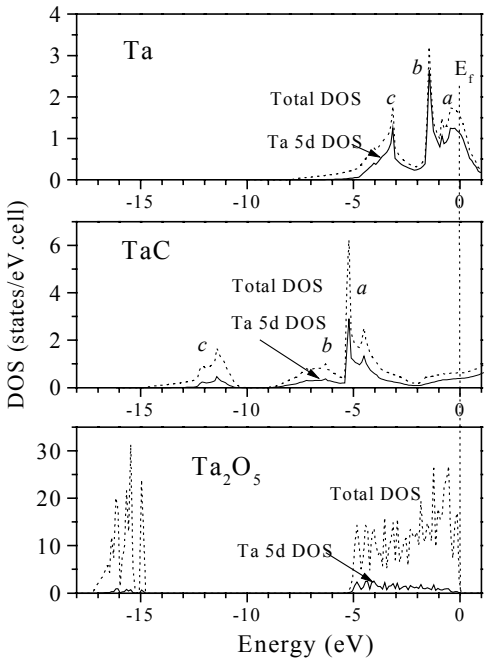

Fig. 1 (b) Total and Ta 5d DOS

We succeeded in measuring non-resonant 5d-metal N_3 ($5d \rightarrow 4p_{3/2}$ transition) soft X-ray emission spectra for Ta, TaC and Ta_2O_5 [5]. The measurements are displayed in Fig. 1(a). X-ray emission is governed by the dipole selection rule, $\Delta l = \pm 1$, which allows only for d- or s-valence electrons to fill the p-type core holes in 5d atoms. The intensity of $N_{2,3}$ non-resonant X-ray emission spectra of 5d elements maps the d-density at the atomic site, or in a band structure picture, the contribution of partial d-type density of states. The measured spectra have a signal to noise ratio of about 10 and show different spectral shape for metal, carbide and oxide evidencing the sensitivity to chemical bonding. According to band structure calculations [5] displayed in Fig. 1b, the main features of Ta 5d DOS are the same as in the total DOS and different in pure metal, carbide and oxide. Ta 5d DOS in pure metal have three subbands (*a*-*c*) and occupy less energy range than that of TaC. Ta 5d DOS in TaC are strongly hybridizing with the C 2p band giving rise to the structures labeled (*a* to *b*). The additional subband labeled *c* is due to hybridization with C 2s-states. The rather complicated band structure of TaC is reflected in Ta N_3 XES. The energy position of calculated and experimental peaks is in reasonable agreement though the ratio of peaks is rather different. In the case of tantalum pentoxide (Ta_2O_5), the band structure calculations show simpler structure because all Ta 5d electrons occupy the O 2p-band and the d-like band is empty (metal atoms have d^0 configuration). Therefore only the O 2p–Ta 5d band and the atomic-like O 2s-band are present in the valence band of Ta_2O_2. In good agreement with the calculated spectrum, the Ta N_3 emission is of simpler structure for Ta_2O_5 than for TaC. O 2s-states are not seen in Ta N_3 XES of Ta_2O_5 because they are more localized than the C 2s-states and less hybridized with Ta 5d-states.

$5d \rightarrow 4p$ transitions seem to be more favorable for studying the electronic structure of 5d-metals than $5d \rightarrow 5p$ and $5d \rightarrow 4f$ transitions, which are present in the ultra-soft region of 20-90 eV [3]. The reason is that the corresponding metal N_3 X-ray emission spectra are less influenced by core-level vacancies due to the higher localization of 4p-levels compared to 5p and 4f-levels. Therefore one can measure the undistorted density of 5d states.

REFERENCES

1. R. Nyholm, A. Berndtson, and N. Martensson, J. Phys. C 13 (1980) L109.
2. J.A. Beardeen, Rev. Mod. Phys. 39 (1967) 78.
3. V.A. Fomichev, T.M. Zimkina, A.V. Rudnev, and S.A. Nemnonov, in *Band Structure Spectroscopy of Metals and Alloys* (ed. by D.J.Fabian and L.M.Watson), Academic Press, London and New York, 1973, pp. 259-293.
4. J.J. Jia, T.A. Callcott, J. Yurkas, A.W. Ellis, F.J. Himpsel, M.G. Samant, J. Stohr, D.L. Ederer, R.C.C. Perera, Rev. Sci. Inst. 66 (1995) 1394
5. E.Z. Kurmaev, A. Moewes, Z.V. Pchelkina, I.A. Nekrasov, A.A. Rempel and D.L. Ederer, Phys. Rev. B 63 (2001) 73108.

This work was supported by the Russian Foundation for Basic Research (Projects 00-15-96575), the National Sciences and Engineering Research Council (NSERC). The work at the Advanced Light Source at Lawrence Berkeley National Laboratory was supported by U.S. Department of Energy (Contract No. DE-AC03-76SF00098).

Principal investigator: Ernst Kurmaev, Institute of Metal Physics, Russian Academy of Sciences-Ural Division, 620219 Yekaterinburg GSP-170, Russia. Email: kurmaev@ifmlrs.uran.ru. Telephone: +7-3432-744183.